Dissertation

Submitted to the Department of Earth Sciences

of Freie Universität Berlin

Luminescence dating of transgressions in the Bohai Coast China since the Middle Pleistocene

Yan Li

李 琰

Luminescence dating of transgressions in the Bohai Coast China since the Middle Pleistocene

Inaugural-Dissertation zur Erlangung des Doktorgrades

Dr. rer. nat.

im Fachbereich Geowissenschaften

der Freien Universität Berlin

vorgelegt von

YAN LI

李 琰

aus Linyi County, Shandong, China

Gutachter:

Prof. Dr. Manfred Frechen (Erster Gutachter)

Prof. Dr. Margot Böse (Zweiter Gutachter)

Tag der Disputation: 25.04.2018

Table of contents

Abstract

Coastal areas hold major social and economic value. Understanding past coastal evolution is therefore crucial to anticipate future changes which will affect these areas of high significance. The Bohai Sea, situated at the transition zone between the East Eurasian Continent and West Pacific Ocean, is an area particularly sensitive to sea-level changes and sediment inputs. Due to the continuous subsidence of the Bohai basin since the Cenozoic, thick sediment sequences accumulated progressively in the Bohai Coast, providing a valuable proxy record of climate and environmental evolution. Sedimentary sequences in the Bohai Coast indicate three main transgressive and regressive phases, associated with the regional sea-level change and terrestrial influence since the Middle Pleistocene. The chronology of these transgressions and regressions is however not well constrained, and requires a thorough investigation.

The main objective of this thesis is to establish a reliable chronological framework for the three transgressions identified in the Bohai Coast since the Middle Pleistocene, using Optically Stimulated Luminescence (OSL) dating. A careful validation of different OSL approaches is first conducted. The quartz OSL signal was fully reset for materials from the North Bohai Coast, while the K-feldspar luminescence signals were well bleached for the pre-Holocene deposits, validating the use of this dosimeter to establish a robust chronology of the Bohai sediments. To correct the undesirable signal loss over geological time scale associated with the use of this mineral, the fading correction method based upon the theory of power-law decay of tunnelling is tested. Fading corrected ages in agreement with the reference chronology confirm the validity of this fading correction method. Quartz OSL dating is applied to the coastal core sediments and dune sands from the North Bohai Coast. The quartz and feldspar luminescence chronologies indicate that the earliest transgression occurred ca. 200 ka, correlating with the sea-level highstand during Marine Isotope Stage (MIS) 7. Based on the age-depth relation, the second transgression very likely occurred during MIS 5. Both the radiocarbon dates and the quartz OSL ages show that the transgressive sedimentary facies in association with the rising of the sea-level during MIS 3 is not preserved in the Bohai cores. The last transgression correlates with the Holocene sea-level rise.

Luminescence chronology, in conjunction with the historical records of the shoreline migration, reveals that the sea-level constantly stayed at highstand between *ca.* 6 and 1 ka in the North Bohai Coast, and then retreated rapidly causing the delta progradation. Thin transgressive deposits, equivalent to an annual sediment increment of 2.7×10^4 $m^3\cdot a^{-1}$ between 6-1 ka, are explained by the flat relief and insufficient sediment supply. The rapid deltaic progradation, which includes an episodic deposition by multiple flooding events at *ca.* 700 a, resulted in the dramatic increase of sediment increment (9.1×10^6 $m^3\cdot a^{-1}$) over the last millennia. This sudden increase was triggered by both the

winter monsoon enhancement and the reduction of plant cover and soil erosion by human activity. On the contrary, a rapid inland sand deposition after the Little Ice Age was most likely related to the Immigrant and Reclamation Policy.

Zusammenfassung

Durch die hohe sozio-ökonomische Bedeutung von Küstenregionen ist es wichtig, deren geologische Entwicklungsgeschichte zu verstehen, um Aussagen zu künftigen Küstenveränderungen prognostizieren zu können. Das Bohai-Meer, welches in der Übergangszone zwischen dem Eurasischen Kontinent und dem Pazifischem Ozean liegt, reagiert sehr sensibel auf Meeresspiegelschwankungen, sowie auf Änderungen im Sedimenteintrag. Die seit dem Känozoikum anhaltende Subsidenz führte zur Ablagerung von mächtigen Sedimentabfolgen entlang der Küste von Bohai. Diese enthalten wertvolle Informationen über die Klima- und Umweltentwicklung dieses Zeitabschnittes. Sedimentologische Variationen, besonders die der drei Hauptzyklen mit transgressiven und regressiven Sedimente, spiegeln die Umweltveränderungen wider, welche verbunden sind mit Schwankungen des Meeresspiegels und terrestrischer Einflüsse seit dem mittleren Pleistozän. Trotz ihrer Bedeutung ist die zeitliche Abfolge der Transgressionen und Regressionen kaum bekannt und bedarf daher einer eingehenden Untersuchung.

Das Hauptziel der vorliegenden Dissertation ist die Erstellung einer belastbaren chronologischen Altersabfolge für drei Transgressions-Phasen, welche seit dem Mittleren Pleistozän entlang der Küste von Bohai stattgefunden haben. Hierzu erfolgte zuerst eine sorgfältige Überprüfung der zur Verfügung stehenden Lumineszenz-Methoden. Das Lumineszenz-Signal des Kaliumfeldspat erwies sich als gut gebleicht und deshalb als geeignet zum Datieren der Bohai-Ablagerungen. Die Fading-Korrekturmethode basiert auf power-law decay of tunnelling ergibt Alter die mit der Referenzchronologie übereinstimmen und somit die Richtigkeit der Fading korrigierten Alter bestätigen. Sedimente aus Bohrkernen der Küstenregion, sowie Dünensande von der Nord-Küste von Bohai wurden mit Hilfe der optisch stimulierte Lumineszenz (OSL) Methode datiert. Die Quarz OSL (innerhalb 50 ka) und Feldspat pIRIR (10-250 ka) Lumineszenz Alter zeigen, dass die früheste Transgression vor c. 200 ka erfolgte, was mit dem Meeresspiegel-Hochstand im Marinen Isotopen Stadium (MIS) 7 korreliert. Basierend auf Alter-Tiefe Verhältnissen ist die zweite Transgression höchstwahrscheinlich im MIS 5 aufgetreten. Sowohl die Radiokarbon- als auch die Quarz-OSL-Alter ergaben, dass transgressive Ablagerungen des Meeresspiegel-Hochstandes während des MIS 3 nicht in den Bohai-Kernen erhalten geblieben sind. Die letzte Transgression korreliert mit dem holozänen Meeresspiegelanstieges.

Die Lumineszenz-Chronologie in Verbindung mit Aufzeichnungen über historische Küstenverlagerungen verweisen auf einen konstant oszillierenden Meeresspiegel mit einem Höchststand zwischen ca. 6 und 1 ka entlang der Nord-Küste von Bohai. Hierauf folgt ein schneller Rückgang, welcher eine Delta-Progradation bewirkt. Geringmächtige transgressive Ablagerungen, korrespondierend mit einem jährlichem Sedimentzuwachs von 2.7×10^4 $m^3 \cdot a^{-1}$ im Zeitraum zwischen 6-

1 ka, sind durch das flache Relief und die insuffiziente Sedimentzufuhr bedingt. Die schnelle Progradation, inklusive der episodischen Ablagerung durch häufige Flutereignisse der letzten 700 a, resultiert in einem dramatischen Anstieg des Sedimentzuwachses auf 9.1×10^{6} $m^{3}\cdot a^{-1}$ im letzten Jahrtausend. Diese Zunahme wurde ausgelöst durch die Intensivierung des Wintermonsuns, sowie durch menschliche Aktivität. Die Ablagerung von Sand steigt seit dem Ende der Kleinen Eiszeit rapide an, welches in Zusammenhang mit menschlichen Eingriffen in den Naturhaushalt steht.

Acknowledgements

This PhD is funded by China Scholarship Council (CSC No. 201406400050. September 2014 to August 2017) at Leibniz Institute for Applied Geophysics and Freie Universität Berlin.

First of all, I would like to thank my supervisor Prof. Dr. Manfred Frechen sincerely who accepted my PhD proposal in November 2013. During the past three and half years in Hannover, I benefited a lot from his scientific supervision and suggestions. I appreciate very much that he created many opportunities for me to attend academic workshops and conferences, which have spread my field of version and allowed me to connect with other colleagues. I will never forget the kindness, support and encouragement from him.

I would like to express my genuine gratitude to Dr. Sumiko Tsukamoto for her hand-by-hand supervision throughout my PhD. Her supervision started from the first aliquot and sequence I have prepared in my life. Each of my paper, conference poster, abstract and presentation was carefully corrected by her. I was always encouraged to resolve the scientific problems after the discussions with her. It is my honour to work with you, Sumiko!

I would like to thank Prof. Dr. Margot Böse for reviewing the thesis and her constructive comments on this thesis and my presentation which I gave in Lankwitz. I would also like to thank Dr. Robert Hebenstreit, Dr. Jacob Hardt and Shih-Hung Liu for their help during my PhD period.

Special thanks go to Hao Long and Jingran Zhang. During the first two years of my PhD, they helped me very much not only in the laboratory, but also in daily life. They are so supportive that make my life in Germany much easier. I always felt like at home when we celebrated our holidays, cooking together, etc. I was also super enjoying the scientific discussions with them that I learned a lot.

I am grateful to Prof. Hong Wang (Tianjin Geological Survey, CGS) for his recommendation and huge support. I had the opportunity to join the collaborations with colleagues from Tianjin. I would like to thank Dr. Zhiwen Shang and Dr. Fu Wang (Tianjin Geological Survey, CGS) for the fruitful discussions and helps in the field. Thanks go to Dr. Jianfen Li, Xingyu Jiang, Hongwei Ma (CGS) and Kexin Zhang (CUGB) for their help during drilling and sampling.

I am thankful to Dr. Benny Guralnik (Risø, DTU) for showing me how to run the fading correction model. Furthermore, I want to thank Dr. Georgina King (University of Bern) for her help in my paper and the discussions about application of fading correction model. Thanks go to Dr. Toru Tamura (Geological Survey of Japan) for his help in sedimentological interpretation in my PhD research. Special thanks to Dr. Tobias Lauer (MPI, Leipzig) who supported and taught me in the laboratory at the very beginning of my luminescence career. I would like to thank Dr. Christian Rolf (LIAG-S5) for his support in magnetic

measurement and data analysis, and allowing me to stay in the cosy guest house in Grubenhagen. I would also like to thank Stephanie Scheidt and Lena Wallbrecht for their kind help during the two weeks in Grubenhagen. Dr. Michael (Ede) Kenzler and Dr. Natacha Gribenski helped me a lot to improve this thesis during the last days before submission. I appreciate it! Ede, I also appreciate a lot for your help at the beginning of my PhD. Natacha, your working attitude with passion always encourages me. Thanks go to my collaborators Dr. Gerald Gabriel (LIAG-S1), Dr. Liang Yi (Tongji University) and Prof. Ke Hu (CUGB) for your help in data analysis, interpretation and publications.

Moreover, I am very grateful to my colleagues in the team of section S3, LIAG. I got a lot of support from Gudrun Drewes, Frank Oppermann, Karsten Vollmer, Petra Posimowski, Dr. Melanie Sierralta, Astrid Jaeckel, Dr. Christine Thiel, Sabine Mogwitz, Dr. Astrid Techmer and Ragna Bergmann. Special thanks go to Sonja Reimenschneider for her generous help and the huge support from her international office. I would also like to thank the PhD students Marcus Richter and Neda Rahimzadeh in our section, for sharing knowledge and experience.

Finally, I would like to thank my parents sincerely, who are waiting for my return. I could not finish my PhD without their constant support. Special thanks to my beloved girlfriend Congyue for her super encouragement and patience.

Yan Li

16.11.2017 Hannover

Chapter 1 Introduction

Coastal areas are sensitive to the sea-level change, which is driven by a combination of natural processes and anthropogenic factors (e.g. IPCC, 2014). Since the majority of human activities occurs along coasts, exploring past coastal processes under marine-terrestrial interaction with a reliable chronological framework is of crucial socio-economic significance. Investigations of the past environmental evolution in coastal areas help us to understand the coastal reshaping, i.e. accumulation and erosion, triggered by the global sea-level change and sediment input. Furthermore, a better understanding of the past coastal evolution is mandatory to predict future coastal development and develop appropriate strategies of protection for vulnerable coastal zones in the future ''greenhouse world''.

Coastal deposits, which record detailed climatological and environmental information, are regarded as ideal archives of former coastal processes. The palaeo-coastline migration can be documented by multiple sea-level indicators, such as marine terraces, shore platforms, cheniers and beach rocks (Murray-Wallace and Woodroffe, 2014). The sea flooding ranges in different periods can also be reconstructed by down-core distributions of marine strata, based on the identification of the marine deposits from the terrestrial sediments using indicators such as macro- and micro-fossils,

mineral and sediment architecture (Department of Marine Geology, Tongji University, 1980). If the information about palaeo-coastline migration is complemented with a chronology, the geomorphological evolution during a certain period can be subsequently interpreted. Furthermore, the climate change is reflected by environmental proxies recorded in the coastal deposits.

The Bohai Sea is situated at the transition zone between the East Eurasian Continent and the West Pacific Ocean, sensitive to both continental input and sea-level change. Due to their regional and global significance, the Quaternary deposits have been widely investigated in terms of sea-level change and environmental evolution (e.g. Bradley et al., 2016; IOCAS, 1985; Lambeck et al., 2014; Li et al., 2015; Liu et al., 2004, 2009, 2016; Shi et al., 2016; Wang et al., 2015; Xu et al., 2015; Xue, 2014; Yao et al., 2014; Zhao et al., 1979; Yi et al., 2012, 2015). Based upon the numerous cores obtained from the coastal area since the 1970s, alternated sedimentary strata associated with marine and terrestrial environment were found, showing the existence of several main transgressions in the Bohai area in the past (e.g. Y. K. Chen et al., 2008; Y. S. Chen et al., 2012; Han, 2001; IOCAS, 1985; Liaoning Geology Bureau, 1983; Liu et al., 2016; Yi et al., 2013; Zhao et al., 1978, 1986). Most of the cores indicate three major transgressive-regressive cycles postdating the Brunhes-Matuyama (B/M) boundary (IOCAS, 1985; Liu et al., 2016; Yi et al., 2015). These sequences of transgression and regression were also observed in the adjacent coasts of East China (e.g. Wang and Tian, 1999; Yang and Lin, 1991). However, the poorly constrained chronology for the marine-terrestrial deposition has held back a convincing palaeo-environmental interpretation. Most of the existing numerical dating results were derived using the radiocarbon dating method, which has a limited dating range within ca. 40-50 ka. In addition, datable materials for radiocarbon dating occur sporadically, resulting in discontinuously constrained chronologies.

Luminescence dating method is advantageous as it permits to extend the dating range and to establish a high-resolution chronological data beyond the limits of radiocarbon dating. During the last decade, luminescence dating has been widely applied to coastal deposits (Lamothe, 2016). Luminescence dating methods, using quartz and feldspar have been previously applied to determine the transgression-regression chronology in the Bohai Coast (e.g. Y.K. Chen et al., 2008; Y.S. Chen et al., 2012; Liu et al., 2016; Yi et al., 2013). However, the reliability of the published luminescence ages, in terms of signal bleaching, saturation and signal loss (i.e. anomalous fading), was not well assessed. Furthermore, the reliability of the methods (Huntley and Lamothe, 2001; Kars et al., 2008; Lamothe et al., 2003; Wallinga et al., 2007) applied to correct the underestimated feldspar ages affected by anomalous fading was not well discussed and partly missing in previous studies. Consequently, there is a significant uncertainty associated with the luminescence ages published in earlier studies.

1.1 Objectives

In this thesis, multiple luminescence signals are used to date the deposits from the North Bohai Coast, which consist in a sand dune a priori formed during the Holocene transgression, and sediments from a coastal core recording several transgression-regression phases. The main aim of this thesis is to establish a reliable chronology for the three main transgressions in the Bohai Coast since the Middle Pleistocene. The second objective is to understand the sedimentary processes concomitant with sea-level change and fluvial input during the last deglaciation. The accumulation history during the post sea-level highstand in the North Bohai Coast is subsequently interpreted.

Prior to the establishment of chronology and environmental interpretation of the transgression and regression in the Bohai Coast, the degree of bleaching is evaluated for multiple luminescence signals, in order to validate the application of the K-feldspar infrared signals for the Bohai coastal deposits. In addition, the reliability of the fading correction models for the feldspar luminescence dating is tested on samples with reference chronology, from the Heidelberg Basin (Upper Rhine Graben), Germany, and from the Chinese Loess Plateau. The validated fading correction method is finally applied to determine reliable feldspar ages for the Bohai sediments.

1.2 Study area and core LZK06

1.2.1 Bohai Sea and Quaternary sedimentation

The Bohai Sea is a semi-enclosed sea with an average water depth of 18 m, located in northeastern China (37°07'-41°00' N, 117°35'-121°10' E). It consists of three bays (the Liaodong Bay, Bohai Bay and Laizhou Bay), the central Bohai Basin and the Bohai Strait (IOCAS, 1985. Fig. 1.1).

The Liaodong (North Bohai) Coast comprises bedrock-sandy and sandy-clayey coasts. It includes the estuaries of Daliao River, Liao River, Daling River and Xiaoling River, which contribute mostly to the sedimentary loads into the Liaodong Bay, and the formation of the Lower Liao Plain. The coastal area of the Bohai Bay is mainly occupied by clayey-silty material, which are the finest in the entire Bohai area, because significant amount of sediments are transported by the Yellow River and Haihe River. The water depth is generally shallower than 20 m in this bay. The Laizhou Bay is the southern part of the Bohai Sea, and its coastal sediments are dominated by clayey silt. The sediments are mainly derived from the Luzhong mountain area and transported in a short distance by several local rivers. The water depth varies from 10 to 15 m. In contrast to the three bay areas, only small amount of sediment is deposited in the Bohai Strait owing to the strong currents. The Bohai Sea is connected to the Yellow Sea through the Bohai Strait, comprising the Miaodao Archipelago and six main submarine water channels with whole width of approximately 100 km.

Quaternary sediments with a thickness of 300-400 m were deposited in the Bohai basin, which includes the areas of Bohai Sea and adjacent coastal plains (IOCAS, 1985), as a consequence of continuous subsidence since the onset of the Cenozoic (Allen et al., 1997). The rivers draining into the Bohai Sea contribute mostly to the sediment loads. The lower Quaternary succession mainly comprises terrigenous deposits, such as lacustrine and fluvial sediments. The upper succession consists of marine, fluvial and lacustrine deposits, revealing the cyclic marine-terrestrial interaction. The definition of transgressive layers is mainly based on the results from macro- and micro-fossil analysis (e.g. IOCAS, 1985; Yao et al., 2010).

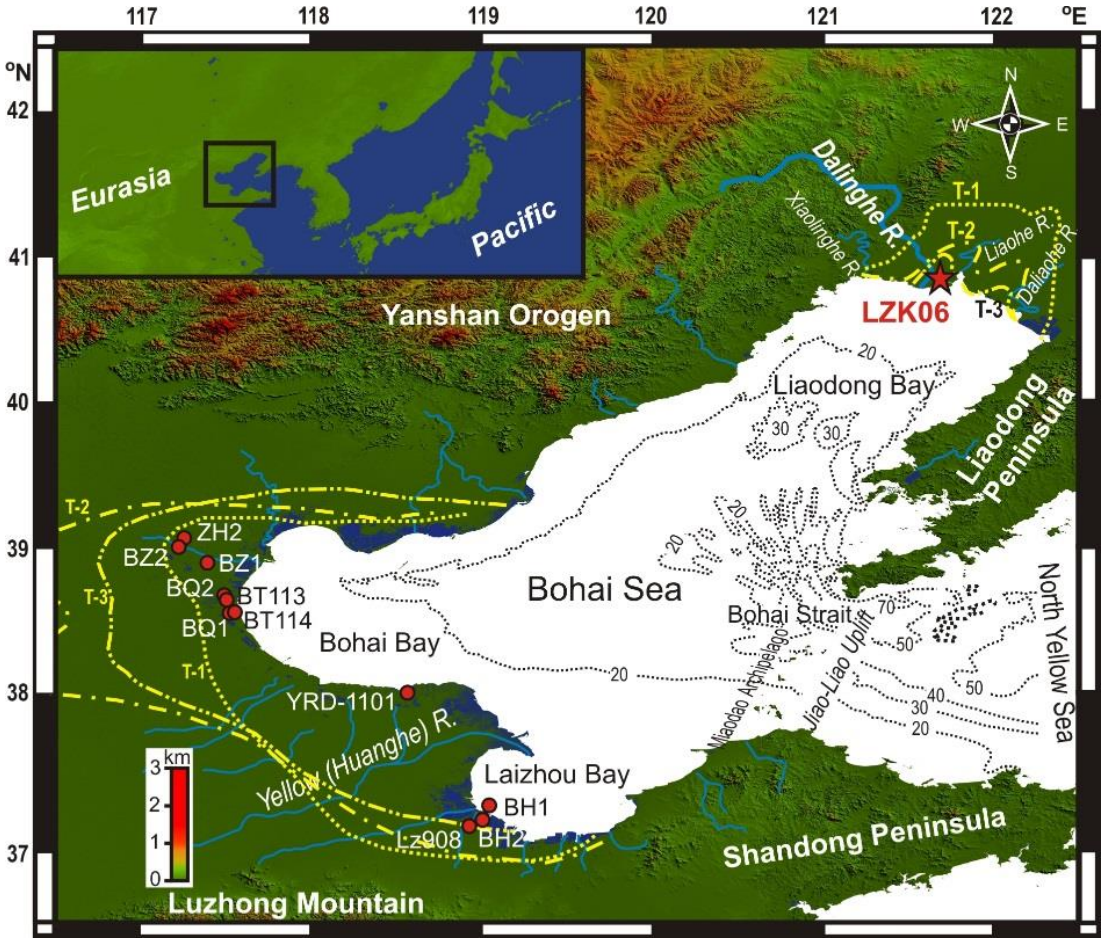

Fig. 1.1 Topographic map of Bohai Sea and location of the studied borehole LZK06. The three transgression ranges (T-1, T-2 and T-3) in the Bohai Coast are modified from Wang et al. (1986) and Zhao et al. (1986). The main local streams and OSL dated cores are shown. The digital elevation model (DEM, 90 m) was downloaded from http://www.cgiar-csi.org. Isobaths are following He et al. (2006). The OSL dated coastal cores are from Chen et al. (2008) (BZ1 and BZ2), Chen et al. (2012) (BT113 and BT114), Liu et al. (2016) (YRD-1101), Yan et al. (2006) (BQ1 and BQ2), Yi et al. (2013) (Lz908, BH1 and BH2), Zhao et al. (2002) (ZH2).

1.2.2 Core LZK06

The borehole LZK06 (40°54.44' N, 121°37.77' E, elevation +4.51 m a.s.l.; Fig. 1.1) was drilled in the North Bohai Coast in 2015. It is situated on the left bank of the present channel of the Dalinghe River, 10 km north of the river mouth. The length of the core is 100 m and the recovery rate is approximately

92%. The three transgressive layers occurring in the upper 55 m of the core were identified based on: 1) the identification of mollusc shells indicative of the marine environment, and 2) lithological correlation in the North Bohai Coast (Liaoning Geology Bureau, 1983). The three transgression layers are referred to as T-1, T-2 and T-3, respectively, in ascending order. The terrestrial deposits in between representing the regression periods are named as R-1, R-2 and R-3, respectively (Fig 1.2). R-3 occurs at 50.1-100 m, comprising massive fluvial and lacustrine sediments. T-3(49.0-50.1 m) contains high-moist dark-grey clayey sand with mollusc shells and fragments. R-2 consists of brownish-grey fluvial sand (44.0-48.5 m), dark-grey lacustrine silty clay (39.2-44.0 m) and bluish-grey fluvial sand (28.7-39.0 m). T-2 occurring at 21.0-28.7 m comprises a basal mollusc shell-rich layer with well-rounded carbonate concretions, a clayey silt layer at depth of 23.5-24.3 m, and also rich mollusc shell fragments. Shell fragments in millimetre size were found throughout the middle T-2. R-1 comprises fining-upward silty sand with the top organic-rich layer, occurring at a depth of 13.6-19.0 m. T-1 occurs at 4.2-13.6 m depth and comprises grey clayey silt to sand with mollusc shells and fragments.

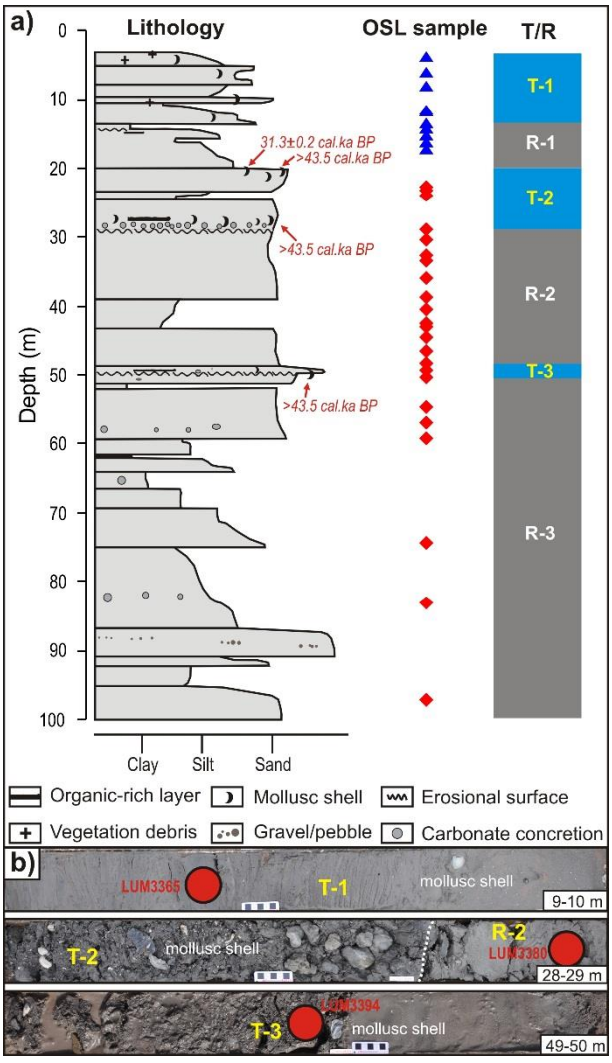

Fig. 1.2 Lithology of core LZK06. a) shows the lithological variations, OSL sample positions and definition of transgression or regression layers. Radiocarbon dates for the lower two transgression layers are shown (Shang et al., in prep.). b) shows pictures of the representative transgressive deposits. The position of OSL samples, mollusc shells and boundary between R-2 and T-2 are sketched.

1.3 Current state of research

1.3.1 Transgressions and regressions in the Bohai Coast

In the review paper by Lamothe (2016), sediment architectures in different tectonic settings of coastal areas are summarised. For uplifting systems, marine terraces can be recognised. High to low elevation of these terraces generally represents the old to young transgressive processes. In contrast, for continuously subsiding coastal systems, the marine deposits associated to the earlier transgression are in general submerged under the later transgressive layer (Fig. 1.3). The Bohai sediment basin has been slowly subsided since the Cenozoic (Allen et al., 1997). Consequently, thick Quaternary sediments were deposited there, recording the evolution of the sedimentary environment. The widely discovered transgressive and regressive sediments in cyclicity in the Bohai coastal stratigraphy thus record the main transgressions during the Quaternary. According to the studies on the Bohai Coast, as well as the adjacent Yellow Sea area, three main transgressive layers have been recognised (e.g. IOCAS, 1985; Liu et al., 2016; Yi et al., 2015; Wang and Tian, 1999; Yang and Lin, 1991). Palaeomagnetic results show that the three transgressions postdate the Brunhes/Matuyama boundary, and these events were explained to be consecutive to the subsidence of Miaodao Islands in the Bohai Strait, at ca. 300 ka before present (Yi et al., 2015). However, this assumption has not been supported by numerical dating.

The transgressions in the Bohai Sea since the Middle Pleistocene have been extensively investigated in aspects of long-term and short-term chronologies, coastal sedimentary processes and the correlation to the global sea-level change (e.g. IOCAS, 1985; Shi et al., 2016; Yao et al., 2014; Liu et al., 2016). In particular, the regional sea-level change has been explored over the last 50 years. The investigation of the relative water-depth change since the late deglaciation was carried out using grain-size parameters (Yi et al., 2012). Pico et al. (2016) corrected the relative sea-level height during the Marine Isotope Stage (MIS 3) period in the Yellow Sea area and refined the estimate of global ice volume. Except for these two studies, most of the research carried out in this area mainly focuses on the sea-level change since the Last Glacial Maximum (LGM). Previous studies on global sea-level change showed that after MIS 3 it continuously fell to a lowstand of ca. -130 m with the glacial maximum at ca. 20 ka (Yokoyama et al., 2000; Lambeck and Chappell, 2001; Clark et al., 2009). The main phase of deglaciation occurred from 16.5 to 7 ka BP with an abrupt sea-level rise, after an initial sea level rise and a short stagnation phase (Lambeck et al., 2014). The rate of sea-level rise decreased in the last 7 ka and subsequently reached the Holocene sea-level highstand.

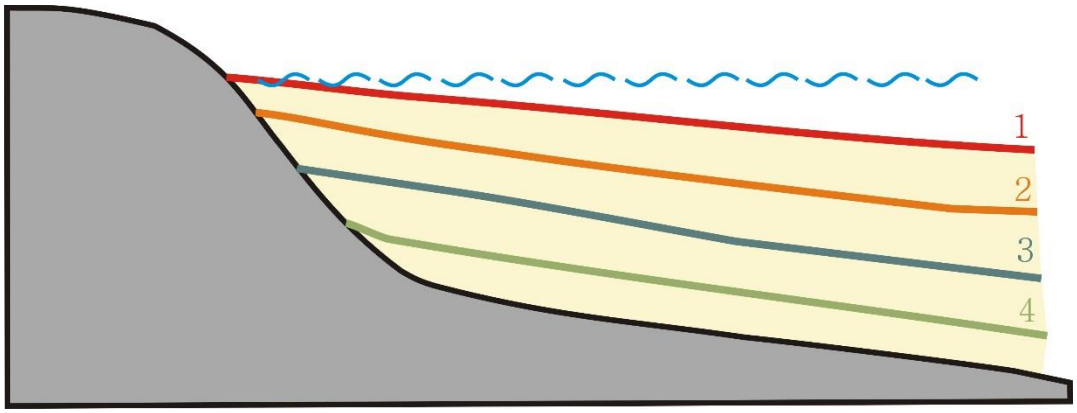

Fig. 1.3 Sediment architecture along the subsiding coast modified from Lamothe (2016). The latest to earliest transgressive layers (in colour) are marked in ascending order.

The relative sea-level change since the LGM in the East China seas including the Bohai Sea was commonly obtained based on the burial depth of multiple sea-level indicators and radiocarbon chronology. Zhao et al. (1979) proposed a sea-level rise curve in the East China seas which demonstrated a sea-level lowstand of -150 - -160 m from 20 to 15 ka BP, whilst other studies indicate that the sea-level lowstand reached ca. -120 m at 21-19 ka BP, broadly consistent with the global sea-level change (Liu, 2001; Liu et al., 2004). Afterwards, the sea-level rose rapidly and reached the highstand at ca. 6 ka (Zhao et al., 1979; Liu et al., 2004; Xue, 2014; Li et al., 2015). These earlier studies suggested the existence of a stepwise sea-level rise (Zhao et al., 1979; Liu, 2001; Liu et al., 2004). However, Xue (2014) challenged this model owing to unreliable radiocarbon dates substantially used for determination of the stepwise sea-level curve. The sea-level highstand was assumed to be higher than the present level (Zhao et al., 1979; Xu, 1994; Liu et al., 2004), but some latter studies revealed that there was no evidence of a higher sea-level than present (Xue, 2014; Li et al., 2015). The coastline changes in recent centuries were documented in historical records (e.g. Lin, 1991) and also interpreted from remote sensing for the last decades (Chen et al., 2010).

Based on the results of the past sea-level history, its sedimentary responses since the LGM have also been widely investigated in the Bohai Sea (e.g. Zhao et al., 1978; IOCAS, 1985). On the basis of studies of numerous cores from the modern alluvial plain, coastal plain and the offshore area, the pre-Holocene lacustrine and fluvial sediments were deposited in the Bohai area, as a consequence of relatively sea-level lowstand since the LGM (IOCAS, 1985). With the abrupt sea-level rise, the transgressive system tract was developed, overlying the regionally comparable organic-rich layer (Wang et al., 2004; Wang and Fan, 2005), which was regarded as the upper limit of the mean high tidal range (Li et al., 2015). The maximum Holocene sea flooding range, correlating to the sea-level highstand, was recognised by the down-core transgressive deposits in the Bohai coastal plains (IOCAS, 1985; Xue, 2009; Wang et al., 2015). However, for the post sea-level highstand period, the

reconstruction of precise sea-level fluctuations and the corresponding sedimentary processes in the Bohai Coast have not been widely explored.

1.3.2 Chronologies for the transgression-regression cycles in the literature

To constrain the timing of transgression and regression periods in the Bohai Coast, several dating methods have been applied to fluvial/lacustrine-marine sediments in the Bohai Sea. Palaeomagnetism was applied to restrict the chronological framework for the whole Quaternary. These studies showed that the main transgressive layers are above the Brunhes-Matuyama (B/M) boundary (ca. 781 ka), suggesting that the main transgressions in the Bohai Coast have occurred since the Middle Pleistocene (e.g. Yi et al., 2015; Liu et al., 2016; Yao et al., 2014; IOCAS, 1985). Some weak transgressions occurring at ca. 0.83 Ma have also been revealed using a core drilled in the modern Yellow River delta (Liu et al., 2016). For the three main transgressions in the Bohai Coast, radiocarbon dating has been widely carried out using organic materials from numerous coastal cores (e.g. IOCAS, 1985; Wang et al., 2004; Wang and Fan, 2005), oyster reefs (e.g. Wang et al., 2004; Wang and Fan, 2005), cheniers (e.g. Xu, 1994; Wang, 1996) and cultural layer (e.g. Shang et al., 2016). The radiocarbon dates showed that the latest transgression (T-1) is related to the sea-level rise since the last deglaciation, as most of the dated materials provide Holocene ages. Mollusc shells, foraminifera and peat were dated using the radiocarbon method to reconstruct the history of coastal deposition. The special distribution of the Holocene sea-level highstand in three bays was mapped by stratigraphic correlation and radiocarbon dates. Radiocarbon dating of the oyster reefs and cheniers provided evidence for sea-level oscillations during the middle and late Holocene after the sea-level highstand (Xu, 1994; Wang, 1996; Wang et al., 2004; Wang and Fan, 2005). The sea-level oscillations, corresponding to the shoreline migration in the Bohai Coast since the Middle Holocene, has been discussed by Xue (2009) who shows that the shoreline migration was dominated by river delta development. In addition, radiocarbon dating of mollusc shells from the ceramic sinker-rich layer has been applied to determine human activity and the position of the coastline at that time (Shang et al., 2016). The dating results show a consistency with the reference age of *ca.* 200 BC for one buried coin. The radiocarbon ages for the last transgression (T-1) are generally reliable when intact *in situ* material was employed for dating. However, to establish a chronological framework for coastal sediments, suitable material for radiocarbon dating can only be found sporadically. In consequence, the chronological framework of the sediment succession has not been continuously constrained, and therefore, the interpretation is still under discussion.

For the second transgression (T-2), radiocarbon dating was conducted on samples mainly obtained from coastal cores. According to the foraminifera assemblage, the second transgressive layer was

recognised, and mollusc shells or foraminifera were dated. Some radiocarbon dates yielded infinite results for the T-2 succession (Shang et al., in prep; Yi et al., 2013), indicating that the radiocarbon ages are minimum ages (> 43.5 cal ka BP). The finite ages are generally between ca. 30 and 45 cal ka BP (e.g. Liu et al., 2009, 2016), and are also close to the upper limit for the reliability of radiocarbon dating. In several studies, the radiocarbon dates close to the limit are proven to be underestimated (Pigati et al., 2007; Yi et al., 213; Long et al., 2015). These finite radiocarbon ages for the T-2 deposition, however, were previously used to determine the timing of the second transgression (Liu et al., 2009, 2016), and suggested its correlation with MIS 3. The earliest transgression (T-3) was then interpreted as a result of the sea-level highstand during MIS 5, based on the correlation between the transgression in the Bohai Sea and warm periods from the deep-sea oxygen isotope records (Liu et al., 2016; Spratt and Lisiecki, 2016).

With the development of optically stimulated luminescence (OSL) dating, the previous radiocarbon results have been re-evaluated. Since the dating limit has been largely extended by using OSL dating, the radiocarbon ages close to the upper limit are thought to be unreliable and most likely underestimate the true age. In the last 15 years, luminescence dating method has been significantly improved and widely applied to determine the age of various deposits along the Bohai Coast (e.g. aeolian deposits: Du et al., 2016; Xu et al., 2015, in press; coastal cores: Liu et al., 2016; Yi et al., 2013; Zhao et al., 2002; oyster reef: Zhang et al., 2007). To constrain the timing of the main transgressions, several coastal cores in the Bohai Coast have been dated using luminescence dating (Fig. 1.1).

The OSL samples collected from the latest transgression (T-1) were mainly dated using the quartz OSL signal. The quartz OSL ages range from 0.22±0.20 to 10.8±0.1 ka. The quartz OSL ages for T-1 are broadly consistent with the radiocarbon dates and considered to be reliable for core BH-2 (Yi et al., 2013). It is also concluded that the feldspar infrared stimulated luminescence (IRSL) ages agree with the radiocarbon age in the validation study using feldspar IRSL dating by Zhao et al. (2002). However, the bleaching characteristics for the quartz OSL signal were barely discussed, restricted to a comparison of OSL ages using different grain sizes solely for core sediments from the South Bohai Coast (Yi et al., 2013). As the transportation process and sources vary in different bays, it is mandatory to investigate the degree of bleaching for the luminescence signals prior to the application of OSL dating for the coastal deposits. It is possible that the luminescence signals are partially bleached in the water-lain environment and thus resulting in age overestimation (Wallinga, 2002. See details in Chapter 1.3).

The terrestrial layer R-1, i.e. between T-1 and T-2, was dated using quartz OSL, feldspar IRSL and post-IR IRSL signal (pIRIR) signals in previous studies. The quartz OSL ages for R-1 spread between 10.0±0.7 and 73.6±6.0 ka with the density peak centred between ca. 10 and 30 ka (Fig. 1.4). The quartz

OSL signal normally reaches saturation at ca. 150 Gy (Chapot et al., 2012). This is equivalent to ca. 40-80 ka for the Bohai sediments, if we use typical quartz environmental dose rates of 2-4 Gy/ka. Thus, the R-1 quartz ages are thought to be reliable. The feldspar IRSL ages ranging from 30 to 50 ka as determined by Zhao et al. (2002) for the R-1 deposition are well discussed and provide a reliable chronology. However, the pIRIR ages of 104±9 to 157±10 ka for R-1 for sediments from cores BT113 and BT114, as proposed by Chen et al. (2012), are significantly overestimated, most likely owing to insufficient bleaching (Fig. 1.4. See details in Chapter 1.3).

The quartz ages related to T-2, between 23±2 and 128±12 ka, were yielded from sediments from different cores. There are two main age clusters, correlating to MIS 4 and 5(Fig. 1.4). The feldspar pIRIR ages range from ca. 110 to 140 ka (Chen et al., 2012). For the underlying terrestrial layer R-2, the quartz OSL ages are between 60±6 and 144±14 ka, which correlates to MIS 6-4. The quartz OSL ages for the underlying T-3 range from 88±9 to 127±10 ka. In each case, the corresponding quartz equivalent doses are larger than 300 Gy (Yan et al., 2006; Chen et al., 2008; Liu et al., 2016). Chen et al. (2012) used K-feldspar pIRIR dating for the Pleistocene succession in cores BT113 and BT114 (Fig. 1.1). The ages are between 144±11 and 200±14 ka for the layers R-2 and R-3, respectively (Fig. 1.4).

Concerning the upper quartz OSL timing, most of the MIS 4 ages under discussion fulfil quality criteria and appear to be reliable. However, the high doses associated with quartz OSL ages of 90-130 ka for T-2, R-2 or T-3 from several cores (Chen et al., 2008; Liu et al., 2016; Yan et al., 2006; Yi et al., 2013), indicating that the quartz OSL signal is very likely beyond the saturation threshold, and hence the clustered quartz ages should be regarded as minimum ages. Thus, some of the old quartz OSL ages should be reassessed. Insufficient signal bleaching, which could result in age overestimation, is also a potential problem for the water-lain sediments. Most of the dating results for transgression and regression in the Bohai Coast were published without detailed information and sufficient discussion, hence it is challenging to evaluate their reliability. The quartz OSL ages determined using equivalent doses larger than 300 Gy very likely underestimate the timing of sedimentation (i.e. T-2 in Liu et al. (2016) and T-3 in Chen et al. (2008)).

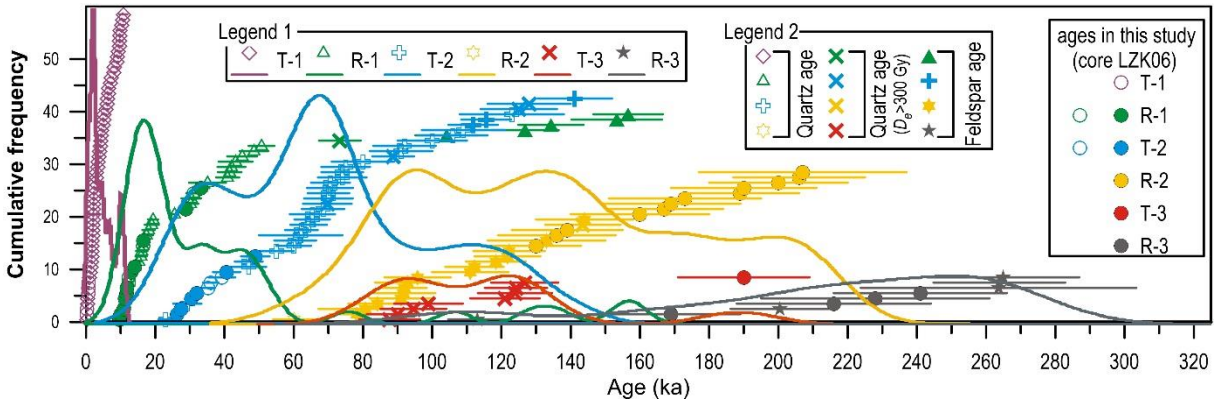

Fig. 1.4 Summary of the published OSL ages in the Bohai Coastal area. The dating results for core LZK06 are included for comparison (see details in Chapter 4.3). The luminescence ages are from the dated cores in drawn in Fig 1.1.

The pIRIR ages were determined using equivalent doses of ca. 300-700 Gy in Chen et al. (2012), is well below the saturation (ca. 1000 Gy) and therefore allowing to largely extend the dating range compared with the quartz OSL signal. However, anomalous fading and signal bleaching characteristics of the pIRIR signal were not investigated (pers. communication Chen, 2016). Although fading for pIRIR signal is relatively insignificant compared with the conventional IRSL signal (See details in Chapter 1.3), it could result in large underestimation for relatively old ages. As the dated materials are all from the water-lain environment, bleaching is also a crucial issue which should be explored. Indeed it has been demonstrated that the pIRIR signal bleaches much slower than the quartz OSL signal and the low temperature IRSL signals (Kars et al., 2014; Colarossi et al., 2015; Tsukamoto et al., 2017).

1.3.3 Development of optically stimulated luminescence (OSL) dating approaches

1.3.3.1 Brief principles of OSL dating

Luminescence dating is used to determine the time elapsed since the sediments were last exposed to daylight (optical) or heated (thermal). The luminescence signal stored in the minerals (mainly quartz and feldspar used) of the deposits can be either optically (optically stimulated luminescence (OSL); Huntley et al., 1985) or thermally (thermoluminescence (TL); Aitken, 1985) stimulated. Basically, during erosion and transportation, the light-sensitive signals in minerals are zeroed in response to daylight exposure. When the sediments are deposited and buried, the mineral grains are isolated from the sunlight, and the luminescence signal accumulates again mainly as a consequence of radioactivity from the surrounding materials. When using luminescence dating method, the total dose absorbed during the last burial period, known as equivalent dose, is determined in the laboratory. If the luminescence signal was not fully reset before deposition, the problem of insufficient bleaching will arise (Fig. 1.5). Assuming that the OSL signal has been properly bleached prior deposition, the burial time can be calculated by dividing the measured equivalent dose by the environmental dose rate, which is shown as

$$\text{Age (ka)} = \frac{D_e \text{ (Gy)}}{\dot{D} \text{ (Gy/ka)}} \quad (1.1)$$

where D_e is the equivalent dose and $\dot{D}$ is the environmental dose rate. In the laboratory, D_e for the separated mineral (quartz and feldspar) can be determined by quantifying the relationship between the natural and artificial luminescence intensities. To determine the environmental dose rate, the radioactivity of the surrounding sediments, i.e. the concentrations of the radionuclides, is measured by gamma spectrometry or neutron activation analysis. The cosmic dose rate is calculated according to the geographic position, elevation and depth (Prescott and Stephan, 1982). Furthermore, as water in the sediments will attenuate the ionising radiation, water content of the material should be carefully determined.

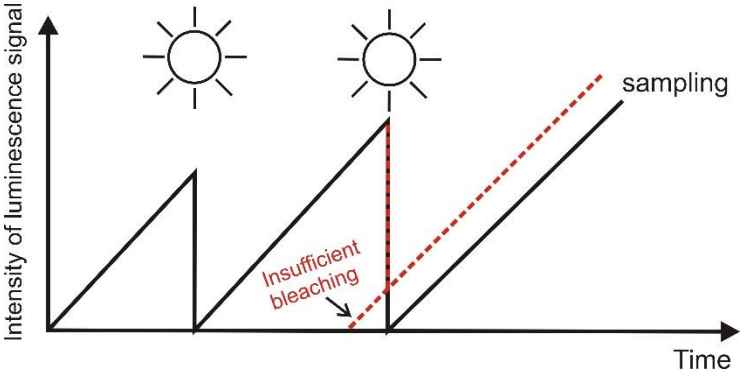

Fig. 1.5 Resetting and accumulation of luminescence signal (modified from Preusser et al., 2008).

1.3.3.2 Luminescence dating: main dosimeters and application

Quartz is the most favoured dosimeter applied in luminescence dating due to its abundance in the sediments. It is also advantageous for luminescence dating, in terms of rapid bleaching (Godfrey-Smith et al., 1988) and lack of anomalous fading. Under optical stimulation at 470 nm, the quartz OSL signal is generally detected using optical filters that pass wavelengths centred at 340 nm. The quartz OSL dating was previously reviewed by Preusser et al. (2008) and more recently by Wintle and Adamiec (2017). Since the single-aliquot regenerative-dose (SAR) protocol was developed (Murray and Wintle, 2000, 2003), quartz OSL dating has been widely applied for sediment dating from various environments (e.g. Fuchs and Owen, 2008; Lamothe, 2016; Long et al., 2012; Roberts, 2008; Wallinga, 2002). In the SAR protocol, a test dose is exploited to correct sensitivity changes following each regenerative dose, which is used to artificially simulate the natural signal growth in response to increasing absorbed dose. After fitting the dose response curve, the natural OSL intensity, which is measured prior to the regenerative procedure, is projected onto the dose response curve to retrieve the equivalent dose, representing the palaeo-dose accumulated during the last depositional period, and corresponding to

the time elapsed since the last exposure to daylight. Prior to the estimation of the equivalent dose, appropriateness of thermal treatment is determined by several performance tests, i.e. the preheat plateau, dose recovery and thermal transfer tests. Recycling ratio and recuperation are also crucial criteria to evaluate the applicability of the SAR protocol using specific thermal treatment (Wintle and Murray, 2006).

The upper dating limit for the conventional quartz OSL signal corresponds to a maximum dose of ca. 150 Gy, equivalent to 50-75 ka assuming an environmental dose rate of ca. 2-3 Gy/ka (Timar-Gabor et al., 2010). The maximum dating range is generally quantified utilizing the $2D_0$ value of the dose response curve, representing a saturation level of 86%, when the dose response curve is fitted using the single saturating exponential function (Wintle and Murray, 2006). Several young quartz samples were measured using the SAR protocol, showing that quartz OSL dating could yield reliable ages as young as few decades (Madsen and Murray, 2009). However, problems of quartz OSL dating should be addressed. First, for very young deposits, quartz OSL dating might be problematic, as the quartz grains are too dim to provide a high enough signal to noise ratio, especially when the environmental dose rate is low (Madsen and Murray, 2009). Second, some studies show discrepancies of luminescence characteristics for different grain-size fractions, as the fine grained quartz OSL ages are likely underestimated when D_e is larger than 100 Gy. This grain-size effect was reported and investigated recently using the reference age controlled Chinese loess samples (Timar-Gabor et al., in press and the references therein). Third, for samples from certain depositional environments, such as water-lain (fluvial, glaciofluvial and coastal, etc.) deposits, a potential problem of signal partial bleaching may arise due to the lack of daylight exposure during transportation and deposition. Insufficient bleaching could be assessed and minimised by applying the single-grain dating approach (Duller, 2008) and multiple age models (e.g. Galbraith et al., 1999). In addition, some volcanic quartz might also be affected by significant fading (Tsukamoto et al., 2007).

Potassium rich (K-) Feldspar is another luminescence dosimeter commonly used, as proposed initially by Hütt et al. (1988). During optical stimulation at 870 nm, the K-feldspar IRSL signal is generally detected using optical filters that pass wavelengths centred at ca. 390 nm. Feldspar IRSL dating is advantageous to extend the dating range as it has a much higher saturation dose than quartz OSL. Moreover, the IRSL signal is much brighter than the quartz OSL signal and thus ensures a detectable signal especially for young deposits (Preusser et al., 2008). After using the SAR protocol for IRSL dating by Wallinga et al. (2000), the conventional K-feldspar IRSL signal stimulated at 50 ^{o}C has been applied for dating (e.g. Frank et al., 2005; Wallinga et al., 2001; Frechen et al., 2009). However, there are several disadvantages associated with the use of feldspar IRSL dating. First the feldspar IRSL signal is less light sensitive than the quartz OSL signal, which results in a slower bleaching process during

daylight exposure (Godfrey-Smith, 1988). The discrepancy of the bleaching rate may result in the presence of a residual signal, which if not taken in account, may lead to age overestimation. Second, the spontaneous signal loss during the depositional period, i.e. anomalous fading (Aitken, 1985), has been observed, and can result to up to 30-40% age underestimation. Anomalous fading, as well as the existing correction and minimising approaches, are summarised below.

1.3.3.3 Anomalous fading of K-feldspar luminescence signal

Anomalous fading, caused by quantum-mechanical tunnelling (Visocekas, 1985), was generally observed for various feldspar minerals (Spooner, 1994), and could result in undesirable age underestimation in feldspar luminescence dating. Some experimental observations for anomalous fading for both the young and old faded feldspar luminescence ages were presented by Huntley and Lian (2006). It showed that anomalous fading is related to the source of feldspar minerals, concentrations of calcium and iron in the mineral, and received irradiation dose.

Fading correction models

To overcome anomalous fading for the conventional feldspar IRSL signal measured at 50°C (IR_{50}; hereafter the subscript refers to the IR stimulation temperature), several fading correction models have been proposed (Huntley and Lamothe, 2001; Kars et al., 2008; Lamothe et al., 2003; Wallinga et al., 2007). Prior to fading correction, the fading rate for feldspar need first to be quantified in the laboratory (e.g. Auclair et al., 2003; Huntley and Lamothe, 2001; Huntley, 2006), by measuring repeatedly the luminescence intensities after variable storage times. The fading rate, *g* value (Aitken, 1985. generally normalized to 2days, g_{2days}: %/decade) was fitted with the following logarithmic decay function:

$$I = I_c \left[1 - \frac{g}{100} \log_{10}\left(\frac{t}{t_c}\right)\right] \quad (1.2)$$

where I_c is the intensity at an arbitrary time t_c (Huntley and Lamothe, 2001. Fig. 1.6). However, the logarithmic decay cannot explain the experimental data for very short and long-term signal decay (Huntley and Lamothe, 2001). An alternative model to describe anomalous fading was proposed by Huntley (2006), which explained the tunnelling of electron to a nearby recombination centre using power-law decay (See equation 2.2). In contrast to the *g* value after Huntley and Lamothe (2001), the density of recombination centres, referred to as *ρ'*, is used to quantify anomalous fading (Fig. 1.6). The relationship between the laboratory determined fading rates, i.e. *g* and *ρ'*, and irradiation dose or the related natural intensity were investigated in several studies (Huntley and Lian, 2006; Lamothe et al., 2012; Li and Li, 2008; Li et al., 2016; Wallinga et al., 2007). The results showed that the fading rates are

probably irradiation dose dependent, which should be carefully investigated before the application of fading correction using different models.

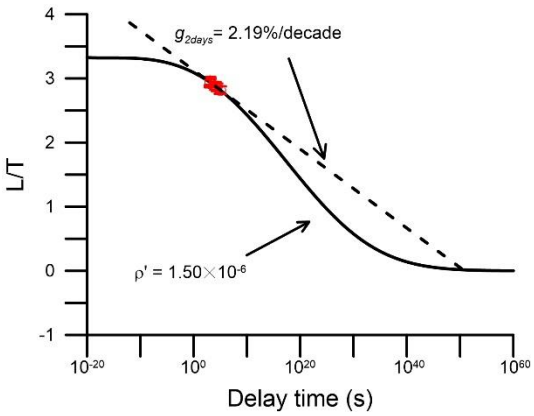

Fig. 1.6 Comparison of fittings between logarithm (dotted line) and power-law decay (solid line) of the luminescence signal. The red dots represent the measured luminescence intensities after arbitrary delay times. The sample (lab code: LUM1510) was collected from core Heidelberg UniNord1.

Several fading correction models have been proposed during the last two decades. Huntley and Lamothe (2001) presented a correction procedure applicable for the linear part of the signal growth, which could theoretically be used to correct fading for ages up to 20-50 ka. For the correction of older samples, a procedure was proposed by Lamothe et al. (2003), named the dose-rate correction method, which was considered to be applicable for ages falling into the linear part of the dose response curve to ages close to the signal saturation. This model is using a signal loss factor based upon the relationship between the laboratory and environmental dose rates (See equation 2.1). Wallinga et al. (2007) modified the fading correction model after Lamothe et al. (2003). The signal loss factor is used to correct the laboratory luminescence intensities, which are then used to construct a faded dose response curve. All the fading correction models mentioned above are according to the logarithm function-fitted fading rate, i.e. *g* value (Aitken, 1985). On the contrary, Kars et al. (2008) proposed a fading correction model according to the power-law decay of tunnelling in Huntley (2006), which is used to simulate the natural dose growth including fading. The measured, unfaded and simulated dose response curves can be constructed and the saturation level for the conventional feldspar IR_{50} signal was yielded (See details in Chapter 2.1). After a comparison between the natural and simulated saturation levels, the results showed that there is potential fading over-correction of ca. 10%. Although these fading correction models have existed for at least a decade, the reliability of these models has not been thoroughly investigated using independent age-controlled materials.

Athermally more stable feldspar luminescence signals

To minimise anomalous fading, some novel feldspar luminescence signals, which are more athermally stable, were investigated and proposed in the last decade. Thomsen et al. (2008) first compared the laboratory determined fading rates for the conventional IR_{50} and the post-IR IRSL (pIRIR) signal stimulated at higher temperatures, both detected through a blue filter pack. The results showed that

the fading rates for the pIRIR signals decreased with the increasing stimulation temperatures. Buylaert et al. (2009) further tested the $pIRIR_{225}$ signal measured following a preheat at 250 °C and an IR stimulation. The applicability of this approach was assessed in terms of dose recovery, recycling and recuperation. The much smaller fading rate compared to that for IR_{50} was promising to minimise fading. Furthermore, Thiel et al. (2011) found that the $pIRIR_{290}$ signal after preheating at 320 °C and IR_{50} stimulation was in saturation for loess samples in Austria. The $pIRIR_{290}$ signal was thus considered to be non-fading, and no need for fading correction. Fading rates of 1-1.5%/decade were actually measured but regarded as laboratory artefact from fading experiment and so negligible (Buylaert et al., 2012). In the meantime, the multiple-elevated temperature (MET) post-IR IRSL signals were investigated by Li and Li (2011). Using the SAR protocol (Murray and Wintle, 2000), a set of IR stimulation at 50, 100, 150, 200, 250 °C after preheating at 300 °C was conducted to investigate the characteristics for all the signals in terms of fading, bleaching and age. The ages from the MET-pIRIR signal stimulated at 200 and 250 °C (last study showing those at 250 and 300 °C after preheating at 320 °C. Li and Li, 2012) agreed with the independent chronology, and therefore, these MET-pIRIR signals were also considered to be non-fading.

Both the two-step and MET-pIRIR signals show that these feldspar luminescence signal tends to be more athermally stable with increased stimulation temperature, as shown by the generally decreased trend of fading rate (Li and Li, 2011; Zhang et al., 2015). It is promising to minimise fading to yield a non-fading signal, for which no fading correction is needed. During the last decade, the $pIRIR_{290}$ and MET-$pIRIR_{250}$ signals have been widely applied to date the sediments from various environments (e.g. Buylaert et al., 2013; Li and Li, 2012; Lowick et al., 2012; Schmidt et al., 2014). However, in several studies non-negligible fading was observed for the $pIRIR_{290}$ signal, which requires further investigation (Li et al., 2014 and the references therein).

Furthermore, more and more studies have shown that the pIRIR signal stimulated at higher temperature is more difficult to bleach (e.g. Li and Li, 2011; Kars et al., 2014; Colarossi et al., 2015; Tsukamoto et al., 2017). The slow bleaching rate increases the risk of insufficient signal resetting and significant residual signal, which in turn may yield to age significantly overestimated. Investigations in the suitability of the $pIRIR_{290}$ signal to date several modern sediments were carried out, showing that the residual doses dominated the laboratory determined equivalent dose, and yielded large age overestimates (e.g. Buylaert et al., 2011; Alexanderson and Murray, 2012). Therefore, it should be avoided to apply the high temperature stimulated pIRIR luminescence dating for young deposits. In order to avoid large residual doses and permit the dating of young deposits, pIRIR protocols with low preheat and stimulation temperatures were later developed. Reimann et al. (2011) proved that the two-step pIRIR dating results measured at 180 °C ($pIRIR_{180}$) are in agreement with quartz ages and radiocarbon dates, after subtracting the residual dose. Madsen et al. (2011) and Reimann and

Tsukamoto (2012) proposed the pIRIR protocol with preheating at 180 °C and pIRIR stimulation at 150 °C ($pIRIR_{150}$) to date young coastal sand deposits. Fu and Li (2013) modified the MET-pIRIR protocol with low stimulation temperatures up to 170 °C for dating Holocene samples. The low temperature stimulated pIRIR signals have been applied successfully for the Holocene aeolian deposits, lacustrine sediments and marine deposits using coarse-grained feldspar and polymineral fine-grained materials (e.g. Long et al., 2014, 2015; Yang et al., 2015).

An alternative athermally stable signal, known as the pulsed IRSL signal, was investigated during the last decade (Jain and Ankjærgaard, 2011; Jain et al., 2015; Tsukamoto et al., 2006, 2017). The pulsed IRSL signal was previously reported to be more stable than the continuous wave IR signal (Sanderson and Clark, 1994). The pulsed IR_{50} signal is advantageous to improve both the bleachability and athermal stability compared with the elevated temperature pIRIR signals. Recently, Tsukamoto et al. (2017) thoroughly investigated the pulsed IR_{50} signal from three fluvial samples with reference ages, in terms of bleaching rate, anomalous fading and thermal stability. Comparisons with the two-step $pIRIR_{225}$ and $pIRIR_{290}$ signals were systematically conducted. The results showed that bleaching rate for the pulsed IR_{50} signal was similar with the CW IR_{50} signal. It is also as stable as the pIRIR signals. However, this signal has not been widely applied for dating the Quaternary sediments.

According to the distinguishable bleaching rate for the feldspar luminescence signals stimulated at various temperatures, if the fast-bleached and slow-bleached signals yield consistent ages, the fast-bleached signal is considered to be well bleached during the last depositional event. Consequently, recent studies compared the ages obtained from multiple signals to evaluate the degree of bleaching for the luminescence signal (Murray et al., 2012; Reimann et al., 2015; Yang et al., 2015).

1.4 Outline of the thesis

The thesis consists of six chapters. In the Chapter 1, I have broadly presented the objectives, study area and and studied materials, and the current state of knowledge. The coming four chapters (2-5) include five manuscripts which have been published, submitted or will be submitted to peer-reviewed journals.

Chapter 2 contains two manuscripts, presenting the validation of fading correction methods for K-feldspar IR and pIRIR ages beyond the linear part of dose response curve. In Chapter 2.1, the fluvial deposits collected from core Heidelberg UniNord1 in the Heidelberg Basin are dated using the K-feldspar $pIRIR_{225}$ and $pIRIR_{290}$ protocols. Two fading correction models are used to correct the apparent feldspar ages. The fading corrected ages are compared with the regional biostratigraphy from pollen analysis and palaeomagnetic results, which provide a reference age control, in order to assess the reliability of different fading correction models. Chapter 2.2 further tests the reliability of fading correction models for feldspar samples below and near saturation using Chinese loess-palaeosol

sequences. The reference ages and environmental dose rates for the Chinese loess are first used to estimate the expected accumulated doses, which are then used to construct the natural dose response curve for the three feldspar luminescence signals, (IR_{50} (pre-$pIRIR_{225}$), $pIRIR_{225}$ and pulsed IR_{50}). The simulated dose response curve after fading correction is compared with the natural one to evaluate the appropriateness of the fading correction models. The manuscript associated to Chapter 2.1 is published in journal *Boreas*. The content in Chapter 2.2 is submitted to the journal *Radiation Measurements*.

In Chapter 3, the chronology of a sand dune in the Lower Liao Plain is well established using quartz optically stimulated luminescence (OSL) dating method. As the sand dune is situated in the range of the Holocene maximum sea flooding, the relationship between sand accumulation and sea-level change is discussed to understand whether the dune developed close to the coast or further inland In addition, the suitability of potassium feldspar post-infrared (IR) infrared stimulated luminescence (IRSL) dating protocol at low stimulation temperature (150°C) for the young sand sediments is investigated. The driving factors of sand accumulation are finally discussed in aspects of climate change and human activity. The content of Chapter 3 is published in the journal *Geochronometria*.

Chapter 4 represents the reconstruction of accumulation history during the Holocene for the North Bohai Coast China according to a refined chronology by luminescence dating. First, the degree of bleaching for multiple luminescence signals, i.e. the quartz OSL, K-feldspar IR_{50}, $pIRIR_{150}$ and $pIRIR_{225}$ signals is fully investigated by comparing the ages from 1) different luminescence signals and radiocarbon dating, and 2) different aliquot sizes for quartz. The age comparison is also to performed to validate the applicability of K-feldspar pIRIR dating for the pre-Holocene Bohai samples. Subsequently, the chronology of sedimentation documented in core LZK06 since the late Pleistocene is established using the most reliable luminescence ages. The stratigraphic correlation in the North Bohai Coast is conducted using both the lithological and age constraints from the studied core LZK06 and the other three reference cores. The variation of sediment accumulation during the Holocene is recognised by estimating the sediment increments according to the luminescence chronology and historical shoreline migrations, for which the driving factors are also discussed. The manuscript on the basis of this study is published in *Journal of Asian Earth Sciences*.

Following the evaluation of the existing fading correction models in Chapter 2, as well as the validation of feldspar pIRIR dating for the Bohai samples in Chapter 4, the application of feldspar luminescence dating for the relatively old samples in core LZK06 is presented in Chapter 5. The motivation of this study is to investigate the timing of the three transgressions since the Middle Pleistocene in the Bohai Coast. The relationship between anomalous fading and signal saturation level for both $pIRIR_{225}$ and $pIRIR_{290}$ is discussed. The bleaching characteristics for these two signals are

investigated by age comparison. The reliable feldspar pIRIR ages, in conjunction with the quartz OSL ages presented in Chapter 4, are used to construct the age-depth model. Timing of the three transgressions is determined and its correlation to the driving factors are discussed.

Chapter 6 comprises the main conclusions drawn from all the studies included in the thesis and the outlook for further research. Main contributions from the five manuscripts in terms of Bohai Sea coast evolution and methodology of luminescence dating are outlined.

References

Aitken, M.J., 1985. Thermoluminescence dating. Academic Press, London, UK.

Alexanderson, H., Murray, A.S., 2012. Luminescence signals from modern sediments in a glaciated bay, NW Svalbard. Quaternary Geochronology 10, 250-256.

Allen, M.B., Macdonald, D.I.M., Zhao, X., Vincent, S.J., Brouet-Menzies, C., 1997. Early Cenozoic two-phase extension and late Cenozoic thermal subsidence and inversion of the Bohai Basin, northern China. Marine and Petroleum Geology 14, 951-972.

Bradley, S.L., Milne, G.A., Horton, B.P., Zong, Y., 2016. Modelling sea level data from China and Malay-Thailand to estimate Holocene ice-volume equivalent sea level change. Quaternary Science Reviews 137, 54-68.

Bureau, L.G., 1983. Quaternary in Liaoning. Geology Press, Beijing, China.

Buylaert, J.P., Jain, M., Murray, A.S., Thomsen, K.J., Thiel, C., Sohbati, R., 2012. A robust feldspar luminescence dating method for Middle and Late Pleistocene sediments. Boreas 41, 435-451.

Buylaert, J.P., Murray, A.S., Gebhardt, A.C., Sohbati, R., Ohlendorf, C., Thiel, C., Wastegård, S., Zolitschka, B., 2013. Luminescence dating of the PASADO core 5022-1D from Laguna Potrok Aike (Argentina) using IRSL signals from feldspar. Quaternary Science Reviews 71, 70-80.

Buylaert, J.P., Murray, A.S., Thomsen, K.J., Jain, M., 2009. Testing the potential of an elevated temperature IRSL signal from K-feldspar. Radiation Measurements 44, 560-565.

Buylaert, J.P., Thiel, C., Murray, A., Vandenberghe, D., Yi, S., Lu, H., 2011. IRSL and post-IR IRSL residual doses recorded in modern dust samples from the Chinese Loess Plateau. Geochronometria 38.

Chen, Y., Fang, G., Ni, J., Hu, K., 2010. Research on century's changes of coastlines of Liaohe Estuary. Journal of marine sciences 28, 14-21. (in Chinese with English Abstract)

Chen, Y., Li, Z., Shao, Y., Wang, Z., Gao, W., Yang, X., 2008. Study on the Quaternary chronostratigraphic section in Tianjin Area. Seismology and Geology 30, 483-493. (in Chinese with English Abstract)

Chen, Y., Wang, H., Pei, Y., Tian, L., Li, J., Shang, Z., 2012. Division and its geological significance of the late Quaternary marine sedimentary beds in the west coast of Bohai Bay, China. Journal of Jilin University (Earth Science Edition) 42, 747-759. (in Chinese with English Abstract)

Clark, P.U., Dyke, A.S., Shakun, J.D., Carlson, A.E., Clark, J., Wohlfarth, B., Mitrovica, J.X., Hostetler, S.W., McCabe, A.M., 2009. The Last Glacial Maximum. Science 325, 710-714.

Colarossi, D., Duller, G.A.T., Roberts, H.M., Tooth, S., Lyons, R., 2015. Comparison of paired quartz OSL and feldspar post-IR IRSL dose distributions in poorly bleached fluvial sediments from South Africa. Quaternary Geochronology 30, 233-238.

Department of Marine Geology, T.U., 1980. Identification of marine and terrestrial strata. Science Press, Beijing, China.

Du, S., Li, B., Chen, M., Xiang, R., Niu, D., Si, Y., 2016. Paleotempestology evidence recorded by aeolian deposition in the Bohai Sea coastal zone during the last interglacial period. Marine Geology 379, 78-83.

Duller, G.A., 2008. Single-grain optical dating of Quaternary sediments: why aliquot size matters in luminescence dating. Boreas 37, 589-612.

Frechen, M., Kehl, M., Rolf, C., Sarvati, R., Skowronek, A., 2009. Loess chronology of the Caspian Lowland in Northern Iran. Quaternary International 198, 220-233.

Fu, X., Li, S., 2013. A modified multi-elevated-temperature post-IR IRSL protocol for dating Holocene sediments using K-feldspar. Quaternary Geochronology 17, 44-45.

Fuchs, M., Owen, L.A., 2008. Luminescence dating of glacial and associated sediments: review, recommendations and future directions. Boreas 37, 636-659.

Galbraith, R.F., Roberts, R.G., Laslett, G.M., Yoshida, H., Olley, J.M., 1999. Optical dating of single and multiple grains of quartz from Jinmium Rock Shelter, northern Australia: Part I, experimental design and statistical models. Archaeometry 41, 339-364.

Godfrey-Smith, D.I., Huntley, D.J., Chen, W.H., 1988. Optical dating studies of quartz and feldspar sediment extracts. Quaternary Science Reviews 7, 373-380.

Han, D., 2001. Geochemistry of Core E in the Laizhou Bay since late stage of Middle Pleistocene. Acta Oceanologica Sinica 23, 79-85. (in Chinese with English Abstract)

He, Q., 2006. Marine Sedimentary Geology of China. Ocean Press, Beijing, China.

Huntley, D.J., 2006. An explanation of the power-law decay of luminescence. Journal of Physics: Condensed Matter 18, 1359-1365.

Huntley, D.J., Godfrey-Smith, D.I., Thewalt, M.L.W., 1985. Optical dating of sediments. Nature 313, 105-107.

Huntley, D.J., Lamothe, M., 2001. Ubiquity of anomalous fading in K-feldspars and the measurement and correction for it in optical dating. Canadian Journal of Earth Sciences 38, 1093-1106.

Huntley, D.J., Lian, O.B., 2006. Some observations on tunnelling of trapped electrons in feldspars and their implications for optical dating. Quaternary Science Reviews 25, 2503-2512.

Hütt, G., Jaek, I., Tchonka, J., 1988. Optical dating: K-feldspars optical response stimulation spectra. Quaternary Science Reviews 7, 381-385.

IOCAS, 1985. Geology of the Bohai Bea. Science Press, Beijing. (in Chinese with English Abstract)

IPCC, 2014. Climate change 2014: Impacts, adaptation, and vulnerability, in: Field, C.B., Barros, V.R. (Eds.), New York, USA.

Jain, M., Ankjærgaard, C., 2011. Towards a non-fading signal in feldspar: insight into charge transport and tunnelling from time-resolved optically stimulated luminescence. Radiation Measurements 46.

Jain, M., Buylaert, J.P., Thomsen, K.J., Murray, A., 2015. Further investigation on 'non-fading' in K-feldspar. Quaternary International 362.

Kars, R.H., Reimann, T., Ankjaergaard, C., Wallinga, J., 2014. Bleaching of the post-IR IRSL signal: new insights for feldspar luminescence dating. Boreas 43, 780-791.

Kars, R.H., Wallinga, J., Cohen, K.M., 2008. A new approach towards anomalous fading correction for feldspar IRSL dating — tests on samples in field saturation. Radiation Measurements 43, 786-790.

Lambeck, K., Chappell, J., 2001. Sea-level change though the last glacial cycle. Science 292, 679-686.

Lambeck, K., Rouby, H., Purcell, A., Sun, Y., Sambridge, M., 2014. Sea level and global ice volumes from the Last Glacial Maximum to the Holocene. Proceedings of the National Academy of Sciences of the United States of America 111, 15296-15303.

Lamothe, M., 2016. Luminescence dating of interglacial coastal depositional systems: Recent developments and future avenues of research. Quaternary Science Reviews 146, 1-27.

Lamothe, M., Auclair, M., Hamzaoui, C., Huot, S., 2003. Towards a prediction of long-term anomalous fading of feldspar IRSL. Radiation Measurements 37, 493-498.

Lamothe, M., Barré, M., Huot, S., Ouimet, S., 2012. Natural luminescence and anomalous fading in K-feldspar. Radiation Measurements 47, 682-687.

Li, B., Jacobs, Z., Roberts, R., Li, S.-H., 2014. Review and assessment of the potential of post-IR IRSL dating methods to circumvent the problem of anomalous fading in feldspar luminescence. Geochronometria 41, 178-201.

Li, B., Li, S.-H., 2008. Investigations of the dose-dependent anomalous fading rate of feldspar from sediments. Journal of Physics D: Applied Physics 41, 225502.

Li, B., Li, S.-H., 2011. Luminescence dating of K-feldspar from sediments: A protocol without anomalous fading correction. Quaternary Geochronology 6, 468-479.

Li, B., Li, S., 2012. Luminescence dating of Chinese loess beyond 130 ka using the nno-fading signal from K-feldspar. Quaternary Geochronology 10, 24-31.

Li, B., Roberts, R.G., Brumm, A., Guo, Y., Hakim, B., Ramli, M., Aubert, M., Gruen, R., Zhao, J. X., Saptomo, E.W., 2016. IRSL dating of fast-fading sanidine feldspars from Sulawest, Indonesia. Ancient TL 34, 1-13.

Li, J., Shang, Z., Wang, F., Chen, Y., Tian, L., Jiang, X., Wang, H., 2015. Holocene sea level change on the west coast of the Bohai Bay. Quaternary Science 35, 243-264. (in Chinese with English Abstract)

Lin, T., 1991. Coastline change in the Liaodong Bay. Collections of Essays on Chinese Historical Geography 2, 1-13.

Liu, J., Saito, Y., Wang, H., Zhou, L., Yang, Z., 2009. Stratigraphic development during the Late Pleistocene and Holocene offshore of the Yellow River delta, Bohai Sea. Journal of Asian Earth Sciences 36, 318-331.

Liu, J., Wang, H., Wang, F., Qiu, J., Saito, Y., Lu, J., Zhou, L., Xu, G., Du, X., Chen, Q., 2016. Sedimentary evolution during the last ~1.9Ma near the western margin of the modern Bohai Sea. Palaeogeography, Palaeoclimatology, Palaeoecology 451, 84-96.

Liu, J.P., Milliman, J.D., Gao, S., Cheng, P., 2004. Holocene development of the Yellow River's subaqueous delta, North Yellow Sea. Marine Geology 209, 45-67.

Long, H., Haberzettl, T., Tsukamoto, S., Shen, J., Kasper, T., Daut, G., Zhu, L., Mäusbacher, R., Frechen, M., 2015a. Luminescence dating of lacustrine sediments from Tangra Yumco (southern Tibetan Plateau) using post-IR IRSL signals from polymineral grains. Boreas 44, 139-152.

Long, H., Lai, Z., Frenzel, P., Fuchs, M., Haberzettl, T., 2012. Holocene moist period recorded by the chronostratigraphy of a lake sedimentary sequence from Lake Tangra Yumco on the south Tibetan Plateau. Quaternary Geochronology 10, 136-142.

Long, H., Shen, J., Tsukamoto, S., Chen, J., Yang, L., Frechen, M., 2014. Dry early Holocene revealed by sand dune accumulation chronology in Bayanbulak Basin (Xinjiang, NW China). The Holocene 24, 614-626.

Long, H., Shen, J., Wang, Y., Gao, L., Frechen, M., 2015b. High-resolution OSL dating of a late Quaternary sequence from Xingkai Lake (NE Asia): Chronological challenge of the 'MIS 3a Mega-paleolake' hypothesis in China. Earth and Planetary Science Letters 428, 281-292.

Lowick, S.E., Trauerstein, M., Preusser, F., 2012. Testing the application of post-IR IRSL dating to fine grain waterlain sediments. Quaternary Geochronology 8, 33-40.

Madsen, A., Buylaert, J.-P., Murray, A., 2011. Luminescence dating of young coastal deposits from New Zealand using feldspar. Geochronometria 38, 378-390.

Madsen, A.T., Murray, A.S., 2009. Optically stimulated luminescence dating of young sediments: A review. Geomorphology 109, 3-16.

Murray-Wallace, C.V., Woodroffe, C.D., 2014. Quaternary sea-level changes: A global perspective. Cambridge University Press, New York, USA.

Murray, A.S., Thomsen, K.J., Masuda, N., Buylaert, J.P., Jain, M., 2012. Identifying well-bleached quartz using the different bleaching rates of quartz and feldspar luminescence signals. Radiation Measurements 47, 688-695.

Murray, A.S., Wintle, A.G., 2000. Luminescence dating of quartz using an improved single-aliquot regenerative-dose protocol. Radiation Measurements 32, 57-73.

Murray, A.S., Wintle, A.G., 2003. The single aliquot regenerative dose protocol: potential for improvements in reliability. Radiation Measurements 37, 377-381.

Pico, T., Mitrovica, J.X., Ferrier, K.L., Braun, J., 2016. Global ice volume during MIS 3 inferred from a sea-level analysis of sedimentary core records in the Yellow River Delta. Quaternary Science Reviews 152, 72-79.

Pigati, J.S., Quade, J., Wilson, J., Jull, A.J.T., Lifton, N.A., 2007. Development of low-background vacuum extraction and graphitization systems for 14C dating of old (40-60 ka) samples. Quaternary International 166, 4-14.

Preusser, F., Andersen, B.G., Denton, G., Schlüchter, C., 2005. Luminescence chronology of Later Pleistocene glacial deposits in North Westland, New Zealand. Quaternary Science Reviews 24, 2207-2227.

Preusser, F., Degering, D., Fuchs, M., Hilgers, A., Kadereit, A., Klasen, N., Krbetschek, M.R., Richter, D., Spencer, J., 2008. Luminescence dating: basics, methods and application. E&G Quaternary Science 57, 95-149.

Reimann, T., Notenboom, P.D., De Schipper, M.A., Wallinga, J., 2015. Testing for sufficient signal resetting during sediment transport using a polymineral multiple-signal luminescence approach. Quaternary Geochronology 25, 26-36.

Reimann, T., Tsukamoto, S., 2012. Dating the recent past (<500 years) by post-IR IRSL feldspar – Examples from the North Sea and Baltic Sea coast. Quaternary Geochronology 10, 180-187.

Reimann, T., Tsukamoto, S., Naumann, M., Frechen, M., 2011. The potential of using K-rich feldspars for optical dating of young coastal sediments – A test case from Darss-Zingst peninsula (southern Baltic Sea coast). Quaternary Geochronology 6, 207-222.

Roberts, H.M., 2008. The development and application of luminescence dating to loess deposits: a perspective on the past, present and future. Boreas 37, 483-507.

Sanderson, D.C.W., Clark, R.J., 1994. Pulsed photostimulated luminescence of alkali feldspar. Radiation Measurements 23, 633-639.

Schmidt, E.D., Tsukamoto, S., Frechen, M., Murray, A., 2014. Elevated temperature IRSL dating of loess sections in the East Eifel regions of Germany. Quaternary International 334-335, 141-154.

Shang, Z., Wang, F., Li, J., Marshall, W.A., Chen, Y., Jiang, X., Tian, L., Wang, H., 2016. New residence times of the Holocene reworked shells on the west coast of Bohai Bay, China. Journal of Asian Earth Sciences 115, 492-506.

Shi, X., Yao, Z., Liu, Q., Larrasoaña, J.C., Bai, Y., Liu, Y., Liu, J., Cao, P., Li, X., Qiao, S., Wang, K., Fang, X., Xu, T., 2016. Sedimentary architecture of the Bohai Sea China over the last 1 Ma and implications for sea-level changes. Earth and Planetary Science Letters 451, 10-21.

Spooner, N.A., 1994. The anomalous fading of infrared-stimulated luminescence from feldspars. Radiation Measurements 23, 625-632.

Spratt, R.M., Lisiecki, L.E., 2016. A late Pleistocene sea level stack. Climate of the past 12, 1079-1092.

Thiel, C., Buylaert, J.-P., Murray, A., Terhorst, B., Hofer, I., Tsukamoto, S., Frechen, M., 2011. Luminescence dating of the Stratzing loess profile (Austria) – Testing the potential of an elevated temperature post-IR IRSL protocol. Quaternary International 234, 23-31.

Thomsen, K.J., Murray, A.S., Jain, M., Bøtter-Jensen, L., 2008. Laboratory fading rates of various luminescence signals from feldspar-rich sediment extracts. Radiation Measurements 43, 1474-1486.

Timar-Gabor, A., Buylaert, J.P., Guralnik, B., Trandafir-Antohi, O., Constantin, D., Anechitei-Deacu, V., Jain, M., Murray, A., Porat, N., Hao, Q., Wintle, A.G., in press. On the importance of grain size in luminescence dating using quartz. Radiation Measurements.

Timar-Gabor, A., Vandenberghe, D., Panaiotu, E.C., Panaiotu, C.G., Necula, C., Cosma, C., van den haute, P., 2010. Optical dating of Romanian loess using fine-grained quartz. Quaternary Geochronology 5, 143-148.

Tsukamoto, S., Denby, P.M., Murray, A.S., Bøtter-Jensen, L., 2006. Time-resolved luminescence from feldspars: New insight into fading. Radiation Measurements 41, 790-795.

Tsukamoto, S., Kondo, R., Lauer, T., Jain, M., 2017. Pulsed IRSL: A stable and fast bleaching luminescence signal from feldspar for dating Quaternary sediments. Quaternary Geochronology 41, 26-36.

Tsukamoto, S., Murray, A., Huot, S., Watanuki, T., Denby, P.M., Boetter-Jensen, L., 2007. Luminescence property of volcanic quartz and the use of red isothermal TL for dating tephras. Radiation Measurements 42, 190-197.

Visocekas, R., 1985. Tunnelling radiative recombination in labradorite: its association with anomalous fading of thermoluminescence. Nuclear Tracks and Radiation Measurements 10, 521-529.

Wallinga, J., 2002. Optically stimulated luminescence dating of fluvial deposits: a review. Boreas 31, 303-322.

Wallinga, J., Bos, A.J.J., Dorenbos, P., Murray, A.S., Schokker, J., 2007. A test case for anomalous fading correction in IRSL dating. Quaternary Geochronology 2, 216-221.

Wallinga, J., Murray, A., Duller, G.A., Törnqvist, T.E., 2001. Testing optically stimulated luminescence dating of sand-sized quartz and feldspar from fluvial deposits. Earth and Planetary Science Letters 193, 617-630.

Wallinga, J., Murray, A., Wintle, A.G., 2000. The single-aliquot regenerative-dose (SAR) protocol applied to coarse-grain feldspar. Radiation Measurements 32, 529-533.

Wang, F., Li, J., Chen, Y., Fang, J., Zong, Y., Shang, Z., Wang, H., 2015. The record of mid-Holocene maximum landward marine transgression in the west coast of Bohai Bay, China. Marine Geology 359, 89-95.

Wang, H., 1996. Palaeoenvironment of the Holocene cheniers and oyster reefs in the Bohai Bay, China. Quaternary Research 1, 71-79. (in Chinese with English Abstract)

Wang, H., Fan, C., 2005. The 14C database (II) on the circum-Bohai sea-coast. Quaternary Science 25, 141-156. (in Chinese with English Abstract)

Wang, H., Li, F., Fan, C., Frechen, M., van Strydonck, M., Fei, D., Wang, Y., 2004. The 14C database (I) on the circum-Bohai sea-coast. Quaternary Science 24, 601-613. (in Chinese with English Abstract)

Wang, H., Tian, G.Q., 1999. The neotectonic settings of late Quaternary transgression on the eastern coastal plain of China. Journal of Geomachanics 5, 41-48. (in Chinese with English Abstract)

Wang, Q., Li, F., Li, Y., 1986. Shoreline changes in west-southern coastal plain of the Bohai Sea since 150 ka, in: Qin, Y., Zhao, S. (Eds.), Late Quaternary sea-level changes, Beijing, China, pp. 62-71. (in Chinese with English Abstract)

Wintle, A.G., Adamiec, G., 2017. Optically stimulated luminescence signals from quartz: A review. Radiation Measurements 98, 10-33.

Wintle, A.G., Murray, A.S., 2006. A review of quartz optically stimulated luminescence characteristics and their relevance in single-aliquot regeneration dating protocols. Radiation Measurements 41, 369-391.

Xu, J., 1994. Changes of sea level and chenier along Huanghua beach of the Bohai Bay. Acta Oceanologica Sinica 16, 68-77. (in Chinese with English Abstract)

Xu, Q., Yang, J., Yuan, G., Chu, Z., Zhang, Z., 2015a. Stratigraphic sequence and episodes of the ancient Huanghe Delta along the southwestern Bohai Bay since the LGM. Marine Geology 367, 69-82.

Xu, S., Ding, X., Yu, L., Ni, Z., 2015b. Palaeoclimatic implications of aeolian sediments on the Miaodao Islands, Bohai Sea, East China, based on OSL dating and proxies. Aeolian Research 19, 259-266.

Xu, S., Kong, F., Jia, G., Miao, X., Ding, X., in press. An integrated OSL chronology, sedimentary and geochemical approach to loess deposits from Tuoji Island, Shandong Province: Implications for the late Quaternary palaeoenvironment in East China. Aeolian Research.

Xue, C., 2009. Historical changes of coastline on West and South Coast of Bohai Sea since 7000 a B.P. Scientia Geographica sinica 29, 217-222.

Xue, C., 2014. Missing evidence for stepwise postglacial sea level rise and an approach to more precise determination of former sea levels on East China Sea Shelf. Marine Geology 348, 52-62.

Yan, Y., Wang, H., Li, F., Li, J., Zhao, C., Lin, F., 2006. Sedimentary environment and sea-level fluctuations revealed by Borehole BQ1 on the west coast of the Bohai Bay. China Geological Bulletin 25, 264-279. (in Chinese with English Abstract)

Yang, L., Long, H., Yi, L., Li, P., Wang, Y., Gao, L., Shen, J., 2015. Luminescence dating of marine sediments from the Sea of Japan using quartz OSL and polymineral pIRIR signals of fine grains. Quaternary Geochronology 30, 257-263.

Yang, Z., Lin, H.M., 1991. Quaternary processes in eastern China and their international correlation. Geological Publishing House, Beijing, China.

Yao, J., Yu, H., Xu, X., Yi, L., Su, Q., 2010. Deposition characteristics in brine aquifers and brine formation in Laizhou Bay area. Advances in Marine Science 28, 473-477. (in Chinese with English Abstract)

Yao, Z., Shi, X., Liu, Q., Liu, Y., Larrasoaña, J.C., Liu, J., Ge, S., Wang, K., Qiao, S., Li, X., Shi, F., Fang, X., Yu, Y., Yang, G., Duan, Z., 2014. Paleomagnetic and astronomical dating of sediment core BH08 from the Bohai Sea, China: Implications for glacial-interglacial sedimentation. Palaeogeography, Palaeoclimatology, Palaeoecology 393, 90-101.

Yi, L., Lai, Z., Yu, H., Xu, X., Su, Q., Yao, J., Wang, X., Shi, X., 2013. Chronologies of sedimentary changes in the south Bohai Sea, China: constraints from luminescence and radiocarbon dating. Boreas 42, 267-284.

Yi, L., Yu, H.-J., Ortiz, J.D., Xu, X.-Y., Chen, S.-L., Ge, J.-Y., Hao, Q.-Z., Yao, J., Shi, X.-F., Peng, S.-Z., 2012. Late Quaternary linkage of sedimentary records to three astronomical rhythms and the Asian monsoon, inferred from a coastal borehole in the south Bohai Sea, China. Palaeogeography, Palaeoclimatology, Palaeoecology 329-330, 101-117.

Yokoyama, Y., Lambeck, K., Deckker, P.D., Johnston, P., Fifield, L.K., 2000. Timing of the Last Glacial Maximum from observed sea-level minima. Nature 406, 713-716.

Zhang, J., Fan, C., Wang, H., Zhou, L.P., 2007. Chronology of an oyster reef on the coast of Bohai Bay, China: Constraints from optical dating using different luminescence signals from fine quartz and polymineral fine grains of coastal sediments. Quaternary Geochronology 2, 71-76.

Zhang, J., Tsukamoto, S., Nottebaum, V., Lehmkuhl, F., Frechen, M., 2015. De plateau and its implications for post-IR IRSL dating of polymineral fine grains. Quaternary Geochronology 30, 147-153.

Zhao, H., Lu, Y.C., Zhang, J., Wang, H., 2002. IRSL dating of late Quaternary sediments and chronology of environmental changes at Dazhigu area, Tianjin. Chinese Journal of Geology 37, 174-183. (in Chinese with English Abstract)

Zhao, S., 1986a. Transgression and coastal changes in Bohai Sea and its vicinities since the Late Pleistocene, in: Qin, Y., Zhao, S. (Eds.), Late Quaternary sea-level changes. China Ocean Press, Beijing, pp. 53-61.

Zhao, S., 1986b. Transgression and coastal changes in Bohai Sea and its vicinities since the Late Pliestocene, in: Qin, Y., Zhao, S. (Eds.), Late Quaternary sea-level changes, Beijing, China, pp. 53-61.

Zhao, S., Yang, G., Cang, S., Zhang, H., Huang, Q., Xia, D., Wang, Y., Liu, F., Liu, C., 1978. On the marine stratigraphy and coastlines of the western coast of the Gulf of Bohai. Oceanologia et Limnologia Sinica 9, 15-25. (in Chinese with English Abstract)

Zhao, X., Geng, X., Zhang, J., 1979. Sea level changes of the eastern China during the past 20,000 years. Acta Oceanologica Sinica 1, 269-281. (in Chinese with English Abstract)

Chapter 2 Reliability assessment of fading correction for the K-feldspar luminescence signals using reference chronologies

In this chapter, the reliability of fading correction methods for feldspar luminescence ages is investigated using the fluvial deposits from the loess-palaeosol deposits from the Chinese Loess Plateau (Chapter 2.1) and the Heidelberg Basin (Upper Rhine Graben. Chapter 2.2), which hold the reference chronologies from orbital tuning, palynological stratigraphy and palaeomagnetism respectively. Reliability of two main fading correction models were evaluated by comparing 1) the simulated and natural dose response curves, and 2) fading corrected and reference ages.

Chapter 2.1 Timing of fluvial sedimentation in the Upper Rhine Graben since the Middle Pleistocene: constraints from quartz and feldspar luminescence dating

Yan Li, Sumiko Tsukamoto, Manfred Frechen, Gerald Gabriel

Leibniz Institute for Applied Geophysics (LIAG), Stilleweg 2, 30655, Hannover, Germany.

Published in ***Boreas***

Volume 47, Issue 1 (January 2018), pages 256-270

https://doi.org/10.1111/bor.12266

Chapter 2.2 Testing the reliability of fading correction methods for feldspar IRSL dating: A comparison between natural and simulated-natural dose response curves

Yan Li[1,*], Sumiko Tsukamoto[1], Hao Long[2], Jingran Zhang[3], Linhai Yang[4], Zhong He[5], Manfred Frechen[1]

[1] Leibniz Institute for Applied Geophysics, Hannover, 30655, Germany

[2] Nanjing Institute of Geography & Limnology, CAS, Nanjing, 210008, China

[3] Nanjing Normal University, Nanjing, 210023, China

[4] Northwest Institute of Eco-environment and Resources, CAS, Lanzhou, 730000, China

[5] Northwest A&F University, Yangling, 712100, China

* Corresponding author: Yan.Li@liag-hannover.de, geo-liyan@foxmail.com (Y. Li)

Submitted to the Journal ***Radiation Measurements***

in revised form (11.04.2018)

Abstract

The reliability of the fading correction methods for feldspar infrared stimulated luminescence (IRSL) dating in the non-linear part of the dose response curve proposed by Wallinga et al. (2007) (modified from Lamothe et al., 2003) and Kars et al. (2008) was evaluated using samples from the Chinese loess-palaeosol sequence in Luochuan with the reference ages. Two protocols, the post-infrared (IR) IRSL at 225 ˚C ($pIRIR_{225}$) and the pulsed IR at 50 ˚C, were applied in this study. The natural dose response curve (DRC) for the IR_{50} (pre-$pIRIR_{225}$), $pIRIR_{225}$ and pulsed IR_{50} was first constructed. The simulated-natural DRC and the fading corrected ages were then determined. The characteristic saturation dose (D_0) of the simulated-natural DRC was found to be larger than that of the natural DRC for the IR_{50} (pre-$pIRIR_{225}$) and $pIRIR_{225}$ signals, whilst the two D_0 values agreed with each other for the pulsed IR_{50}. The saturation ratio (*n/N*) of the simulated-natural DRC agreed with the natural one within 10% uncertainty for all three signals. The fading corrected ages using these two methods agreed with the reference ages, confirming the reliability of the two fading correction methods. However, our numerical simulation on the fading correction showed that the method by Wallinga et al. (2007) significantly overcorrect ages when the fading rates are larger than *ca.* 4-5%/decade.

Keywords: Anomalous fading; Dose response curve; Saturation level; Characteristic dose; Chinese loess

2.2.1 Introduction

The much higher saturation dose of the K-feldspar infrared stimulated luminescence (IRSL) signal compared to the quartz optically stimulated luminescence (OSL) signal, should enable to significantly extend the age range of luminescence dating. However, the IRSL signal is commonly affected by athermal signal loss, known as anomalous fading (Spooner, 1994). It is most likely caused by quantum-mechanical tunnelling (Visocekas, 1985), which results in age underestimation, and has therefore held back the application of K-feldspar IRSL dating. During the last decade, several more athermally stable luminescence signals were proposed and thoroughly investigated to overcome or minimise anomalous fading, such as the post-IR IRSL signal at an elevated preheat temperature (pIRIR; Thomsen et al., 2008; Buylaert et al., 2009), the multiple-elevated temperature pIRIR signal (MET-pIRIR; Li and Li, 2011) and the pulsed IR signal (Jain and Ankjærgaard, 2011; Jain et al., 2015; Tsukamoto et al., 2006; 2017). In particular, the pIRIR signal stimulated at 290°C ($pIRIR_{290}$; the stimulation temperature is labelled as subscripts) by Thiel et al. (2011) and the MET-$pIRIR_{250}$ signals by Li and Li (2011) were thought to be not affected by anomalous fading. However, these athermally stable signals tend to be more difficult to bleach (Li and Li, 2011; Kars et al., 2014; Colarossi et al., 2015; Tsukamoto et al., 2017). Therefore, for dating sediments from depositional environments where sufficient light exposure is known to be

challenging (e.g. fluvial, glacial), it may be more suitable to use a signal which is faster to bleach although still slightly fading, such as $pIRIR_{225}$ and pulsed IR_{50}, combined with a proper fading correction.

The fading correction method of Huntley and Lamothe (2001) predicts a logarithmic decay of a luminescence signal with decadal time, and is only applicable for the linear part of the dose response curve (DRC), corresponding to ages not older than 20-50 ka. To correct anomalous fading for older ages lying in the non-linear part of the DRC up to saturation, Lamothe et al. (2003) proposed the 'dose-rate fading correction' method, based upon the relationship between the laboratory and environmental dose rates. Using this method, a fading corrected DRC can be constructed, representing a fading corrected DRC which is affected by anomalous fading during the burial time (Wallinga et al., 2007). A new physical model of anomalous fading was proposed by Huntley (2006), based upon a power-law decay of the luminescence signal due to the tunnelling of electrons to the nearest neighbour recombination centre. Kars et al. (2008) presented a fading correction method using the model of Huntley (2006); they reconstructed a simulated-natural DRC and predicted the natural saturation level and the fading corrected age. This method was tested using fluvial sediment samples from the Roer Valley Graben and the fading corrected ages agreed with the corresponding quartz OSL ages (Kars et al., 2009). However, the reliability of these fading correction methods for the part of dose non-linearly growing up to saturation has not yet been thoroughly tested against independent age control. In addition, the accuracy of the simulated-natural DRC has not been evaluated by the natural signal intensity plotted against the equivalent dose (De), i.e. the natural DRC.

The loess-palaeosol sequences from the Chinese Loess Plateau contain homogenous and quasi-consistent wind-blown dusts with a well-established reference chronology based on the orbital tuning of high resolution grain size and magnetic susceptibility records for the entire Quaternary (Liu et al., 1985; Ding et al., 2002). Therefore, the Chinese Loess Plateau provides an ideal material to test the reliability of the fading correction methods beyond the linear part of the DRC. Using this chronostratigraphy, the natural and laboratory-generated DRCs were compared for the quartz luminescence signals (e.g. Ankjærgaard et al., 2016; Chapot et al., 2012, 2016). The natural DRC was also constructed for the K-feldspar IRSL (Li and Li, 2008) and MET-pIRIR (Li and Li, 2012) signals.

In this study, the accuracy of the fading correction methods following Lamothe et al. (2003) and Kars et al. (2008) is assessed using K-feldspar samples from the Luochuan profile on the Chinese Loess Plateau. The $pIRIR_{225}$ and pulsed IR_{50} protocols are applied to construct the natural DRC of the IR_{50} (pre-$pIRIR_{225}$), $pIRIR_{225}$ and pulsed IR_{50} signals. The saturation ratio (n/N; Table 2.2.3 for the full detail about the abbreviations used in this paper) and characteristic saturation dose (D_0) of the simulated-natural DRC are compared with those of the natural DRC for each luminescence signal. The reliability of the fading correction methods is evaluated by comparing the fading corrected ages with the reference chronology, and is further tested using numerical simulations.

2.2.2 Samples and methodology

2.2.2.1 Sample collection and preparation

Eleven loess and palaeosol samples were collected from Unit S0 (0-11 ka) to Unit L9 (865-943 ka) (Ding et al., 2002) from the Luochuan profile (Fig. 2.2.1). The samples were either taken using steel cylinders or as blocks. Under subdued red light, sample material was prepared for mineral separation. The 63-100 µm fraction was first isolated after wet-sieving. Carbonate and organic matter in the subsamples were then removed using hydrochloric acid (HCl) and hydrogen peroxide (H_2O_2). The K-feldspar grains were finally extracted after heavy liquid separation (<2.58 g/cm^3).

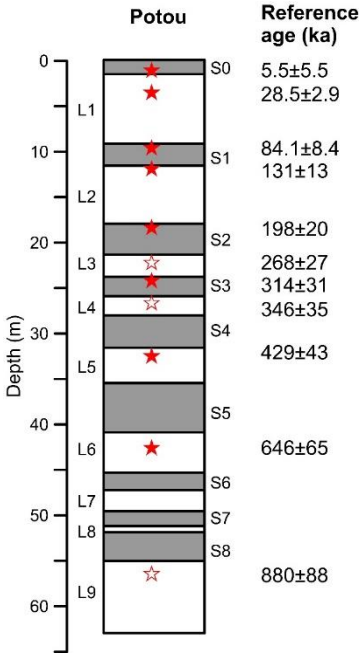

Fig. 2.2.1. The graphic sedimentary log of the Luochuan Profile and the sampling position. Fading correction was conducted for all the 11 samples using the pIRIR$_{225}$ protocol. The eight samples marked with filled star were also used for the pulsed IR$_{50}$ dating.

2.2.2.2 Luminescence instrumentation, protocols and dosimetry

Luminescence measurements were carried out using two automated Risø TL/OSL readers (DA-20), both equipped with a ^{90}Y/^{90}Sr beta source. The dose rates of the two beta sources (D_{lab}) are *ca.* 0.12 and 0.13 Gy/s, respectively. The K-feldspar luminescence signals in the UV-blue wavelengths (320-480 nm) were detected during the infrared stimulation at 870±40 nm. The pIRIR$_{225}$ protocol following Thomsen et al. (2008) and the pulsed IR$_{50}$ protocol following Tsukamoto et al. (2017) were applied (Table 2.2.1). The initial 5 s of the signal was subtracted by the last 15 s to calculate the intensities of the IR$_{50}$ (pre-pIRIR$_{225}$) and pIRIR$_{225}$, while the signal between 10 and 30 s was subtracted by the last 50 s for pulsed IR$_{50}$ (Fig. 2.2.2). The on-time and off-time of the IR-LEDs were set to 100 and 400 µs respectively in the pulsed IR$_{50}$ protocol. The pulsed IR$_{50}$ signal was recorded after rejecting the initial 100 µs of the off-time.

For each sample, six aliquots were measured to determine the sensitivity corrected natural luminescence intensity (I_n) for each signal. The full DRC was measured using three of the six aliquots for all samples for pIRIR$_{225}$, and eight samples for pulsed IR$_{50}$ (Fig. 2.2.1). A constant test dose of *ca.*

254 Gy was exploited to normalise the luminescence sensitivity for all the natural and regenerative intensities.

The concentrations of uranium (U, ppm), thorium (Th, ppm) and potassium (K, %) of the sediments were measured using both neutron activation analysis (NAA) and high-resolution gamma spectrometry, and the mean concentrations from both analyses were used to determine the total environmental dose rate (Table 2.2.2). The environmental dose rate was calculated using the estimated water contents of 15±5% and 20±5% for the loess and palaeosol samples, respectively (e.g. Lu et al., 2007). The conversion factors of Guérin (2011) and beta attenuation factors of Mejdahl (1979) were used. The cosmic dose rate was calculated following Prescott and Hutton (1994). The a-value was set to 0.09±0.02 following Balescu et al. (2007). The internal dose rate was calculated using K concentration of 12.5±0.5% (Huntley and Baril, 1997) and ^{87}Rb content of 400±100 ppm (Huntley and Hancock, 2001). The results of environmental dose rate are shown in Table 2.2.2.

Table 2.2.1 Details of the applied protocols.

post-IR $IRSL_{225}$ ($pIRIR_{225}$)			pulsed $IRSL_{50}$ (pulsed IR_{50})		
Step	Treatment	Observed	Step	Treatment	Observed
1	N, beta dose		1	N, beta dose	
2	Preheat for 60 s at 250 °C		2	Preheat for 60 s at 250 °C	
3	IR stimulation for 110 s at 50 °C	Ln, Li	3	Pulsed IR stimulation for 500 s at 50 °C [b]	Ln, Li
4	IR stimulation for 210 s at 225 °C	Ln, Li	4	Beta dose (Test dose) [a]	
5	Beta dose (Test dose) [a]		5	Preheat for 60 s at 250 °C	
6	Preheat for 60 s at 250 °C		6	Pulsed IR stimulation for 500 s at 50 °C	Tn, Ti
7	IR stimulation for 110 s at 50 °C	Tn, Ti	7	Return to 1	
8	IR stimulation for 210 s at 225 °C	Tn, Ti			
9	Return to 1				

[a] Test dose of ca. 254 Gy is given for the natural intensity and laboratory DRC measurements.
[b] 100 µs on-time and 400 µs off-time. Intensity was recorded between 100-400 µs of the off-time period.

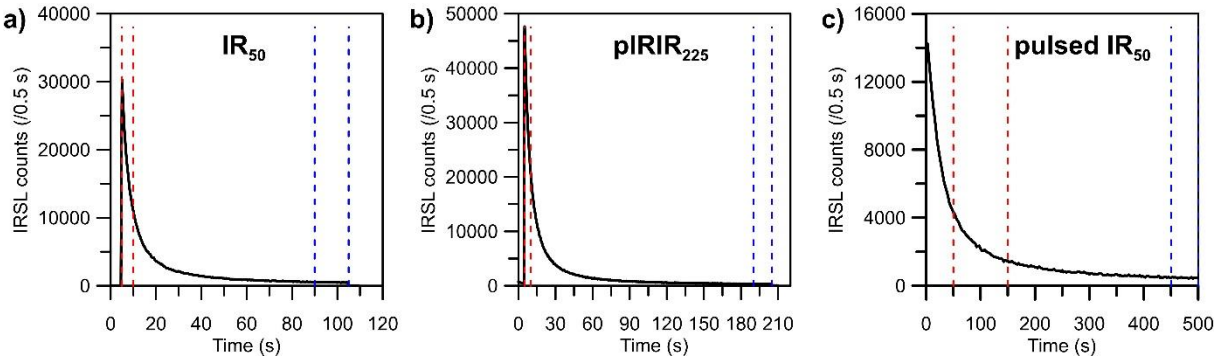

Figure 2.2.2 Decay curves and integration limits for the three signals. The initial 5 s of the signal was subtracted by the last 15 s to calculate the intensities of the IR_{50} (pre-$pIRIR_{225}$) and $pIRIR_{225}$, while the signal between 10 and 30 s was subtracted by the last 50 s for pulsed IR_{50}.

2.2.3 Natural and laboratory DRCs

The reference ages for the loess and palaeosol samples were calculated assuming a constant accumulation rate between the boundary ages for the loess-palaeosol transitions determined by Ding et al. (2002) (Table 2.2.2). The expected natural dose was calculated by multiplying the reference age by dose rate ($\dot{D}$). The natural DRC was built by plotting I_n against the associated expected natural dose, and then was fitted with a single saturating exponential function (Fig. 2.2.3). The saturation intensity (I_s) of the natural DRCs was calculated to 1.82±0.03, 1.77±0.03 and 1.57±0.04 for IR_{50} (pre-$pIRIR_{225}$), $pIRIR_{225}$ and pulsed IR_{50}, with the corresponding characteristic saturation dose (referred to as $(D_0)_{nat}$) of 592±26, 452±23 and 425±30 Gy, respectively. Thus, the upper dating limit of each signal was estimated to *ca.* 300, 230 and 210 ka for the IR_{50} (pre-$pIRIR_{225}$), $pIRIR_{225}$ and pulsed IR_{50} signals, respectively, according to a mean dose rate of 4 Gy/ka and the $2D_0$ value (Wintle and Murray, 2006). To evaluate the reliability of the fading corrected ages from the simulated-natural DRC, especially for the samples in saturation, the natural DRC-generated age was also determined by interpolation of the natural signal intensity onto the natural DRC (Table 2.2.4). However, several of the natural DRC-generated ages are slightly inconsistent with the reference ages, suggesting that the reference ages might contain uncertainty.

The laboratory DRC of the IR_{50} (pre-$pIRIR_{225}$), $pIRIR_{225}$ and pulsed IR_{50} signals was constructed based on the luminescence signal measurement for increasing regenerative doses up to *ca.* 4400 Gy to reach the laboratory saturation. The recycling ratios of 0.9-1.1 and recuperations smaller than 5% were acceptable for all the measured aliquots. Dose recovery and residual measurements were performed after four-hour bleaching in a Hönle SOL2 solar simulator. The dose recovery ratios for the IR_{50} (pre-$pIRIR_{225}$) and $pIRIR_{225}$ were generally satisfactory (~0.9) after subtracting the residual dose, whilst it deviated by ~-20% from unity for the pulsed IR_{50} signal. For each sample, the laboratory DRC was fitted with a single saturating exponential function. The D_e value for each sample was obtained after projecting the natural intensity onto the laboratory DRC (Fig. 2.2.3).

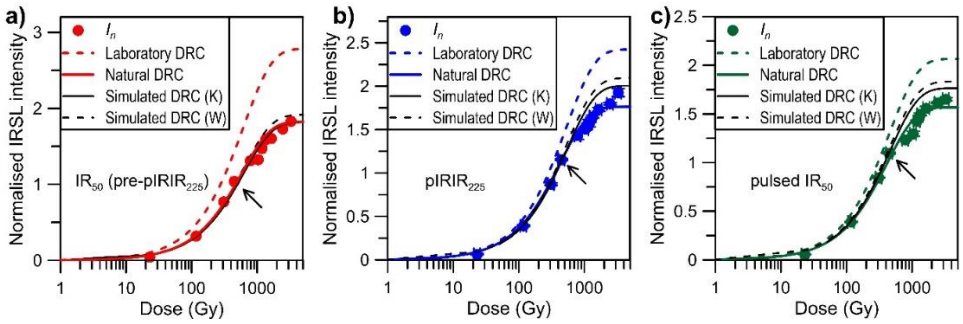

Fig. 2.2.3 Laboratory and simulated-natural DRCs for sample LUM3706 (L1, the arrow in this figure) and the associated natural dose response curve (DRC) for (a) IR_{50} (pre-$pIRIR_{225}$), (b) $pIRIR_{225}$ and (c) pulsed IR_{50}. The black solid and dashed lines show the simulated natural DRC after the fading correction of Kars et al. (2008) (labelled as K) and Wallinga et al. (2007) (labelled as W), respectively.

2.2.4 Construction of the simulated-natural DRC and fading corrections

Prior to fading correction, the fading rate was measured for each signal following the Auclair et al. (2003) procedure. A constant given dose of *ca.* 250 Gy was chosen for all samples to determine the fading rate for the IR_{50} (pre-$pIRIR_{225}$), $pIRIR_{225}$ and pulsed IR_{50} signals after confirming that there is no significant dose dependency on the fading rate (Fig. 2.2.4). The measured luminescence intensities were plotted against their corresponding delay times and then fitted with a logarithmic decay (Huntley and Lamothe, 2001) to calculate g_{2days} (%/decade, delay time normalised to two days), and with a power-law decay to determine the recombination centre density (ρ'; Huntley, 2006). Results for the g_{2days} and ρ' values are shown in Table 2.2.4.

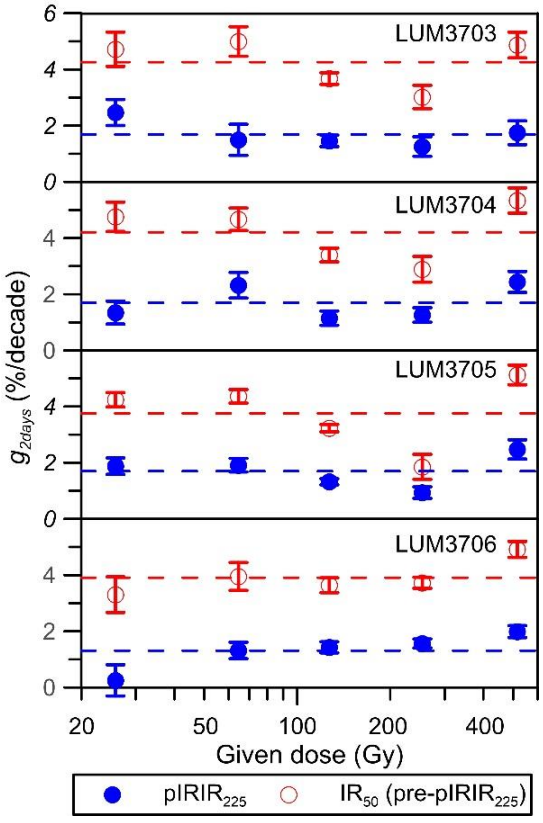

Fig. 2.2.4 Results of investigation of dose-dependent fading rate on the uppermost four samples (LUM3703-3706). Doses of ca. 25, 60, 120, 250 and 500 Gy are first given and fading experiment using pIRIR225 protocol was then conducted on three aliquots of each sample. The dashed line demonstrates mean value of the fading rates for each signal.

For the fading correction using the method of Lamothe et al. (2003), the measured I_n was fading corrected by

$$I_f = I_0 \left[1 - g \log\left(\frac{1}{e}\frac{\dot{D}_{\mathrm{lab}}}{\dot{D}}\right)\right] \tag{2.7}$$

The corrected I_n was then projected onto the laboratory DRC to infer the fading corrected D_e. Based upon this approach, Wallinga et al. (2007) multiplied the measured regenerated intensities (I_x) with the fading factor to construct the simulated-natural DRC. The measured I_n was then projected onto the simulated-natural DRC allowing the determination of the fading corrected D_e. Both Lamothe et al. (2003) and Wallinga et al. (2007) methods yield consistent fading corrected ages (Fig. 2.2.5). For a

further comparison between natural and fading corrected DRCs, the modified method after Wallinga et al. (2007) was applied in this study. Regarding the fading correction method by Kars et al. (2008), the unfaded laboratory DRC was first constructed by eliminating fading effects from the measured laboratory DRC. Parameters of I_s and D_0 from the unfaded laboratory DRC, ρ', D_{lab} and $\dot{D}$ were then used to construct the faded DRC. The fading corrected D_e was determined by projecting I_n onto the simulated-natural DRC (Fig. 2.2.6).

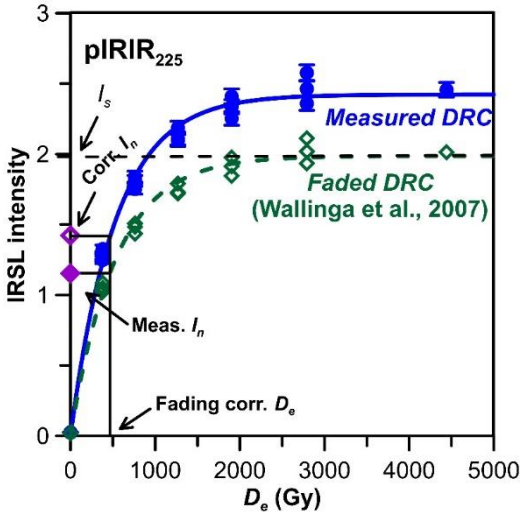

Fig. 2.2.5 Fading correction following Lamothe et al. (2003). The natural intensity was corrected using the laboratory fading rate (g_{2days} value) and then was projected onto the laboratory DRC to yield the fading corrected D_e. The faded (simulated) DRC was constructed following Wallinga et al. (2007). The regenerative intensities are corrected by multiplying the laboratory measured intensities with the fading rate. After fitting with single saturating exponential equation, the fading corrected DRC is constructed. The laboratory determined natural intensity is plotted onto it to obtain the fading corrected D_e.

2.2.5 DRC and age comparisons

In order to evaluate the reliability of the fading correction methods in aspects of simulated-natural DRCs and fading corrected ages, the saturation ratio (n/N), which represents the fraction of the filled trap, and the characteristic saturation dose D_0 for the natural and simulated-natural DRCs were compared. The ratio of the I_s for the simulated-natural DRC to that of the unfaded laboratory DRC represents the simulated saturation level, referred to as $(n/N)_{snd}$, while the natural saturation ratio $(n/N)_{nat}$ was calculated by dividing the I_s for the natural DRC by that of the unfaded laboratory DRC. For the IR_{50} (pre-$pIRIR_{225}$), the $(n/N)_{snd}$ values range between 0.38±0.07 to 0.70±0.06 for Kars et al. (2008), while those range between 0.37±0.01 and 0.73±0.01 following Wallinga et al. (2007). The associated

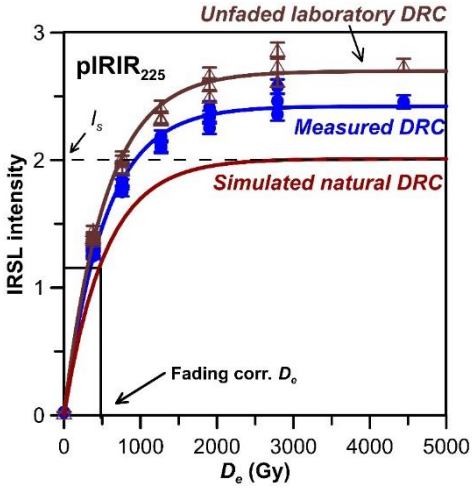

Fig. 2.2.6 Fading correction following Kars et al. (2008). The unfaded laboratory DRC is first built to eliminate fading during D_e measurement and construction of laboratory DRC. The characteristic saturation dose (D0), saturation value of the unfaded laboratory DRC, the recombination-centre-density (ρ') and the environmental dose rate are applied to construct the simulated natural DRC. The fading corrected D_e is finally determined after the laboratory natural intensity being projected onto the simulated natural DRC.

$(n/N)_{nat}$ values are between 0.43±0.01 and 0.56±0.01, showing that the natural saturation levels generally agree with the simulated ones for both methods, with an exception for LUM3705 (Unit S1) (Fig. 2.2.7a, b). For the $pIRIR_{225}$ signal, the $(n/N)_{snd}$ values are between 0.63±0.06 and 0.84±0.04 for the simulated-natural DRC after Kars et al. (2008), while those following Wallinga et al. (2007) vary from 0.66±0.01 to 0.86±0.01. The $(n/N)_{nat}$ values are between 0.60±0.01 and 0.69±0.02, which are ~10% smaller than the $(n/N)_{snd}$. Slight overestimation within 10% of the $(n/N)_{snd}$ is also observed for the pulsed IR_{50} (Fig. 2.2.7a, b). We also noticed that the $(n/N)_{snd}$ values derived after Kars et al. (2008) tend to be slightly smaller than those using the Wallinga et al. (2007) method (Fig. 2.2.7c).

The D_0 value for the natural DRC is in general smaller than the D_0 for the simulated-natural DRCs ($(D_0)_{snd}$) for both the IR_{50} (pre-$pIRIR_{225}$) and $pIRIR_{225}$ signals. On the contrary, the discrepancy between $(D_0)_{nat}$ and $(D_0)_{snd}$ is less pronounced for the pulsed IR_{50} signal (Fig. 2.2.7d-f). Note that the $(D_0)_{snd}$ after Wallinga et al. (2007) is equivalent to D_0 for the laboratory DRC. Our results show that the D_0 for the simulated-natural DRC following Kars et al. (2008) was slightly larger than the corresponding D_0 by Wallinga et al. (2007).

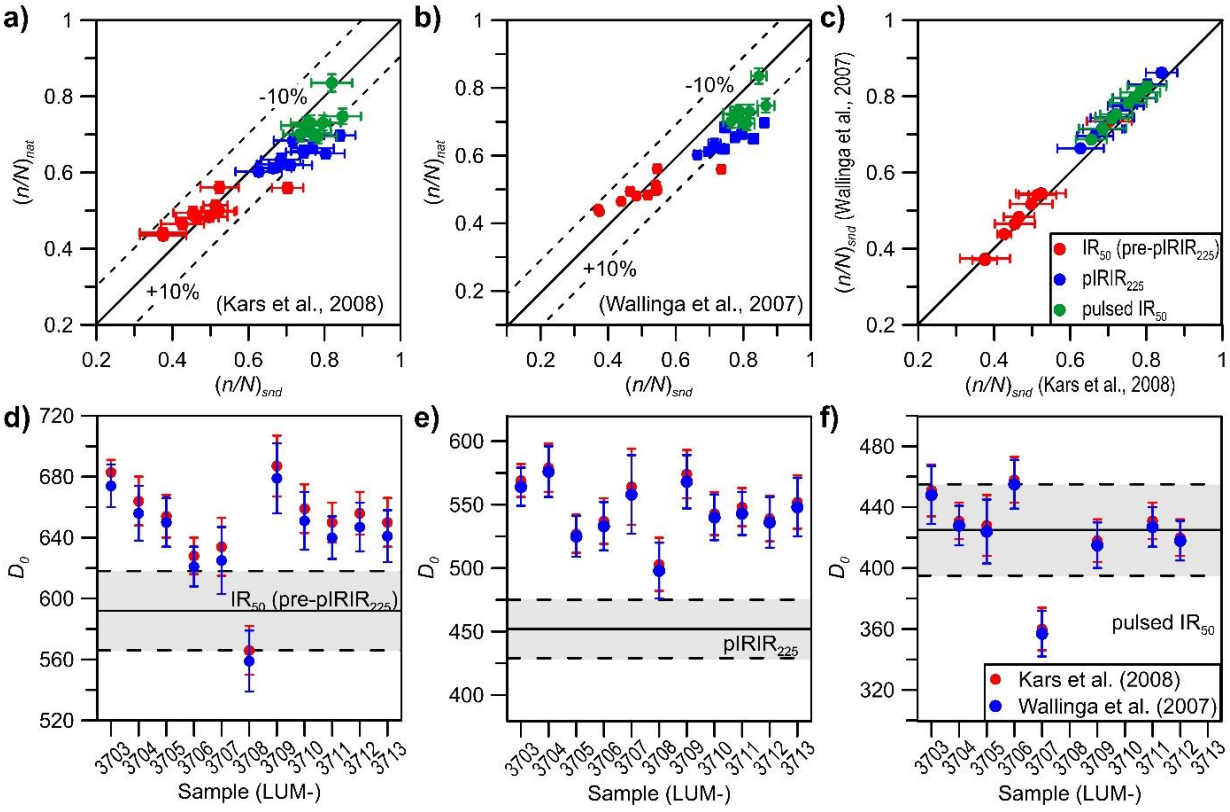

Fig. 2.2.7 Comparison of (n/N) and D_0 values from the natural and simulated-natural DRCs for the IR_{50} (pre-pIR_{225}), $pIRIR_{225}$ and pulsed IR_{50} signals. Comparison of simulated and natural saturation levels following (a) Kars et al. (2008) and (b) Wallinga et al. (2007). (c) Comparison of $(n/N)_{ss}$ values after the two fading correction models. Comparison of D_0 values for the natural and simulated-natural DRCs after fading correction for (d) the IR_{50} (pre-pIR_{225}), (e) $pIRIR_{225}$ and (f) pulsed IR_{50}. The shadow area shows the D_0 value of the natural DRC for each signal. Notice that D_0 values after Wallinga et al. (2007) (blue solid circle) equal to those for the laboratory DRCs.

The fading corrected age was calculated by dividing the fading corrected D_e by $\dot{D}$. The signal was regarded in saturation when the fading corrected D_e was larger than the associated $2(D_0)_{snd}$. A minimum age was then determined using $2(D_0)_{snd}$ for these samples. As shown in Fig. 2.2.8, the fading corrected ages after Kars et al. (2008) and Wallinga et al. (2007) are broadly in agreement, although there is a slight tendency of underestimation for the Wallinga et al. (2007) method compared with the Kars et al. (2008) method. Our results indicate that the IR_{50} (pre-$pIRIR_{225}$) signal reaches saturation at *ca.* 350 ka. The upper finite IR_{50} ages agree with the ages obtained from the natural DRC, and are broadly consistent with the reference ages up to *ca.* 250 ka (Fig. 2.2.8a). Similarly, the upper dating limit for the $pIRIR_{225}$ signal is estimated to be *ca.* 300 ka, based on the fading corrected DRC, while the dating upper limit determined from the natural DRC is *ca*. 230 ka, as the $(D_0)_{nat}$ is generally smaller than the $(D_0)_{snd}$. The finite fading corrected $pIRIR_{225}$ ages are mostly consistent with both the natural-DRC generated and orbital-tuned reference ages up to *ca.* 200 ka (Fig. 2.2.8b). The results suggest that $pIRIR_{225}$ enables the determination of reliable fading corrected ages despite both the $(n/N)_{snd}$ and $(D_0)_{snd}$ are larger than the corresponding $(n/N)_{nat}$ and $(D_0)_{nat}$. The pulsed IR_{50} signal yielded similar $(D_0)_{ss}$ and $(D_0)_{nat}$, that resulted in a consistent upper dating limit of *ca.* 210 ka for both the natural and simulated natural DRCs. As the $(n/N)_{snd}$ is in agreement with the $(n/N)_{nat}$ within 10% uncertainty, the finite fading corrected pulsed IR_{50} ages agree with the reference ages. Only for one sample (LUM3707, S2) the finite fading corrected ages underestimate the reference age (Fig. 2.2.8), which could be explained by the underestimated $(D_0)_{snd}$ of only *ca.* 360 Gy (Fig. 2.2.7f). Overall, both the fading correction methods following Kars et al. (2008) and Wallinga et al. (2007) are applicable for the studied loess-palaeosol sequence.

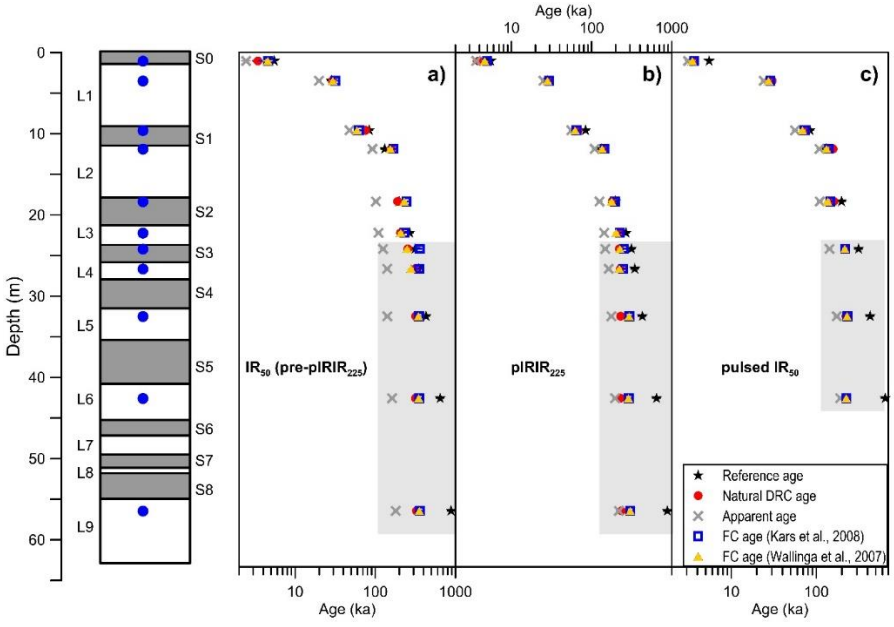

Fig. 2.2.8 Fading corrected ages were compared with the reference ages obtained from the natural DRC and the orbital tuned ages (Ding et al., 2002). The shadow area demonstrates minimum age for each signal.

2.2.6 Comparison of the two fading correction methods

The comparison of the DRC and fading corrected ages obtained by the two correction methods in the previous section shows that the two methods yielded broadly consistent corrected ages. To test if both methods are applicable for various fading rates, a numerical experiment of fading correction was conducted for *g* values ranging from 0 to 11%/decade. The D_0 value of 640 Gy and I_s value of 2.83 for the laboratory DRC for IR_{50} (pre-$pIRIR_{225}$) were used for the numerical simulations, based on the values obtained from the fitting of the regenerative IR_{50} intensities from all the laboratory DRCs (Fig. 2.2.3a). The representative $\dot{D}$ value was fixed to 4 Gy/ka. Dose rate for the beta source was set to 0.127 Gy/s. *g* value of 0-11%/decade was divided into 110 intervals with a bin length of 0.1. The ρ' value corresponding to each *g* were then calculated and employed for the Kars et al. (2008) correction. The D_0 and I_s values for the simulated-natural DRCs following the two correction methods and for each incrementing *g* value were determined using a single saturating exponential fitting approach. $(D_0)_{snd}$ value was constant 640 Gy after Wallinga et al. (2007), but was fading rate dependent for the simulated-natural DRC following Kars et al. (2008) (Fig. 2.2.9a). The I_s values were plotted against the associated fading rates and fitted with linear and exponential decay for the results after Wallinga et al. (2007) and Kars et al. (2008), respectively (Fig. 2.2.9b). It shows that the I_s after the Kars et al. (2008) method was slightly smaller, but broadly in agreement with that for simulated-natural DRC following Wallinga et al. (2007), when the *g* value is smaller than *ca.* 4-5%/decade. The results are consistent with the fading corrected results for Chinese loess and palaeosol samples shown above. Discrepancy of the I_s value arises when the *g* value is larger than *ca.* 4-5%/decade, as the I_s value of Wallinga et al. (2007) correction decreases more rapidly in the simulated-natural DRC than that for Kars et al. (2008) (Fig. 2.2.9b). The fading corrected ages were then calculated based upon $(D_0)_{snd}$ and I_s values obtained from modelling. It showed that the Kars et al. (2008) fading corrected ages are consistently slightly larger than that after Wallinga et al. (2007) for *g* values smaller than *ca.* 4%/decade. With the increase of *g* value, fading corrected ages following Wallinga et al. (2007) significantly overestimate that of the corresponding Kars et al. (2008), as the discrepancy for the simulated I_s becomes dominant in age determination.

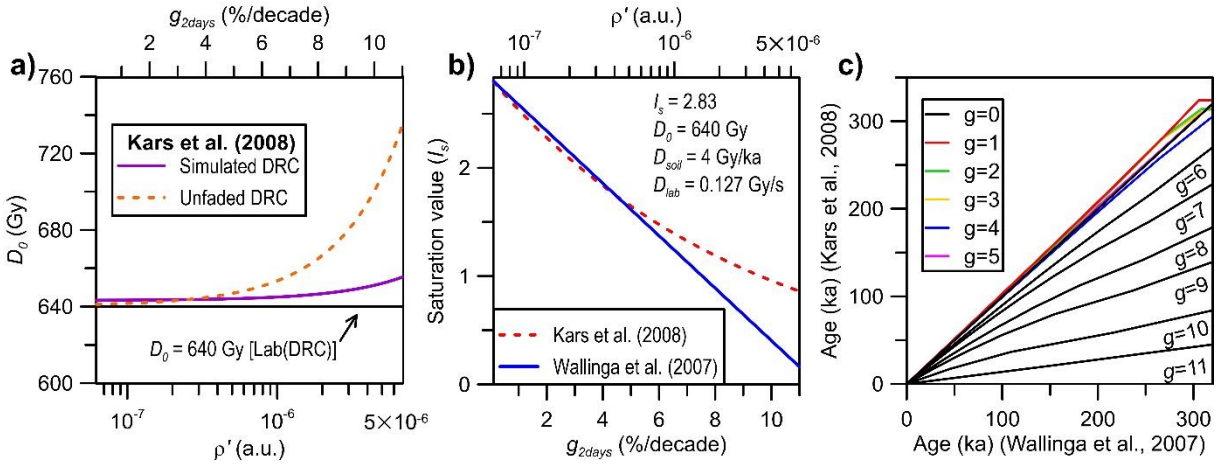

Fig. 2.2.9 Modelling for comparison of fading corrected results using Kars et al. (2008) and Lamothe et al. (2003). D_0 for simulated DRC after Lamothe et al. (2003) is equal to that for the laboratory DRC (Fig. 5A). The unit for *g* in Fig. 5C is %/decade.

2.2.7 Conclusions

In In this study, the natural dose response curve (DRC) for the Chinese loess profile is constructed using the K-feldspar IR_{50} (pre-$pIRIR_{225}$), $pIRIR_{225}$ and pulsed IR_{50} signals. After the fading correction following Wallinga et al. (2007) (on the basis of the dose-rate fading correction by Lamothe et al., 2003) and Kars et al. (2008), the simulated saturation level $(n/N)_{snd}$, the characteristic saturation dose $(D_0)_{snd}$ and the fading corrected ages, are compared with the natural ones. The fading corrected results following these two methods are contrasted with the reference ages. According to the results we conclude that:

- The upper dating limits of *ca.* 300, 230, and 210 ka are obtained from the natural DRCs for the IR_{50} (pre-$pIRIR_{225}$), $pIRIR_{225}$ and pulsed IR_{50} signals.
- The $(n/N)_{snd}$ value following both fading correction methods agrees with the associated $(n/N)_{nat}$ within 10% uncertainty for IR_{50} (pre-$pIRIR_{225}$), $pIRIR_{225}$ and pulsed IR_{50}. The $(D_0)_{snd}$ value overestimates the associated $(D_0)_{nat}$ for $pIRIR_{225}$ and IR_{50} (pre-$pIRIR_{225}$), whilst the $(D_0)_{snd}$ value is similar with the $(D_0)_{nat}$ value for pulsed IR_{50}.
- The Wallinga et al. (2007) method yields broadly consistent ages with only slight underestimation compared with those of the Kars et al. (2008) method for our samples, which agree with the reference ages with uncertainty of the Luochuan loess-palaeosol stratigraphy.
- Our results show that fading corrected ages after Wallinga et al. (2007) significantly overestimate the results after Kars et al. (2008) when the fading rate is larger than *ca.* 4-5%/decade.

Acknowledgements

Gudrun Drewes and Sonja Riemenschneider are thanked for sample preparation in laboratory. The authors are grateful to the participants of the 15th International Conference on Luminescence and Electron Spin Resonance Dating (LED) for their constructive comments and suggestions. Yan Li is supported by China Scholarship Council (201406400050).

References

Ankjærgaard, C., Guralnik, B., Buylaert, J.P., Reimann, T., Yi, S., Wallinga, J., 2016. Violet stimulated luminescence dating of quartz from Luochuan (Chinese loess plateau): Agreement with independent chronology up to ~600 ka. Quaternary Geochronology 34, 33-46.

Auclair, M., Lamothe, M., Huot, S., 2003. Measurement of anomalous fading for feldspar IRSL using SAR. Radiation Measurements 37, 487-492.

Balescu, S., Ritz, J.-F., Lamothe, M., Auclair, M., Todbileg, M., 2007. Luminescence dating of a gigantic palaeolandslide in the Gobi-Altay mountains, Mongolia. Quaternary Geochronology 2, 290-295.

Buylaert, J.P., Murray, A.S., Thomsen, K.J., Jain, M., 2009. Testing the potential of an elevated temperature IRSL signal from K-feldspar. Radiation Measurements 44, 560-565.

Chapot, M.S., Roberts, H.M., Duller, G.A., Lai, Z., 2012. A comparison of natural- and laboratory-generated dose response curves for quartz optically stimulated luminescence signals from Chinese Loess. Radiation Measurements 47, 1045-1052.

Chapot, M.S., Roberts, H.M., Duller, G.A., Lai, Z., 2016. Natural and laboratory TT-OSL dose response curves: Testing the lifetime of the TT-OSL signal in nature. Radiation Measurements 85, 41-50.

Colarossi, D., Duller, G.A.T., Roberts, H.M., Tooth, S., Lyons, R., 2015. Comparison of paired quartz OSL and feldspar post-IR IRSL dose distributions in poorly bleached fluvial sediments from South Africa. Quaternary Geochronology 30, 233-238.

Ding, Z.L., Derbyshire, E., Yang, S.L., Yu, Z.W., Xiong, S.F., Liu, T.S., 2002. Stacked 2.6-Ma grain size record from the Chinese loess based on five sections and correlation with the deep-sea $\delta^{18}O$ record. Paleoceanography 17, 5-1 - 5-21.

Guérin, G., 2011. Dose-rate conversion factors update. Ancient TL 29, 5-8.

Huntley, D.J., 2006. An explanation of the power-law decay of luminescence. Journal of Physics: Condensed Matter 18, 1359-1365.

Huntley, D.J., Baril, M.R., 1997. The K content of the K-feldspars being measured in optical dating or in thermoluminescence dating. Ancient TL 15, 11-13.

Huntley, D.J., Hancock, R.G.V., 2001. The Rb contents of the K-feldspars being measured in optical dating. Ancient TL 19, 43-46.

Huntley, D.J., Lamothe, M., 2001. Ubiquity of anomalous fading in K-feldspars and the measurement and correction for it in optical dating. Canadian Journal of Earth Sciences 38, 1093-1106.

Jain, M., Buylaert, J.P., Thomsen, K.J., Murray, A.S., 2015. Further investigations on 'non-fading' in K-Feldspar. Quaternary International 362, 3-7.

Jain, M., Ankjærgaard, C., 2011. Towards a non-fading signal in feldspar: insight into charge transport and tunneling from time-resolved optically stimulated luminescence. Radiation Measurements 46.

Table 2.2.2. Dose rate and expected natural equivalent dose (Gy) for the employed samples. The total dose rate is calculated using the mean concentrations of uranium, thorium and potassium determined using neutron activation analysis and gamma spectrometry. Water contents of 15±5% and 20±5% are given to loess and palaeosol samples, respectively. Reference ages are following Ding et al. (2002).

Lab ID (LUM)	Sample ID	Depth (m)	U (ppm)			Th (ppm)			K (%)			Dose rate (Gy/ka)	Reference age (ka)	Expected natural dose (Gy)
			NAA	Gamma	Mean	NAA	Gamma	Mean	NAA	Gamma	Mean			
3703	S0	1.1	2.37±0.09	3.21±0.09	**2.79±0.14**	15.20±0.41	13.13±0.18	**14.16±0.43**	2.11±0.06	2.20±0.07	**2.16±0.10**	4.19±0.16	5.5±5.5	23±2
3704	L1-2	3.5	2.20±0.09	2.82±0.08	**2.51±0.13**	13.70±0.38	11.54±0.17	**12.62±0.40**	1.91±0.06	1.93±0.07	**1.92±0.09**	4.12±0.16	28.5±2.9	117±13
3705	S1-1	9.6	3.79±0.14	2.83±0.08	**3.31±0.16**	15.20±0.41	13.66±0.18	**14.43±0.44**	2.14±0.06	2.27±0.08	**2.21±0.10**	4.24±0.16	73±7	310±33
3706	L2-1	11.9	2.21±0.09	2.26±0.08	**2.24±0.12**	9.49±0.28	10.06±0.16	**9.78±0.32**	1.47±0.05	1.62±0.06	**1.55±0.08**	3.42±0.16	131±13	449±49
3707	S2-1	18.3	2.56±0.10	2.77±0.08	**2.66±0.13**	15.90±0.43	13.78±0.19	**14.84±0.45**	2.05±0.06	2.11±0.07	**2.08±0.10**	3.98±0.15	198±20	787±84
3708	L3-1	22.2	3.45±0.12	2.59±0.08	**3.02±0.14**	11.90±0.33	11.56±0.17	**11.73±0.37**	1.67±0.06	1.81±0.07	**1.74±0.09**	3.87±0.16	269±27	1040±113
3709	S3-1	24.2	2.46±0.10	2.59±0.08	**2.53±0.13**	15.80±0.43	13.47±0.18	**14.64±0.44**	1.95±0.06	1.88±0.07	**1.92±0.09**	3.78±0.15	314±31	1188±128
3710	L4-1	26.6	2.96±0.11	2.49±0.08	**2.72±0.14**	12.50±0.35	11.68±0.17	**12.09±0.38**	1.77±0.06	1.86±0.07	**1.82±0.09**	3.89±0.16	346±35	1343±146
3711	L5-1	32.5	3.64±0.13	2.75±0.08	**3.19±0.15**	11.50±0.32	11.18±0.17	**11.34±0.36**	1.64±0.05	1.81±0.07	**1.73±0.09**	3.85±0.17	429±43	1653±180
3712	L6-1	42.6	2.64±0.10	2.45±0.08	**2.55±0.13**	14.50±0.39	11.20±0.17	**12.85±0.40**	1.69±0.06	1.80±0.07	**1.75±0.09**	3.81±0.16	646±65	2462±268
3713	L9-1	56.4	2.38±0.10	2.64±0.08	**2.51±0.13**	13.30±0.37	10.78±0.16	**12.04±0.38**	1.74±0.06	1.72±0.07	**1.73±0.09**	3.72±0.16	880±88	3277±357

Table 2.2.3 Terminology and acronyms.

Parameter (Unit)	Definition	Note
D_e (Gy)	Equivalent dose	
(n/N)	Saturation ratio or the fraction of the filled trap	$(n/N)_{nat}$ is the saturation ratio for the natural DRC, estimated by dividing the saturation value of the natural DRC by the saturation value (I_s) of the unfaded laboratory DRC. $(n/N)_{snd}$ is the saturation ratio for the simulated-natural DRC, showing the ratio of the saturation value of the simulated natural DRC over the saturation value of the unfaded laboratory DRC (same as the term $(n/N)_{ss}$ in Guralnik et al.(2015)).
D_0 (Gy)	Characteristic saturation dose for the DRC	$(D_0)_{nat}$ and $(D_0)_{snd}$ are the characteristic saturation doses for the natural and simulated natural DRCs, respectively.
D_{lab} (Gy/s)	Dose rate of the beta source	
I_n	Natural luminescence intensity	
$\dot{D}$ (Gy/ka)	Environmental dose rate	
I_s	Saturation intensity	
g_{2days} (%/decade)	Fading rate measured in laboratory	Following Huntley and Lamothe (2001)
ρ'	Recombination centre density	

Table 2.2.4. Results of fading correction for the loess and palaeosol samples using the IR_{50} (pre-$pIRIR_{225}$), $pIRIR_{225}$ and pulsed IR_{50} signals.

Lab ID	Signal	g_{2days} (%/decade)	ρ' ($\times10^{-6}$)	$(n/N)_{ss}$[a]	$(n/N)_{ss}$[b]	$(n/N)_{nat}$	$(D_0)_{ss}$[a] (Gy)	$(D_0)_{ss}$[b] (Gy)	D_e (Gy)	Apparent age (ka)	Fading corrected age[a] (ka)	Fading corrected age[b] (ka)	natDRC generated age[c] (ka)	Reference age[d] (ka)
LUM3703	IR_{50}	5.39±0.91	3.62±0.62	0.38±0.07	0.37±0.01	0.43±0.01	683±8	674±14	10±1	2.5±0.3	4.6±1.1	4.6±0.6	3.4±0.5	5.5±5.5
	$pIRIR_{225}$	2.47±0.46	1.73±0.32	0.63±0.06	0.66±0.01	0.60±0.01	569±13	564±15	15±1	3.6±0.2	5.0±0.6	4.6±0.3	4.0±1.1	
	pulsed IR_{50}	1.44±0.27	1.00±0.19	0.77±0.05	0.79±0.02	0.70±0.02	451±17	448±19	13±1	3.1±0.2	3.7±0.4	3.5±0.3	3.7±0.4	
LUM3704	IR_{50}	3.58±0.45	2.43±0.31	0.51±0.05	0.54±0.01	0.50±0.01	664±16	656±18	78±3	20±1	32±3	30±2	29±3	29±3
	$pIRIR_{225}$	1.16±0.26	0.81±0.18	0.80±0.05	0.83±0.01	0.65±0.02	579±19	576±20	98±4	25±1	29±2	28±2	30±3	
	pulsed IR_{50}	1.26±0.26	0.87±0.18	0.80±0.05	0.82±0.02	0.73±0.02	431±17	428±13	94±3	24±1	29±2	27±2	30±3	
LUM3705	IR_{50}	1.91±0.39	1.30±0.27	0.70±0.06	0.73±0.01	0.56±0.01	654±14	650±16	205±6	48±2	63±6	59±3	77±8	73±7
	$pIRIR_{225}$	0.94±0.20	0.65±0.14	0.84±0.04	0.86±0.01	0.69±0.02	527±15	525±16	240±9	56±3	65±4	62±3	74±7	
	pulsed IR_{50}	1.60±0.40	1.10±0.28	0.75±0.07	0.77±0.03	0.72±0.02	428±20	424±21	241±13	56±4	73±8	69±5	75±7	
LUM3706	IR_{50}	3.59±0.19	2.41±0.13	0.51±0.02	0.54±0.01	0.51±0.01	628±12	621±13	291±16	92±6	169±14	154±11	162±18	131±13
	$pIRIR_{225}$	1.56±0.16	1.08±0.11	0.74±0.03	0.78±0.01	0.65±0.02	537±18	533±19	345±13	109±6	146±8	135±8	156±15	
	pulsed IR_{50}	1.31±0.27	0.91±0.18	0.78±0.05	0.81±0.02	0.69±0.02	458±15	455±16	345±13	109±6	141±10	132±8	158±15	
LUM3707	IR_{50}	4.40±0.56	2.90±0.37	0.45±0.05	0.47±0.01	0.49±0.01	634±19	625±22	405±17	102±6	246±30	229±13	199±20	198±20
	$pIRIR_{225}$	2.07±0.29	1.40±0.20	0.69±0.05	0.71±0.02	0.63±0.02	564±30	558±31	496±25	125±9	196±18	178±13	191±18	
	pulsed IR_{50}	1.10±0.27	0.76±0.19	0.82±0.05	0.85±0.02	0.84±0.02	360±14	357±15	437±19	110±6	146±11	136±9	161±14	
LUM3708	IR_{50}	3.58±0.63	2.39±0.42	0.52±0.01	0.55±0.01	0.56±0.01	566±16	559±20	409±21	110±7	230±32	208±14	216±23	269±27
	$pIRIR_{225}$	1.82±0.29	1.23±0.20	0.72±0.05	0.75±0.01	0.68±0.02	503±21	498±22	535±25	143±9	225±18	202±13	232±21	
LUM3709	IR_{50}	3.85±0.54	2.56±0.36	0.50±0.06	0.52±0.01	0.48±0.01	687±20	679±23	480±25	125±8	358±17	250±16	275±29	314±31
	$pIRIR_{225}$	2.23±0.31	1.50±0.21	0.67±0.05	0.70±0.01	0.61±0.02	574±19	568±21	567±27	148±9	254±22	225±13	>253	
	pulsed IR_{50}	1.45±0.31	1.00±0.21	0.76±0.05	0.79±0.03	0.73±0.02	418±14	415±15	548±22	143±8	>218	>216	>216	
LUM3710	IR_{50}	3.57±0.62	2.39±0.41	0.52±0.07	0.55±0.01	0.50±0.01	659±16	651±19	526±23	141±8	>352	280±17	>300	346±35
	$pIRIR_{225}$	1.59±0.28	1.08±0.19	0.75±0.05	0.78±0.01	0.65±0.02	543±17	540±18	612±22	164±9	246	222±12	>259	
LUM3711	IR_{50}	5.45±0.43	3.58±0.28	0.38±0.03	0.37±0.01	0.44±0.01	650±13	640±14	523±18	141±8	>351	>345	>302	429±43
	$pIRIR_{225}$	2.06±0.42	1.41±0.29	0.68±0.06	0.71±0.01	0.62±0.02	548±15	543±17	655±21	177±9	>295	>293	>261	
	pulsed IR_{50}	1.69±0.28	1.15±0.19	0.74±0.05	0.76±0.02	0.70±0.02	431±12	427±13	644±27	174±10	>232	>230	>223	
LUM3712	IR_{50}	4.18±0.41	2.79±0.28	0.47±0.04	0.48±0.01	0.48±0.01	656±14	647±16	602±23	162±9	>352	>348	>302	646±65
	$pIRIR_{225}$	1.42±0.32	0.97±0.22	0.77±0.06	0.80±0.01	0.66±0.02	539±18	536±20	729±29	196±9	>290	>288	>261	
	pulsed IR_{50}	0.89±0.27	0.62±0.18	0.85±0.05	0.87±0.03	0.75±0.02	420±12	418±13	712±25	191±10	>226	>225	>223	
LUM3713	IR_{50}	4.67±0.17	3.09±0.12	0.43±0.02	0.44±0.01	0.46±0.01	650±16	641±17	651±18	180±9	>359	>354	>310	880±88
	$pIRIR_{225}$	1.83±0.34	1.25±0.23	0.71±0.06	0.74±0.01	0.62±0.02	552±21	548±23	791±39	219±14	>305	>303	>268	

The fading corrected results[a] were after Kars et al. (2008), while those marked with [b] showed fading corrected results following Wallinga et al. (2007). Reference ages[c] were obtained from the natural dose response curve, and the reference ages[d] are following Ding et al. (2002).

Kars, R.H., Reimann, T., Ankjaergaard, C., Wallinga, J., 2014. Bleaching of the post-IR IRSL signal: new insights for feldspar luminescence dating. Boreas 43, 780-791.

Kars, R.H., Wallinga, J., 2009. IRSL dating of K-feldspars: Modelling natural dose response curves to deal with anomalous fading and trap competition. Radiation Measurements 44, 594-599.

Kars, R.H., Wallinga, J., Cohen, K.M., 2008. A new approach towards anomalous fading correction for feldspar IRSL dating — tests on samples in field saturation. Radiation Measurements 43, 786-790.

Lamothe, M., Auclair, M., Hamzaoui, C., Huot, S., 2003. Towards a prediction of long-term anomalous fading of feldspar IRSL. Radiation Measurements 37, 493-498.

Li, B., Li, S.-H., 2008. Investigations of the dose-dependent anomalous fading rate of feldspar from sediments. Journal of Physics D: Applied Physics 41, 225502.

Li, B., Li, S.-H., 2011. Luminescence dating of K-feldspar from sediments: A protocol without anomalous fading correction. Quaternary Geochronology 6, 468-479.

Liu, T.S., 1985. Loess and the Environment. China Ocean Press, Beijing.

Lu, Y.C., Wang, X.L., Wintle, A.G., 2007. A new OSL chronology for dust accumulation in the last 130,000 yr for the Chinese Loess Plateau. Quaternary Research 67, 152–160.

Mejdahl, V., 1979. Thermoluminescence dating: beta-dose attenuation in quartz grains. Archaeometry 21, 61-72.

Prescott, J.R., Hutton, J.T., 1994a. Cosmic ray contributions to dose rates for luminescence and ESR dating: Large depths and long-term time variations. Radiation Measurements 23, 497-500.

Prescott, J.R., Hutton, J.T., 1994b. Cosmic ray contributions to dose rates for Luminescence and ESR dating: large depth and long-term time variations. Radiation Measurements 23, 497-500.

Spooner, N.A., 1994. The anomalous fading of infrared-stimulated luminescence from feldspars. Radiation Measurements 23, 625-632.

Thiel, C., Buylaert, J.-P., Murray, A., Terhorst, B., Hofer, I., Tsukamoto, S., Frechen, M., 2011. Luminescence dating of the Stratzing loess profile (Austria) – Testing the potential of an elevated temperature post-IR IRSL protocol. Quaternary International 234, 23-31.

Thomsen, K.J., Murray, A.S., Jain, M., Bøtter-Jensen, L., 2008. Laboratory fading rates of various luminescence signals from feldspar-rich sediment extracts. Radiation Measurements 43, 1474-1486.

Tsukamoto, S., Kondo, R., Lauer, T., Jain, M., 2017. Pulsed IRSL: A stable and fast bleaching luminescence signal from feldspar for dating Quaternary sediments. Quaternary Geochronology 41, 26-36.

Tsukamoto, S., Denby, P.M., Murray, A.S., Bøtter-Jensen, L., 2006. Time-resolved luminescence from feldspars: New insight into fading. Radiation Measurements 41, 790-795.

Visocekas, R., 1985. Tunneling radiative recombination in labradorite: its association with anomalous fading of thermoluminescence. Nuclear Tracks and Radiation Measurements 10, 521-529.

Wallinga, J., Bos, A.J.J., Dorenbos, P., Murray, A.S., Schokker, J., 2007. A test case for anomalous fading correction in IRSL dating. Quaternary Geochronology 2, 216-221.

Wintle, A.G., Murray, A.S., 2006. A review of quartz optically stimulated luminescence characteristics and their relevance in single-aliquot regeneration dating protocols. Radiation Measurements 41, 369-391.

Chapter 3 Quartz OSL and K-feldspar post-IR IRSL dating of sand accumulation in the Lower Liao Plain (Liaoning, NE China)

Yan Li[1], Sumiko Tsukamoto[1], Ke Hu[2] and Manfred Frechen[1]

[1] Leibniz Institute for Applied Geophysics (LIAG), Geochronology and Isotope Hydrology, Stilleweg 2, 30655, Hannover, Germany.

[2] School of Ocean Sciences, China University of Geosciences (Beijing), Xueyuan Road 29, Haidian District, 100083, Beijing, China

Published in ***Geochronometria***

Volume 44, Issue 1 (January 2017), pages 1-15

https://www.degruyter.com/downloadpdf/j/geochr.2017.44.issue-1/geochr-2015-0051/geochr-2015-0051.pdf

https://doi.org/10.1515/geochr-2015-0051

Abstract

The timing of the formation of extensively distributed sand dunes in the Bohai coastal area and its forcing factors are poorly understood. In this study, the chronology of a well-preserved sand dune located in Panjin Forest Park (PJ) in the Lower Liao Plain (LLP) is investigated using quartz optically stimulated luminescence (OSL) and K-feldspar post-infrared (IR) infrared stimulated luminescence (IRSL) (pIRIR) dating. For the pIRIR measurements, the combination of preheating at 180 °C and pIRIR stimulation at 150 °C ($pIRIR_{150}$) is exploited. The quartz results show that the sand dune accumulated from *c*.120 a (1890 AD) to *c*.70 a (1940 AD) before present, and the underlying sandy soil sediments deposited from *c*.5.0 ka to *c*.0.13 ka as marsh sediment after the sea-level highstand since the mid-Holocene. From the evidence in historical coastline records, the PJ sand dune is an inland sand dune and not a coastal sand dune. Based on further information of climate and temperature change after the Little Ice Age (LIA) and human activity in northeastern China, we conclude that the PJ sand dune accumulation was very likely impacted by the immigrants and land reclamation at the end of Qing dynasty. The fading corrected IR_{50} ages, the apparent and fading corrected $pIRIR_{150}$ ages are consistent with quartz ages for two sandy soil samples but overestimate those for six sand samples. The overestimation of the feldspar ages is derived from the residual signal which has not been bleached before burial. The offset obtained from the difference between the quartz OSL and the feldspar $pIRIR_{150}$ ages are ~20-160 a (predicted residual dose; ~0.08-0.60 Gy), whereas the measured residual dose after bleaching 4 h in a solar simulator yielded age overestimation of ~10-40 a (~0.05-0.16 Gy). The age discrepancy calculated from the predicted residual was larger than those obtained from the laboratory measured residuals. We conclude that the $pIRIR_{150}$ of aeolian sediment is applicable for samples older than ~1000 years where the effect of the residual dose become negligible.

Keywords

optically stimulated luminescence (OSL) dating, sand accumulation, the Lower Liao Plain, K-feldspar post-IR IRSL, Holocene

3.1 Introduction

The Bohai Sea is a semi-closed sea in northern China which is known to have thick and continuous Quaternary sediments. Many studies on the geological and environmental evolution around the Bohai coast have been carried out on these Quaternary sediments (Yi et al., 2012; Liu et al., 2009; Wang and Fan, 2005; Wang et al., 2004; IOCAS, 1985). Alterations of marine and terrestrial sediment strata were recognized from numerous sediment cores (e.g. Zhao et al., 1978; Yao et al., 2006; Yi et al., 2015).

During the Holocene, significant geomorphological changes took place in the Bohai coastal area due to coastline migration (sea level change) and fluvial sediment input. These sediments showing the

Holocene transgressive phase are widely distributed, especially in three bays of the Bohai Sea with flat landforms. The regional sea level in Bohai rose to the highest sea level at 5-7 ka, and then oscillated slightly and fell to the present level gradually (Xue, 2009; Xue and Ding, 2008; Xu, 1994; Zhao et al., 1979). Historical documents have also been investigated to provide information about coastline changes during the late Holocene (Lin, 1991; Chen et al., 2010). Sedimentary systems including tidal flat, salt marsh, fluvial, lacustrine, and aeolian sediments along the Bohai coast, which were deposited associated with the sea level oscillation, can be recognized from the surface morphology (IOCAS, 1985). These sediments have documented rich information that promotes the understanding of the sea level fluctuation and the sedimentary process during the post-sea level highstand period. Although the marine strata in the Bohai coast area have been well studied and interpreted, however, the timing and formation of the sediments which were deposited close to the past sea levels within the range of the Holocene transgression are poorly understood due to the lack of datable material and to unreliable chronologies (e.g. Fang and Hu, 2007).

In the past decades, luminescence dating methods have been significantly improved and applied widely to establish chronologies of various sedimentary archives of the late Quaternary, especially after the development of a single aliquot regenerative dose (SAR) protocol (Murray and Wintle, 2000, 2003). The optically stimulated luminescence (OSL) signal from quartz and the infrared stimulated luminescence (IRSL) signal from feldspar are the two main signals that are used for dating. Although there are still challenges (e.g. relatively large uncertainties from insufficient luminescence sensitivity, overestimation caused by thermal transfer, and incomplete bleaching; Madsen and Murray, 2009), the quartz OSL dating using the SAR protocol has been successfully carried out to date young sediments from different environments (e.g. marine deposits: Madsen et al., 2005; Zhang et al., 2014; coastal sand dune: Kunz et al., 2010; Reimann et al., 2011; inland dune: Forman and Pierson, 2003; Yang et al., 2012; Du and Wang, 2014). On the other hand, the feldspar IRSL signal suffers from anomalous fading which causes age underestimation. Recently, it has been found that the post-IR IRSL (pIRIR) signal measured at elevated temperature fades significantly less than the conventional IRSL signal at 50°C (Thomsen et al. 2008). The pIRIR protocol with different preheat and stimulation temperature combinations were tested to date sediments from various environments and in different age range (Thomsen et al., 2008; Thiel et al., 2011; Madsen et al., 2011) . Specifically, the pIRIR protocols (Reimann et al., 2011) and the multi-elevated-temperature pIRIR protocol (Fu and Li, 2013) with low thermal combinations (preheat ≤ 200 °C) were and found to be suitable for dating of young (Holocene) deposits. Reimann et al. (2011) proved that the pIRIR dating results measured at 180 °C ($pIRIR_{180}$) are in agreement with quartz ages and radiocarbon dates, after subtracting the residual dose. Madsen et al. (2011) and Reimann and Tsukamoto (2012) proposed the pIRIR protocol with preheating at 180 °C and pIRIR stimulation at 150 °C ($pIRIR_{150}$) to date young coastal sand deposits. The $pIRIR_{150}$ protocol

has been applied successfully for the Holocene aeolian deposits, lacustrine sediments and marine deposits using coarse-grained feldspar and polymineral fine-grained materials as well (Long et al., 2014, 2015; Yang et al., 2015). However, whether one should correct for small anomalous fading and residual dose for the pIRIR signal is still under discussion (Li B et al., 2014; Buylaert et al., 2012).

We study a well-preserved sand dune and the underlying marsh sediment situated in the Lower Liao Plain, the north coastal area of the Bohai Sea. Our aim is two-fold; first, we apply OSL dating to sand-sized quartz grains extracted from a well-preserved sand dune and marsh sediment to establish the chronology of these deposits. On the basis of coastline changes in historical documents, the timing of sand accumulation and the possible forcing mechanisms of the sand deposition are discussed. Our second aim is to investigate the effects of the residual dose in the pIRIR dating of young sediments. The $pIRIR_{150}$ protocol is applied on K-feldspar fraction for all samples and the results are compared with the quartz ages to determine the applicability of the protocol for the young dune sediments.

3.2 Study area, site description, and sampling

3.2.1 Study area

The Lower Liao Plain (LLP) is an alluvial plain located in northeastern China (Fig. 2.1). To the north of the LLP, the Horqin dune field is located, which is one of the four biggest dune fields in China (Fig. 2.1A). South of the LLP is the Liaodong Bay, which is the northern part of the Bohai Sea. As a consequence of continuous subsidence during the Quaternary (Allen et al., 1997), sediments were carried by several streams and deposited in the LLP and the Liaodong Bay. Two dominant rivers, Liao River and Daling River, contribute most to the sediment load.

The position of the coastline has changed significantly since the late Pleistocene widely along the Bohai coast. Several marine layers were found in cores drilled in the LLP; these have been correlated to transgressions (IOCAS, 1985). The uppermost transgressive phase is widely distributed along the Bohai coast and constrained to the Holocene climate optimum (IOCAS, 1985). The regional sea-level highstand in the Liaodong Bay occurred at 5-7 ka and reached to the area of 50 km inland from the modern coastline (Fu, 1988). Afterwards, the sea level oscillated and fell to the present-day level. Historical documents and remote sensing were applied to examine the coastline changes in the LLP over the last hundred years (Chen et al., 2010). The results show that a significant progradation occurred in the LLP owing to an increased river load (Chen et al., 2010).

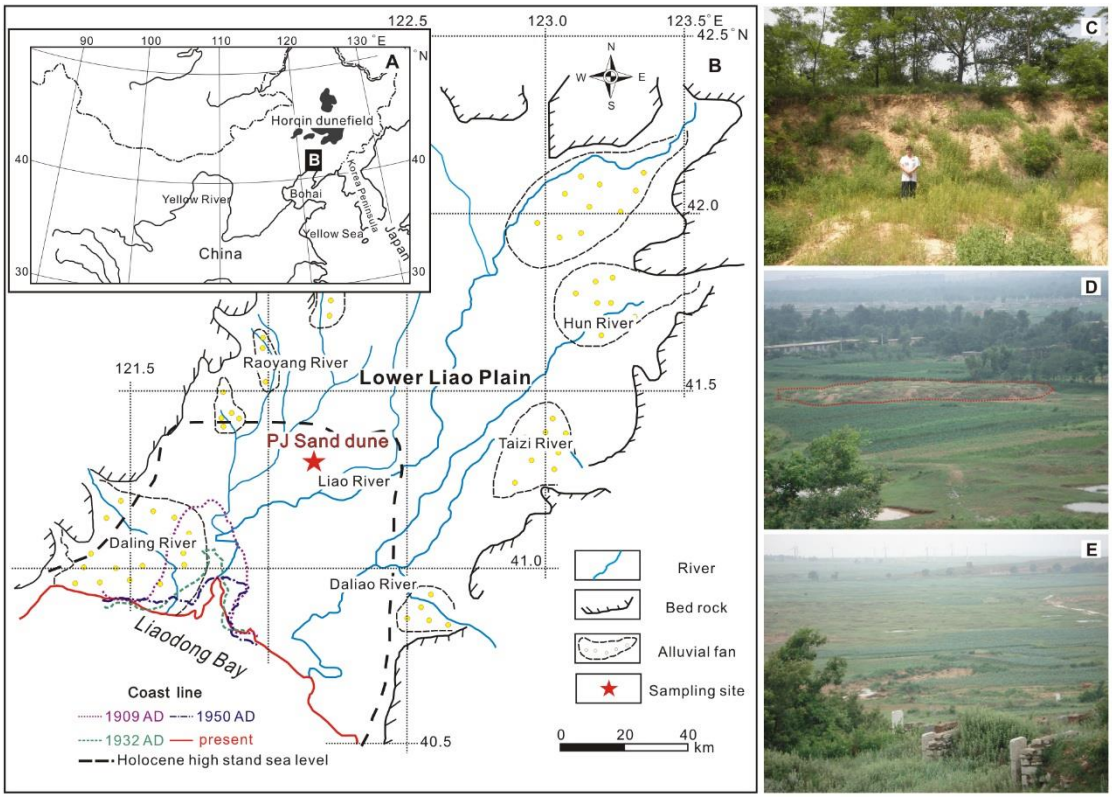

Fig 3.1 (A) The location of the study area in NE China. (B) Map showing the geological setting (Lower Liao River plain, local drainage streams and adjacent mountain areas) and coastline changes (sea level in Holocene, coastlines in 1905 AD, 1932 AD, 1950 AD and present, Fu, 1988; Chen et al., 2010). The location of the sampling site is also shown. (C)-(E) Typical sand deposits in the LLP. (C) is a photo of studied PJ sand dune.

At the present surface, fluvial, alluvial, aeolian, and coastal sediments can be recognized in the LLP. Aeolian sediments in the LLP are mainly reworked sand dunes, which are mobile under strong wind force (e.g. Fig. 3.1C, IOCAS, 1985). Although the sand deposits are distributed extensively, it is difficult to map the distribution as most of the comparatively large sand dunes and ridges are disturbed by human activities (e.g. agricultural movement: residual sand dune in farmland, Fig. 3.1D). The sand deposits at small scales are covered by vegetation and cannot be identified from satellite images (Fig. 3.1E).

The entire region is affected mainly by the East Asian monsoon. The mean annual temperature is 5-10 °C, with the mean temperature at 27-31 °C in summer and the mean temperature at -5-18 °C in winter. The mean annual precipitation is 634 mm, while annual evaporation reaches 1670 mm. During the winter seasons, the wind direction is north-western, whilst the summer seasons is dominated by south or southeastern wind from the Pacific (BGMRL, 1989).

3.2.2 Site description

The sampling site is located in the Panjin (PJ) forest park within the elapsed marine-terrestrial interacted area (Fig. 3.1), where the PJ sand dune is well preserved. Four sedimentary sections (S1-S4; Fig. 3.2B) were investigated and sampled. The sediments can be divided into four units (Fig. 3.2): Unit A contains homogenous yellowish fine sand with a thickness of ca. 4.5 m, covered by vegetation. The sediments are well to moderately sorted. Several roots were found in this layer. Unit B consists of grey fine sand with a thickness of 0.5-0.6 m. The grey sands are moderately to poorly sorted with organic matter. Unit C is a blackish sandy soil layer, consisting of poorly sorted sandy silt and clayey silt with organic-rich matter and soil aggregates. Clear boundaries can be distinguished between the different units. Additionally, at S2, a grey silt layer (Unit D) was found under the blackish sand layer which is not exposed in other sections. Unit A and B are relatively homogenous sands deposited above the sandy silt layer containing organic matter. The darker colour of unit B represents the anoxic condition due to the ground water above the impermeable soil layer.

Eight OSL samples (LUM3191 to LUM3198) were taken by hammering steel tubes (10 cm long cylinders with a diameter of 4 cm) into freshly prepared vertical sections from S1 and S4. The cylinders were fully filled with sediments to make sure that there is no mixing during transportation. The tubes were then covered and sealed with black plastic sheets and tapes to prevent light exposure and moisture loss. Two samples were taken from S1 (LUM3197 and LUM3198) and six samples were taken from S4 (LUM3191 to LUM3196), covering the three sedimentary units A-C.

3.3 Methods

3.3.1 Sample preparation

The preparation of sand-sized samples was conducted under the subdued red light in the luminescence laboratory at Leibniz Institute for Applied Geophysics. Materials of the outer 2 cm from both ends of the tubes were removed and discarded. For the upper six sand samples (LUM3191-3194, LUM3197-3198), the remaining non-light exposed material was dry-sieved to collect grains of 100-150 µm in diameter. With diluted hydrochloric acid (HCl) for two hours, sodium oxalate ($Na_2C_2O_4$) for one day and hydrogen peroxide (H_2O_2) for two hours, the samples were treated to remove carbonate, mineral aggregates and organic matter, respectively. For the lower two sandy soil samples (LUM3195-3196), chemical treatment was carried out first because the grains can be hardly dispersed and dry-sieved.

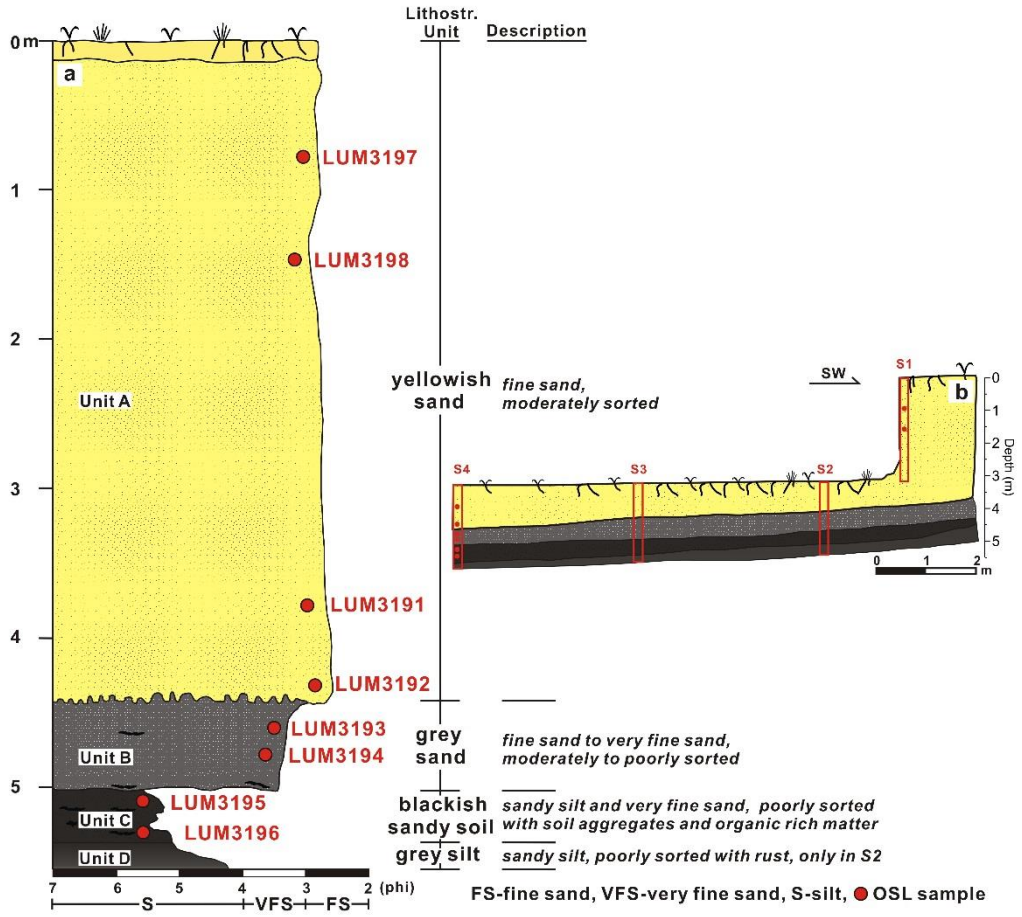

Fig. 3.2 (A) Investigated profile and its description. The positions of OSL samples are shown in the profile. (B) Stratigraphy of the PJ dune showing the positions of four investigated sections and sampling depths.

Subsequently, the remaining material was dry-sieved to extract grains 63-100 µm in diameter. Three steps density separations were performed using heavy liquid to extract quartz grains ($2.62<\rho<2.70$ g/cm^{-3}) and K-feldspar grains ($\rho<2.58$ g/cm^{-3}). The quartz extracts were subsequently treated with 40% hydrofluoric acid (HF) for 1 hour and to remove the remaining feldspar grains and etch quartz grains to eliminate the effect of the alpha-irradiated outer layer. The etched samples were finally treated with HCl and re-sieved to ensure the grains smaller than 100 µm for sand samples and 63 µm for sandy soil samples were removed.

3.3.2 Experimental details and protocols

The quartz and feldspar grains were mounted on stainless steel discs with a diameter of 6 mm and 2.5 mm respectively using silicone oil as adhesive. Luminescence measurements were carried out with an automated Risø TL/OSL system (DA-15) equipped with a calibrated ^{90}Y/^{90}Sr beta source. For quartz measurements, blue light-emitting diodes (LEDs, 470±30 nm) were employed for stimulation, and the quartz OSL signals were detected through a 7.5mm Hoya U-340 filter. The feldspar signals were detected through a combined blue filter pack (Schott BG-39 and Corning 7-59) stimulated by infrared LEDs (870±40 nm).

A single-aliquot regenerative dose (SAR; Murray and Wintle, 2000, 2003) protocol was applied for pre-tests and equivalent dose (D_e) measurements (Table 3.1). 24 aliquots for each sample were measured for the D_e determination of quartz. To test the purity of the quartz extracts, OSL IR depletion ratio (Duller, 2003) was employed in the SAR protocol to check feldspar contamination in the measured quartz. After the standard SAR protocol, an additional recycling dose was given to each aliquot. IR stimulation of grains for 40 s at room temperature using infrared LEDs was set after preheat and blue stimulation. The thermal treatment was set as preheat at 180 °C and cutheat at 160 °C with blue stimulation at 125 °C (Table 3.1). The determination of preheat temperature is described below. The initial OSL signals integrated over 0.80 s (first 5 channels) were subtracted by 'Early background' (6-12 channels, 0.8-1.92 s) to avoid a contribution from medium and slow components (Cunningham and Wallinga, 2010). Among the measured aliquots, aliquots which exceeded the acceptable range (0.9-1.1) for the OSL IR depletion ratio or recycling ratio were excluded from the D_e determination (Wintle and Murray, 2006; Rodnight, 2008).

The $pIRIR_{150}$ protocol (Table 3.1) was applied for K-feldspar D_e determination, residual dose measurement and dose recovery test. First 5 s of IR and post-IR IRSL signals is used for calculating the D_e values, by subtracting a background of the last 15 s of respective signals. Nine or ten feldspar aliquots were measured for the D_e determination for each sample.

3.3.3 Dose rate determination

For dose rate determination, additional 50 g of dried sample material were filled in plastic containers and stored at least four weeks before gamma spectrometry measurements to secure equilibrium between radon and its daughters. The concentrations of uranium (U), thorium (Th) and potassium (K) of the surrounding sediment were calculated from the activity of these nuclides measured by high-resolution gamma spectrometry. Each sample was measured over a period of two to three days. Bulk samples were weighed before and after drying the samples at 130 °C for one day to determine the natural water content. The median water content value of six sand samples with an error which can cover the range of all water contents, 6±4%, was assumed for the water content of sand sediment in antiquity. The water content of the two soil samples was estimated to be 13±3% according to the observed water content. The cosmic dose rate was calculated for each sample as a function of depth, altitude and geomagnetic latitude according to Prescott and Hutton (1994). The conversion factors of Guérin *et al.* (2011) and beta attenuation factors of Mejdahl (1979) were applied for the external beta- and gamma-dose rate calculation using the radionuclide concentration. The additional internal dose rate of each feldspar sample was calculated according to a potassium concentration of 12.5±0.5% (Huntley and Baril 1997) and ^{87}Rb concentration of 400 ± 100 ppm (Huntley and Hancock 2001). A mean a-value of 0.15±0.05 was used for dose rate calculation of the feldspar grains as a contribution

of external alpha radiation (Balescu and Lamothe 1994). The quartz dose rates range from 3.08±0.21 to 3.31 ± 0.24 Gy/ka, and the feldspar dose rates are from 3.92±0.16 to 4.14±0.17 Gy/ka (Table 3.2).

Table 3.1 SAR protocol applied for equivalent dose determination.

Quartz OSL			K-feldspar post-IR $IRSL_{150}$		
Step	Treatment	Observed	Step	Treatment	Observed
1	Give dose [a], D_i		1	Give dose	
2	Preheat for 60 s at 180 °C		2	Preheat for 60 s at 180 °C	
3	IR stimulation [b] for 40 s at 0 °C		3	IR stimulation for 100 s at 50 °C	
4	Stimulation for 40 s at 125 °C	L_n, L_i	4	IR stimulation for 200 s at 150 °C	L_n, L_i
5	Give test dose, D_t		5	Test dose, D_t	
6	Heat to 160 °C		6	Preheat for 60 s at 180 °C	
7	Stimulate for 40 s at 125 °C	T_n, T_i	7	IR stimulation for 100 s at 50 °C	
8	Return to 1		8	IR stimulation for 200 s at 150 °C	T_n, T_i
			9	Return to 1	

[a] For a natural sample, i=0 and D_0 is the natural dose.
[b] Additional recycling step with IR stimulation was added to calculate OSL IR depletion ratio.

3.4 Results and discussions

3.4.1 Performance tests and ages of quartz OSL

To determine the most appropriate preheat temperature for the D_e measurements, the pre-tests including the preheat plateau, dose recovery and thermal transfer tests were conducted on two presentative samples LUM3192 and LUM3196 prior to D_e measurement. The applicability of preheat temperatures between 160 °C and 280 °C with an interval of 20 °C using the SAR protocol was tested with three aliquots for each preheat temperature. The cutheat temperature was fixed at 160 °C suggested for dating young samples by Madsen and Murray (2009). The preheat plateau test was applied to observe the conditions of sensitivity change at different preheat temperatures. Aliquots for the dose recovery and thermal transfer tests were bleached using blue light emitting diodes (LEDs) at room temperature for 300 s before pausing 10000 s and then stimulated for 300s to bleach the natural signals prior to the measurements. The bleached aliquots for the dose recovery test were subsequently given a known beta dose (1.35 Gy for LUM3192 and 16.3Gy for LUM3196) and measured using the SAR protocol. In the thermal transfer test, D_es of bleached aliquots were measured to find out the contribution of transfer of charge into the OSL trap due to preheating. Constrained by the acceptable range (0.9-1.1, Fig. 3.3A and 3.3D) of the dose recovery ratios and the D_e preheat plateau between 160 and 260 °C for both two samples (Fig. 3.3B and 3.3E), as well as the negligible thermal transfer for the preheat temperatures lower than 240 °C (Fig. 3.3C and 3.3F), a preheat temperature of 180 °C was selected for the quartz D_e measurement for all eight samples.

Aliquots out of the acceptable ranges (0.9-1.1) of the recycling ratio, recuperation (Wintle and Murray, 2006) and OSL IR depletion ratio (Duller, 2003) were rejected prior to the D_e determination.

Recycling ratios of all 192 aliquots have a mean value of 1.00 with standard deviation of 0.06. Nine of 179 employed aliquots have recuperation values larger than 5%. Nevertheless, mean recuperation values for all samples are below 2%, suggesting that the undesirable transfer of charge was negligible in quartz measurements. The mean OSL IR depletion ratio of all aliquots is 0.98 with a standard deviation of 0.06. For most measured aliquots, the OSL IR depletion ratios are satisfactory, which suggests that the contribution of feldspar OSL signal is negligibly small.

Table 3.2 Dose rate determination.

Sample ID	Depth (cm)	Grain size Interval (μm)	U(ppm)	Th(ppm)	K%	Water content (%)[a]	Dose rate[Gy/ka]	
							K-feldspar	quartz
LUM3197	80	100-150	0.96±0.06	2.63±0.14	2.85±0.14	6±4 (1.7)	4.02±0.17	3.24±0.24
LUM3198	149	100-150	1.06±0.06	2.82±0.15	2.91±0.15	6±4 (2.1)	4.10±0.17	3.31±0.24
LUM3191	380	100-150	1.00±0.05	2.66±0.14	2.79±0.14	6±4 (2.6)	3.96±0.17	3.13±0.23
LUM3192	434	100-150	0.91±0.05	2.72±0.14	2.83±0.14	6±4 (4.2)	3.92±0.16	3.15±0.24
LUM3193	462	100-150	1.13±0.06	3.27±0.17	2.87±0.14	6±4 (6.6)	4.05±0.17	3.26±0.24
LUM3194	480	100-150	1.31±0.07	4.30±0.22	2.82±0.14	6±4 (9.5)	4.12±0.17	3.32±0.24
LUM3195	511	63-100	1.88±0.10	6.95±0.35	2.61±0.13	13±3 (14)	4.14±0.17	3.20±0.22
LUM3196	532	63-100	2.24±0.12	8.01±0.41	2.34±0.12	13±3 (15)	4.07±0.17	3.10±0.20

[a] The water contents are presented as 'Estimated water content with uncertainty (Observed water content).

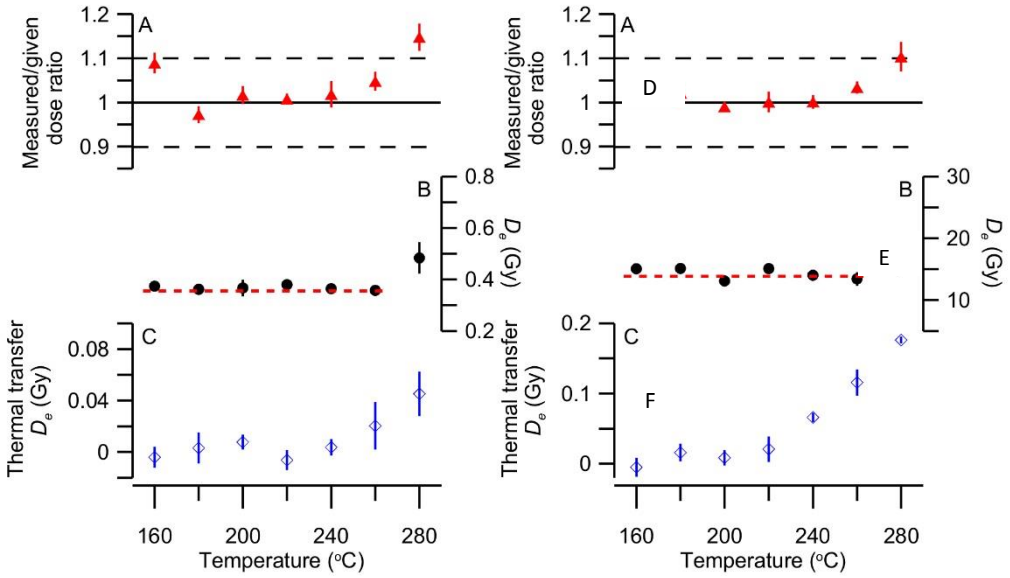

Fig. 3.3 Results of quartz OSL pre-tests. (A) Measured/given ratio (dose recovery test), (B) equivalent dose and (C) thermal transfer at different preheat temperatures for sample LUM3192. (D)-(F) show the results of the same set of tests for sample LUM3196.

Typical decay and dose response curves for both sand sample (LUM3191) and sandy soil sample (LUM3196) are shown in Fig. 3.4. A clear decay of natural quartz OSL signal for each sample was observed. All the samples yielded detectable quartz OSL signal. The dose response curves of the upper six samples were fitted by a linear function, and those of two sandy soil samples were fitted by one

single saturating exponential function. The distributions of D_e values and the overdispersion value (σ_{OD}) which were calculated using the central age model (Galbraith et al., 1999) indicate that employed materials were uniformly bleached owing to the centralized distributions of D_e values. The mean D_e values for the six dune samples range between 0.28±0.01 to 0.42±0.01 Gy, and those for the lowermost two sandy soil samples are 4.69±0.14 Gy and 15.3±0.3 Gy, respectively (Table 3.3).

The quartz ages are calculated by dividing the D_e by the dose rate. The quartz ages of the sand samples range from 85±7 to 126±10 a, and are consistent with the relative stratigraphic order of the sand dune taking the uncertainties into account. The lowermost two sandy soil samples yielded OSL ages of 1.5±0.1 ka and 5.0±0.4 ka.

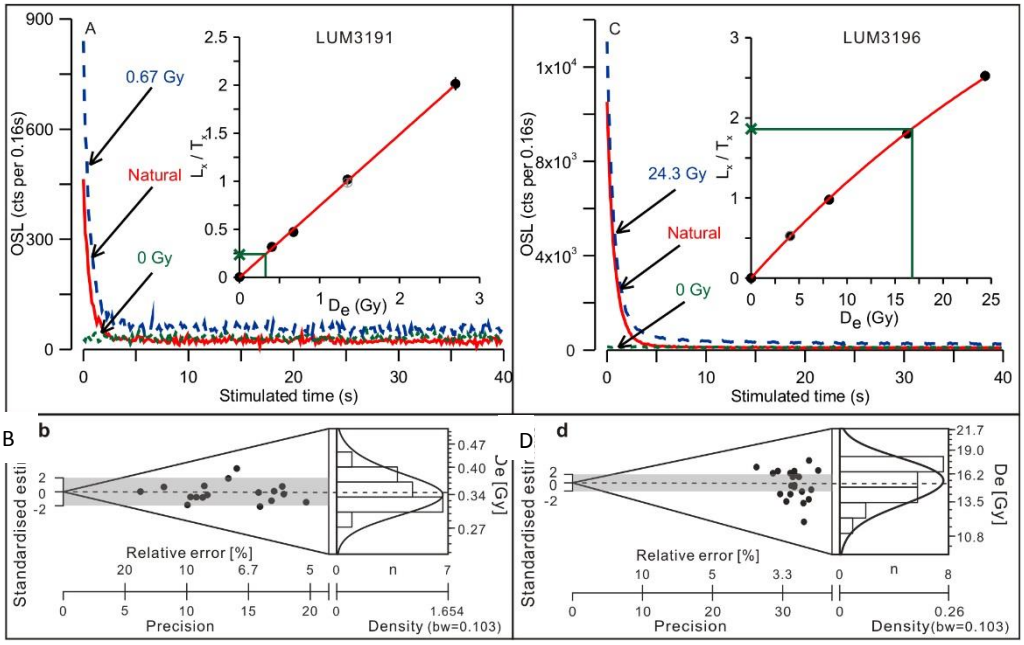

Fig. 3.4 Quartz decay curve, dose response curve and D_e distribution for sample LUM3191—(A) and (B); for sample LUM3196—(C) and (D). D_e distributions are presented using abanico plots (Dietze et al., 2016).

3.4.2 Feldspar luminescence characteristics and ages

3.4.2.1 D_e measurements and apparent ages

Representative decay curves and dose response curves of two samples are shown in Fig. 2.5. The dose response curves of the young sand samples are fitted by linear function, and those of the two sandy soil samples are fitted by single saturating exponential function. Recycling ratios of all aliquots are satisfactory within the acceptable range (0.9-1.1), and almost all of the recuperation values are below 6%. The IR_{50} and $pIRIR_{150}$ D_e distributions of one young sand sample (LUM3191) and one sandy soil sample (LUM3196) are shown in Fig. 2.5B and Fig. 2.5D. It demonstrates that the overdispersion values are generally smaller than 20% according to the central age model (Galbraith et al., 1999). The IR_{50} D_es change between 0.34±0.01 and 0.46±0.03 Gy for sand samples. Two sandy soil samples yield IR_{50} D_e values of 4.28±0.18 and 14.1±0.4 Gy respectively. The $pIRIR_{150}$ D_es range from 0.66±0.05 to 22.1±1.7

Gy, whereas the $pIRIR_{150}$ D_e of sand samples among them are between 0.66±0.05 and 0.88±0.06 Gy. The feldspar ages were subsequently calculated based on the D_e and the feldspar dose rate for each sample. The apparent IR_{50} ages of sand samples vary from 85±4 to 111±8 a, and the $pIRIR_{150}$ ages are between 145±12 and 215±18 a. Two sandy soil samples yield IR_{50} ages of 1.03±0.06 ka and 3.47±0.18 ka, and $pIRIR_{150}$ ages of 1.39±0.08 ka and 5.42±0.47 ka (Table 3.3).

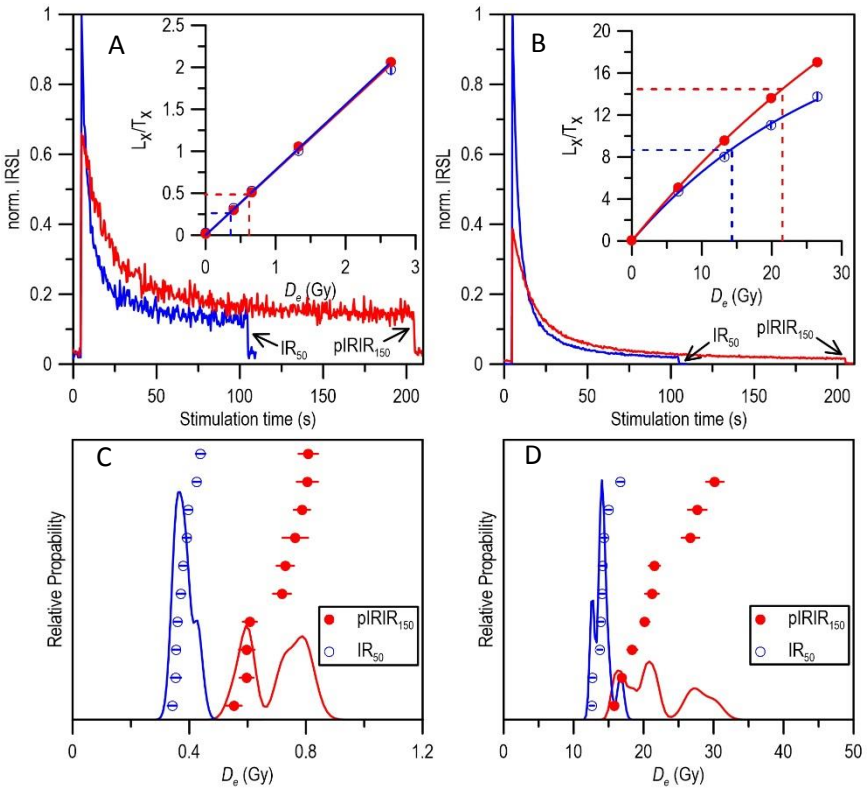

Fig. 3.5 K-feldspar IR_{50} and $pIRIR_{150}$ decay curve, growth curve and D_e distribution for sample LUM3191—(A) and (B), for sample LUM3196—(C) and (D).

The applicability of the $pIRIR_{150}$ protocol on the samples in this study was checked utilizing dose recovery and residual dose tests. Six aliquots of each sample were bleached for 4 hours in the Hönle SOL2 solar simulator. Three aliquots were measured using the $pIRIR_{150}$ protocol after given a beta dose close to the equivalent dose from D_e measurement. The other three aliquots were measured to determine the residual dose. The dose recovery ratio was calculated by dividing the measured dose by giving dose after subtraction by the residual dose. The IR_{50} dose recovery ratios vary from 0.97±0.01 to 1.01±0.01, and those of the $pIRIR_{150}$ signal are between 0.85±0.13 and 0.97±0.05. The IR_{50} and $pIRIR_{150}$ dose recovery ratios for all samples are satisfactory taking uncertainty into account, whereas the $pIRIR_{150}$ dose recovery ratio has a tendency of underestimation for especially two young sand sediments, i.e. LUM3193 and LUM3198. However, the $pIRIR_{150}$ protocol can generally recover the natural dose effectively. The IR_{50} residual doses are generally below 0.05 Gy except that of LUM3196, in a lower level compared with those of $pIRIR_{150}$ signal, which vary from 0.05±0.01 to 0.34±0.02 Gy (Fig. 3.6; Table 3.4). It should be noted that these residual doses were measured to calculate the dose

Table 3.3 Result of OSL dating.

LumNo.	Depth (cm)	Quartz				Feldspar								
						Dose rate (Gy/ka)	pIRIR$_{150}$				IR$_{50}$			
		Dose rate (Gy/ka)	D_e (Gy)	Age (a)	σ_{OD} (%)[a]		D_e (Gy)	g_{2days} (%/decade)	Age (a)	Corrected age (a)	D_e (Gy)	g_{2days} (%/decade)	Age (a)	Corrected age (a)
3197	80	3.24±0.23	0.28±0.01	87±7	6.3	4.02±0.17	0.81±0.05	0.99±0.38	202±15	214±21	0.34±0.01	8.38±0.59	85±4	145±13
3198	149	3.31±0.24	0.28±0.01	85±7	4.4	4.10±0.17	0.88±0.06	1.96±0.41	215±18	243±26	0.35±0.01	9.23±0.64	86±5	159±18
3191	380	3.13±0.23	0.34±0.01	110±9	6.6	3.96±0.17	0.68±0.03	0.38±0.28	173±10	177±14	0.38±0.01	9.18±0.52	96±5	178±17
3192	434	3.15±0.23	0.36±0.01	115±9	5.9	3.92±0.16	0.74±0.03	1.11±0.39	189±12	203±17	0.39±0.01	9.30±0.54	100±4	187±17
3193	462	3.26±0.24	0.37±0.01	114±9	12.5	4.05±0.17	0.66±0.03	0.44±0.31	164±9	168±13	0.39±0.01	9.36±0.74	96±5	181±21
3194	480	3.31±0.24	0.42±0.01	128±10	6.7	4.12±0.17	0.60±0.05	0.62±0.42	145±13	151±17	0.46±0.03	7.80±0.74	111±8	186±25
3195	511	3.19±0.22	4.69±0.14	1470±110	12.3	4.14±0.17	5.77±0.24	0.25±0.41	1390±80	1430±120	4.28±0.18	4.99±0.26	1040±60	1500±120
3196	532	3.08±0.21	15.3±0.3	4970±350	10.1	4.07±0.17	22.1±1.7	0.80±0.28	5420±470	5760±620	14.1±0.4	4.45±0.19	3480±180	4950±350

[a] σ_{OD} values were calculated according to Galbraith et al. (1999).

recovery ratio, because the given dose for the dose recovery test was added on top of the residual dose, and therefore the recovered dose should be calculated after subtracting the residual dose. Since we do not know the natural bleaching condition before burial, the measured residual doses were not subtracted from the D_e values.

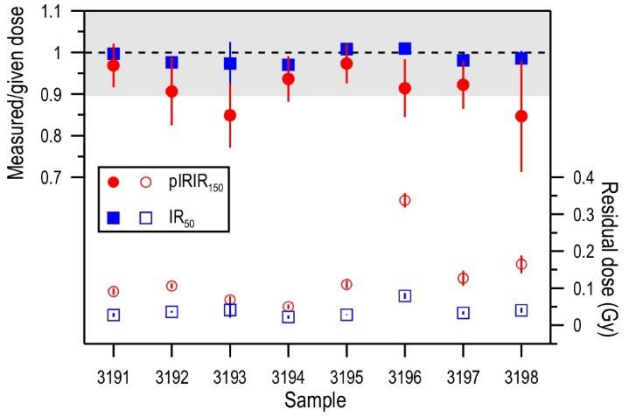

Fig. 3.6 Dose recovery ratio and residual dose for IR_{50} and $pIRIR_{150}$ for each sample.

3.4.2.2 Fading correction

A fading test following Auclair *et al.* (2003) was carried out for all eight samples with 3 aliquots of each sand sample and 6 aliquots of each sandy soil sample (Fig. 3.7). The given dose in the fading experiment was close to the $pIRIR_{150}$ equivalent dose. The delay time for $pIRIR_{150}$ fading vary from a minimum of 0.13 h to a maximum of 24.7 h, whereas that for IR_{50} fading range between 0.06 h and 24.7 h. According to Huntley and Lamothe (2001), the g_{2days} values were calculated (Table 3.3) and subsequently utilized for age correction. The g_{2days} of IR_{50} signal vary from 4.45±0.19 to 9.36±0.74%/decade. The g_{2days} values are much larger for the young sand samples (from 7.80±0.74 to 9.36±0.74%/decade) than for the sandy soil samples (from 4.45±0.19 to 4.99±0.26%/decade). The $pIRIR_{150}$ g_{2days} values are between 0.25±0.41 and 1.96±0.41%/decade, and most of the $pIRIR_{150}$ g_{2days} values are around or below 1%/decade, significantly lower than those of the IR_{50} signal. Based on the fading rates and the correction model following Huntley and Lamothe (2001), we thus corrected the apparent ages which are shown in Table 2.3. The corrected IR_{50} ages of 145±13 a to 186±25 a and the corrected $pIRIR_{150}$ ages of 151±17 a to 243±26 a for sand samples were yielded. We calculated the corrected $pIRIR_{150}$ ages of 1.43±0.12 ka and 5.76±0.62 ka, and the corrected IR_{50} ages of 1.50±0.12 ka and 4.95±0.35 ka for two sandy soil samples.

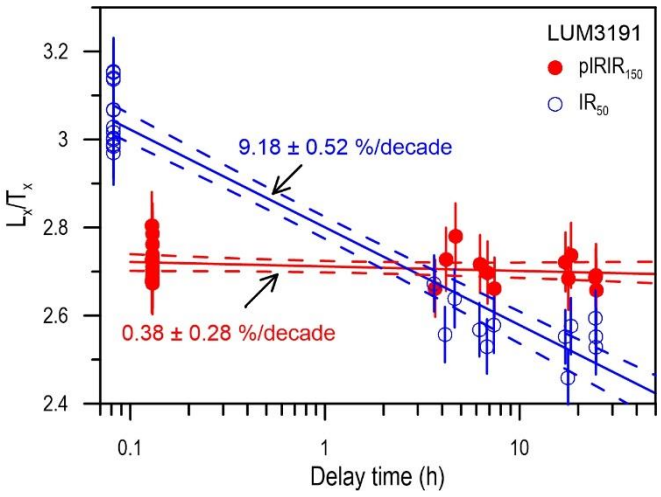

Fig. 3.7 Fading rate (g_{2days}-value) of IR_{50} and $pIRIR_{150}$ signals for one representative sample LUM3191.

3.4.3 Comparison of quartz and feldspar ages

The comparison of ages from quartz OSL, feldspar IR_{50} and $pIRIR_{150}$ signals are shown in Fig. 3.8A and B. In Fig. 3.8A, the apparent IR_{50} ages for the six sand samples are consistent with quartz ages, whereas the fading corrected IR_{50} ages are much older than the associated quartz ages. However, two sandy soil samples shown in Fig. 3.8B yielded the opposite results. The fading corrected IR_{50} ages are in agreement with quartz ages, while the apparent IR_{50} ages underestimated the quartz ages. The fading rates obtained from the fading experiment demonstrate that the sand samples (LUM3191-LUM3194, LUM3197-LUM3198) faded more significantly (g_{2days} values between 7 and 10%/decade) than the sandy soil samples (LUM3195-LUM3196; g_{2days} values from 4 to 5%/decade). The fading rates of $pIRIR_{150}$ signal are much smaller than those of IR_{50} signal, generally around or below 1%/decade. Similar fading behaviours have been observed in previous studies (e.g. Reimann et al., 2011; Long et al., 2014. Fig. 3.7). One exception is sample LUM3198, yielding a fading rate of 1.96±0.41%/decade, reveals more significant fading. The fading corrected $pIRIR_{150}$ ages for the sand samples following Huntley and Lamothe (2001) are much older than the corresponding quartz ages, whereas those for sandy soil samples are consistent with quartz ages.

Compared with the pIRIR signals with high thermal treatment (stimulated at 225 or 290 °C), the $pIRIR_{150}$ signal has an advantage of faster bleaching for dating some young deposits during the Holocene (Reimann et al., 2011; Madsen et al., 2011; Reimann and Tsukamoto, 2012). To determine the applicability of the residual subtraction by artificial bleaching of natural aliquots using solar simulator and to understand the bleaching condition before burial, we exploit the quartz OSL ages as reference, to calculate the predicted feldspar D_e following Zhang et al. (in prep.).

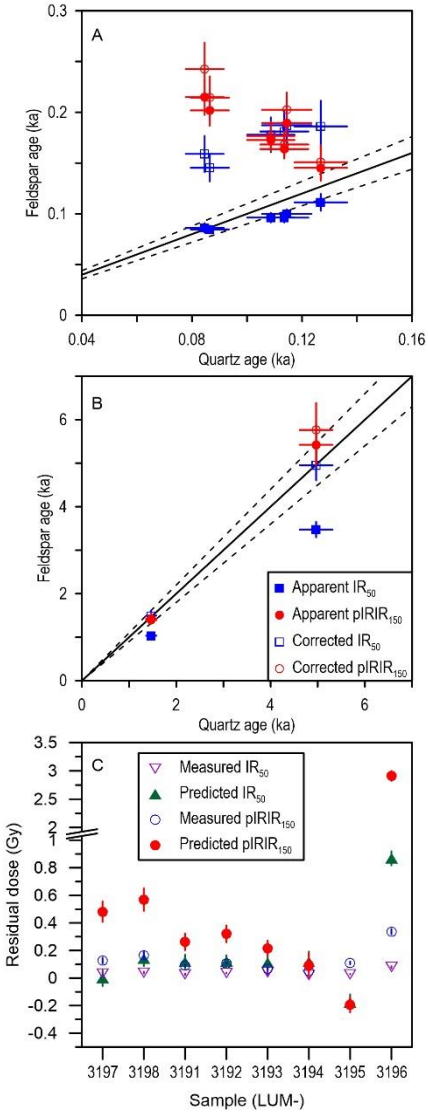

Fig. 3.8 Ages from different luminescence signals and the comparison of the predicted and measured residual doses. A shows the comparison for the sand samples, B shows the comparison for two sandy soil samples. C demonstrates the comparison of the predicted residual dose and measured dose for all samples (See details in text).

We conducted the reverse derivation to simulate the natural growth of the $pIRIR_{150}$ and the associated IR_{50} signals concerning the anomalous fading using the reference (quartz) age, the feldspar dose rate and the fading rate (Kars et al., 2008). The fading rate, feldspar dose rate and measured D_e are the input parameters. The reverse derivation was first conducted to simulate the natural growth of the IR and pIRIR signals (Kars et al., 2008). The natural trap filling was subsequently calculated according to the reference age and employed for natural D_e determination combined with the natural growth. The predicted residual dose was calculated by subtracting the measured D_e by the associated predicted natural D_e (Table 3.4; Fig. 3.8C). The predicted residual dose should be close to the unbleachable residual if the feldspar the IR_{50} and $pIRIR_{150}$ signals were completely bleached before burial. For the sand samples the predicted $pIRIR_{150}$ residual dose range from 0.09±0.09 to 0.57±0.08 Gy (i.e. 23±23 to 140±20 a), whereas the measured $pIRIR_{150}$ residual doses after 4 h bleaching in the solar simulator are between 0.05±0.01 and 0.16±0.02 Gy corresponding to 13±3 to 40±5 a, which are smaller than the predicted values. The predicted IR_{50} residual doses vary from 0.00±0.06 to 0.14±0.06

Gy (0±15 to 35±15 a), whereas the measured IR_{50} residual doses are between 0.02±0.00 and 0.04±0.02 Gy (~5 to 10±5 a). The difference between the predicted and measured residual doses for the IR_{50} signal are smaller than that of the $pIRIR_{150}$ signal, because the IR_{50} signal bleaches much faster that the $pIRIR_{150}$ signal. The predicted $pIRIR_{150}$ residual dose of 2.91±0.09 Gy and IR_{50} residual dose of 0.87±0.05 Gy for sample LUM3196 are much larger than the measured residual doses. However, the apparent and fading corrected $pIRIR_{150}$ ages and fading corrected IR_{50} age are in agreement with the quartz OSL age, because the residual dose of ~1-3 Gy for this sample is close to the uncertainty of the D_e values. The sandy soil sample LUM3195 yields negative predicted $pIRIR_{150}$ and IR_{50} residual doses of -0.19±0.06 and -0.18±0.06 Gy, while the corresponding measured residual doses are 0.11±0.01 and 0.03±0.00 Gy. The negative values of residual doses are not expected, and this was probably caused by the slight underestimation of the fading rate. But the close-to-zero predicted residual doses of this sample suggest that this sample should have been completely bleached before burial.

Table 3.4 Summary of predicted residual dose and measured residual dose (4 h SOL2 bleaching).

Sample	$pIRIR_{150}$		IR_{50}	
	Predicted residual	Measured residual	Predicted residual	Measured residual
3197	0.48 ± 0.07	0.13 ± 0.02	0.00 ± 0.06	0.03 ± 0.00
3198	0.57 ± 0.08	0.16 ± 0.02	0.14 ± 0.06	0.04 ± 0.01
3191	0.26 ± 0.06	0.09 ± 0.01	0.12 ± 0.05	0.03 ± 0.01
3192	0.32 ± 0.06	0.11 ± 0.01	0.12 ± 0.04	0.04 ± 0.00
3193	0.21 ± 0.06	0.07 ± 0.01	0.11 ± 0.05	0.04 ± 0.02
3194	0.09 ± 0.09	0.05 ± 0.01	0.12 ± 0.07	0.02 ± 0.00
3195	-0.19 ± 0.06	0.11 ± 0.01	-0.18 ± 0.06	0.03 ± 0.00
3196	2.91 ± 0.09	0.34 ± 0.02	0.87 ± 0.05	0.08 ± 0.01

The measured residual doses are generally smaller than the predicted residual doses except sample LUM3195, indicating that the natural exposure was less than the equivalent time to 4 h of SOL2 bleaching. The offsets obtained from the difference between the predicted and the measured $pIRIR_{150}$ residual doses are ~0.04-0.40 Gy (~10-100 a) for sand samples and ~2.57 Gy (~630 a) for the sandy soil sample LUM3196, which should cause the overestimation of several tens of percent for sand samples and of ~10% for the old sandy soil sample, if the measured residual dose is subtracted from the D_e value. We conclude that the use of the measured residual subtraction is not appropriate. Furthermore, it demonstrates that the effect of residual component, which is several tens of percent of the measured dose is significant for sand samples younger than 1000 a, whilst the offset of ~10% for the sandy sample becomes insignificant which is roughly equal to the uncertainty of the measured equivalent dose.

3.4.4 Chronology and cause of sand dune accumulation

All OSL ages were calculated in years (a) before 2015 (Table 3.2). All ages derived from the OSL samples are stratigraphically consistent taking uncertainty into account. In the profile a clear boundary between yellowish and grey sand can be identified, but two samples above and below the boundary, LUM3192 and LUM3193, gave almost identical ages (115±9 a and 114±9 a, respectively), indicating the PJ sand dune accumulated successively in a short time interval. The high sedimentation rate for sand deposits and low sedimentary rate for sandy soil layer are observed (Fig. 3.9). Our results are consistent with the mid-Holocene chronostratigraphy presented by Li P et al. (2014) based on radiocarbon and OSL dates of samples from a 24.5 m-long core drilled in modern Liaodong coastal landward.

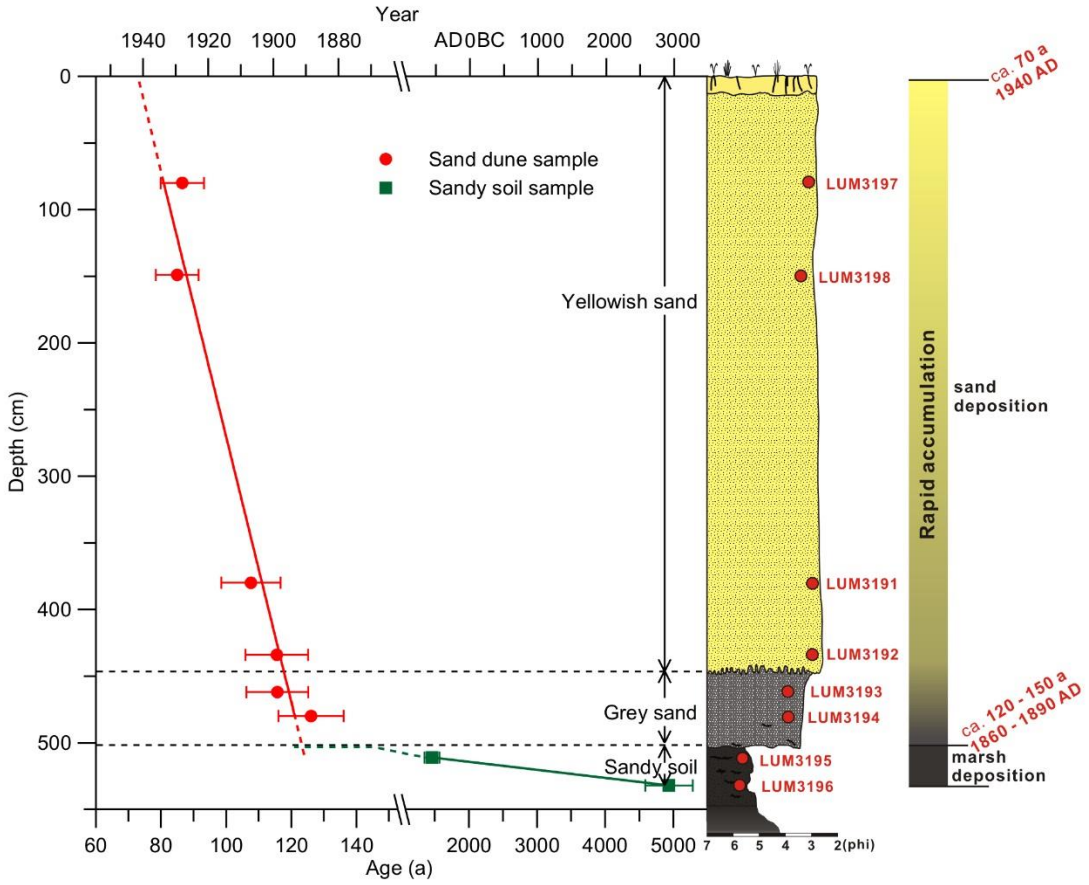

Fig. 3.9 Depth-age relationship of the PJ sand dune and sandy soil layer with a graphic log and all sample codes.

The possible depositional ages for the top and bottom of the sand dune were assumed by extrapolating the fitted age-depth relationship shown in Fig. 3.10. The results after the extrapolation show that the PJ sand dune accumulated from ca.120 a (1890 AD) to ca. 70 a (1940 AD). Although there are only two data points available, the age of the top of sandy soil was also estimated by an extrapolation, resulting in *c.* 150 a. It indicates that no major hiatus occurred during the transition of sandy soil to the sand dune.

The Holocene transgression in the Liaodong coastal area was recorded by marine sediments with buried thicknesses of 6-15 m (Fu, 1988) and 7.85 m (Bing et al., 2013) in the modern Liao River and Daling River estuaries and *c*. 4.5 m (Ma, 2014; Li P et al., 2014) in this coastal lowland near the modern Liao River estuary. The Holocene transgression range has been distinguished based on 11 cores drilled in the LLP according to Fu (1988). Three paleo-coastlines since the late Pleistocene have been reconstructed by IOCAS (1985). The timing of the sea level rise in the LLP was determined by buried shells and peat using ^{14}C (Fu, 1988; Ma, 2014) and OSL dating (Bing et al., 2013; Li P et al., 2014). These previous studies suggest that the location of the PJ sand dune was at the northern edge of the Holocene transgression and was covered by sea water at the sea level high-stand (Fig. 3.1), which occurred at 5-6 ka in the LLP (Fu, 1988). As a consequence of the sea level change during the Holocene, three main depositional units, lacustrine, marine and salt-fresh marsh deposits from early to late Holocene, can be distinguished based on stratigraphic characteristics and down-core distributions of benthic foraminifera, pollen, diatom and grain size from tens of cores drilled in the LLP (Fu, 1988; Ma, 2014; Li P et al., 2014). Using our new data we can compare the timing of sandy soil sedimentation and the sea level high-stand yielded from these previous work. The lowermost sample (LUM3196) provides an OSL age of 5.0±0.4 ka, and the site is located in the northern edge of the postulated Holocene transgression. We infer that the sandy soil section in the studied site deposited after the sea-level highstand. Furthermore, the sediments in this section consist of organic-rich material, soil aggregates and fine grains, constrained to the depositional unit of salt-fresh marsh as a consequence of sea level fluctuation during the sea-level highstand. XRD analysis of soil aggregates larger than 250 μm from LUM3196 gave an approximate mineral composition of quartz (30%), feldspar (15%), vermiculite (30%) and amorphous component (25%). The rich vermiculite component is possibly related to a moderate weathering process and warm environment (Lu, 1997). Evidence from historical documents and archaeological records which were summarized by Lin (1980) and Xiao (2010) also proved that a paleo 'Liao marsh' had widely existed in the LLP since the beginning of the Hongshan Culture (5-6 ka) and perished at the end of Qing dynasty (1860-1912 AD).

More direct evidence is available from historical records of coastline migration (Lin, 1991) and research on recent coastline evolution over the past hundred years conducted by Chen et al. (2010). Three historical military maps were made in 1909 AD, 1932 AD and 1950 AD, demonstrating the coastline change of the Liaodong Bay shown in Fig. 3.1 (Chen et al., 2010). During this period, significant progradational process occurred in the LLP. The PJ sand dune accumulated rapidly at the same time (since *c*. 1890 AD), but it was *c*. 30 km far away from the coastal area.

Previous studies on the Little Ice Age (LIA) in China showed that the last sub-cooling period of the LIA occurred during 1840-1870 AD according to Zhu (1973) and 1830-1890 AD according to Wang and

Wang (1990). Several sand deposits worldwide were correlated to the cold period in the last millennium based on accurate OSL chronology (e.g. Tamura et al., 2016, 2011; Hu et al., 2013). The mean annual temperature variation in northeastern China constructed by Wang et al. (1998) and temperature change in the Liaoning Province presented by Sun and Zhao (2002) indicate that the temperature was steadily increasing between 1880 AD and 1940 AD, indicating that the PJ sand dune accumulated during a warm period after the LIA. The oxygen isotopic record from speleothems for the last 500 years in Li et al. (1998) in northern China (Fig. 3.10) and the tree-ring record of the precipitation in the southern Liao Plain indicate an overall increasing trend with several wet and dry cycles for the precipitation. According to pollen data and historical documents, land types in the LLP were meadow, marsh (wetlands) and river prior to sand deposition (Ma, 2014). From 1860 AD, the Qing government started to open northeastern China gradually, which had been blocked for almost 200 years before 1860 AD and only a few people from central China were allowed to move into this region. The amount of population increased gradually since 1860 AD, and dramatically increased after 1890s, as a result of Immigrant and Reclamation Policy. With the leap of population and traditional cultivation, the natural vegetation in the LLP was largely destroyed. It is most likely that this caused the significant changes in the landscape, resulting in and sand dune formation. Yang et al. (2012) presented a similar sand activation around 1800 AD in Horqin dunefield which was influenced by the Immigrant and Reclamation Policy. Three phases of land cultivation during the last 2300 years in the Mu Us desert were recognized by Sun (2000). Because the sand accumulated in the relatively warm and humid period after the Little Ice Age, we conclude that the accumulation of the PJ sand dune was mostly likely to be influenced by the Immigrant and Reclamation Policy carried out by the Qing government, not due to the climate change.

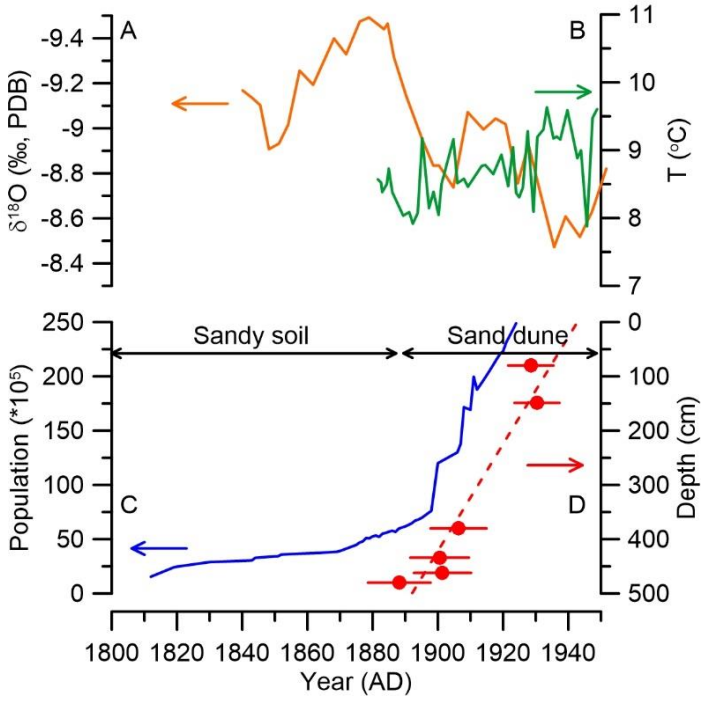

Fig. 3.10 Comparison of different proxies. (A) The precipitation variations in northern China revealed by the $\delta^{18}O$ data from the Shihua Cave stalagmites record (Li et al., 1998; orange solid line). (B) Temperature change in Liaoning Province (Sun and Zhao, 2002; green solid line). (C) Population change in Northeastern China from 1812 to 1911 AD (blue solid line) summarized by Zhao (2004). (D) Quartz OSL ages for the sand deposits.

3.5 Conclusions

A well-preserved sand dune in elapsed marine-terrestrial interacted area in northeastern China is studied in this paper. Based on the results, we conclude:

- Using OSL ages of quartz, the chronology of the PJ sand dune and underlying sandy soil layer based on quartz ages was established: The sandy soil sediments deposited after 5.0 ± 0.4 ka at an extremely low sedimentary rate. The PJ sand dune accumulated from c.120 a (1890 AD) to c.70 a (1940 AD) at a high sediment accumulation rate. There is no major hiatus between sand dune and sand soil layer.
- The quartz OSL chronology shows that the sandy soil layer formed after the sea-level highstand in the Holocene. The sandy soil layer is recognized as a marsh deposition based on the characteristics of the containing organic-rich matter and soil aggregate. Combined with historical coastline change, the PJ sand dune is an inland sand dune instead of a coastal sand dune. Under a humid and warm climate period, the PJ sand dune was very likely impacted by human activity at the end of Qing dynasty but not due to the climate change.
- The IR_{50} fading rates for six sand samples are between ~5 - 10%/decade, whilst he $pIRIR_{150}$ fading rates are generally negligible. The fading corrected IR_{50} and $pIRIR_{150}$ ages are overestimated for six sand samples, and consistent with the quartz ages for two sandy soil samples.
- The predicted residual doses obtained from the quartz OSL ages are generally larger than the measured residual doses for our samples. The use of the measured residual dose for correction is not appropriate, because the true residual dose is highly dependent on the natural bleaching condition. The $pIRIR_{150}$ dating is generally applicable for samples older than ~1000 a when the effect of residual dose becomes insignificant.

Acknowledgements

The authors are grateful to Toru Tamura and one anonymous reviewer for the helpful comments. We thank Dr. Kristian Ufer at Bundesanstalt für Geowissenschaften und Rohstoffe (BGR) in Hannover for the XRD analysis, and also thank Dr. Christine Thiel for her constructive comments. YL was supported by the China Scholarship Council (grant 201406400050).

References

Allen, M.B., Macdonald, D.I.M., Xun, Z., Vincent, S.J., Brouet-Menzies, C., 1997. Early Cenozoic two-phase extension and late Cenozoic thermal subsidence and inversion of the Bohai Basin, North China. Mar. Petrol. Geol.14, 951-972.

Auclair, M., Lamothe, M., Hout, S., 2003. Measurement of anomalous fading for feldspar IRSL using SAR. Radiation Measurement 37, 487-492.

Balescu, S., Lamothe, M., 1994. Comparison of TL and IRSL age estimates of feldspar coarse grains from waterlain sediments. Quartnerary Geochronology (Quaternary Science Reviews) 13, 437-444.

Bing, Z., Chen, X., Zhao, X., Zhao, Y., 2013. Deposition rate and sea-level fluctuations of the major estuarine areas in the coastal zone of Liaoning during ten thousand years. Geology and resources 22, 383-387. (in Chinese with English Abstract)

Bureau of geology and mineral resources of Liaoning (BGMRL), 1989. Regional geology of Liaoning Province. Beijing: Geological Publishing House. (in Chinese with English Abstract)

Buylaert, J.-P., Jain, M., Murray, A.S., Thomsen, K.J., Thiel, C., Sohbati, R., 2012. A robust feldspar luminescence dating method for Middle and Late Pleistocene sediments. Boreas 41, 435-451.

Chen, Y., Fang, G., Ni, J., Hu, K., 2010. Research on century's changes of coastlines of Liaohe Estuary. Journal of marine sciences 28, 14-21. (in Chinese with English Abstract)

Cunningham, A.C., Wallinga, J., 2010. Selection of integration time intervals for quartz OSL decay curves. Quaternary Geochronology 5, 657-666.

Dietze, M., Kreutzer, S., Burow, C., Fuchs, M.C., Fischer, M., Schmidt, C., 2016. The abanico plot: visualising chronometric data with individual standard errors. Quaternary Geochronology 31, 12-18.

Du, J., Wang, X., 2014. Optically stimulated luminescence dating of sand-dune formed within the Little Ice Age. Journal of Asian Earth Sciences 91, 154-162.

Duller, G.A.T., 2003. Distinguishing quartz and feldspar in single grain luminescence measurements. Radiation Measurements 37, 161-165.

Fang, J., Hu, K., 2007. Holocene environment and the highest sea-level based on diatom assemblages from the peat imbedded in the ditch in Dagu Mountain, Liaodong Peninsula. Quaternary sciences 27, 797-805. (in Chinese with English Abstract)

Forman, S.L., Pierson, J., 2003. Formation of linear and parabolic dunes on the eastern Snake River Plain, Idaho in the nineteenth century. Geomorphology 56, 189-200.

Fu, W., 1988. A study of the trasgression process since the late Pleistocene on the coastal zone of Lower Liaohe River Plain and Liaodong Peninsula. Geographical Research 7, 73 - 80. (in Chinese with English Abstract)

Fu, X., Li, S., 2013. A modified multi-elevated-temperature post-IR IRSL protocol for dating Holocene sediments using K-feldspar. Quaternary Geochronology 17, 44-54.

Galbraith, R.F., Roberts, R.G., Laslett, G.M., Yoshida, H., Olley, J.M., 1999. Optical dating of single and multiple grains of quartz from Jinmium rock shelter, Northern Australia: part 1, experimental details and statistical models. Archaeometry 41, 339-364.

Guérin, G., 2011. Dose-rate conversion factors: update. Ancient TL 29, 5-8.

Hu, F., Li, Z., Jin, J., Zhao, Q., Zhang, H., Wang, X., Xia, J., Chen, X., 2013. Coastal environment evolution record from Anshan coastal aeolian sand of Jinjiang, Fujian Province, based on the OSL dating. Acta Geographica Sinica 68, 343-356 (in Chinese with English abstract).

Huntley, K., Baril, M.R., 1997. The K content of the K-feldspars being measured in optical or in TL dating. Ancient TL 15, 11-13.

Huntley, D.J., Hancock, R.G.V., 2001. The Rb contents of the K-feldspar grains being measured in optical dating. Ancient TL 19, 43-46.

Huntley, D.J., Lamothe, M., 2001. Ubiquity of anomalous fading in K-feldspars and the measurement and correction for it in optical dating. Canadian Journal of Earth Sciences 38, 1093-1106.

IOCAS, 1985. Bohai Sea Geology. Science Press, Beijing. (in Chinese with English Abstract)

Kars, R.H., Wallinga, J., Cohen, K.M., 2008. A new approach towards anomalous fading correction for feldspar IRSL dating-tests on samples in field saturation. Radiation Measurement 43, 786-790.

Kunz, A., Frechen, M., Ramesh, R., Urban, B., 2010. Luminescence dating of late Holocene dunes showing remnants of early settlement in Cuddalore and evidence of monsoon activity in south east India. Quaternary International 222, 194-208.

Li, B., Jacobs, Z., Roberts, R. G., Li, S., 2014. Review and assessment of the potential of post-IR IRSL dating methods to circumvent the problem of anomalous fading in feldspar luminescence. Geochronometria 41, 178-201.

Li, P., Xu Y.; Li P., 2014. Evolution of paleoenvironment since late Pleistocene 24 ka of LH01 core in the northern Liaodong Bay. Advances in Marine Science 32. (in Chinese with English Abstract)

Li, H., Gu, D., Stott, L. D., 1998. Application of interannual-resolution stable isotope records of speleothem: climatic changes in Beijing and Tianjin, China during the past 500 years – the $\delta^{18}O$ record. Science in China (Series D) 41, 362-368.

Lin, T., 1980. Wetlands in the Liao River Plain. Journal of Xiamen University, 4, 141-147. (in Chinese with English Abstract)

Lin, T., 1991. Coastline change in the Liaodong Bay. Collections of Essays on Chinese Historical Geography 2, 1-13. (in Chinese with English Abstract)

Liu, J., Saito, Y., Wang, H., Zhou, L., Yang, Z., 2009. Stratigraphic development during the Late Pleistocene and Holocene offshore of the Yellow River delta, Bohai Sea. Journal of Asian Earth Sciences 36, 318-331.

Long, H., Haberzettl, T., Tsukamoto, S., Shen, J., Kasper, T., Daut, G., Zhu, L., Mäusbacher, R., Frechen, M., 2015. Luminescence dating of lacustrine sediments from Tangra Yumco (southern Tibetan Plateau) using post-IR IRSL signals from polymineral grains. Boreas 44, 139-152.

Long, H., Shen, J., Tsukamoto, S., Chen, J., Yang, L., Frechen, M., 2014. Dry early Holocene revealed by sand dune accumulation chronology in Bayanbulak Basin (Xinjiang, NW China). The Holocene 24, 614-626.

Lu, J., 1997. soil geology. Geological publishing house, Beijing. (in Chinese with English Abstract)

Ma, H., 2014. Holocene environmental changes of Liao River delta. Jilin University, Jilin, China, p. 33. (in Chinese with English Abstract)

Madsen, A., Buylaert, J.-P., Murray, A., 2011. Luminescence dating of young coastal deposits from New Zealand using feldspar. Geochronometria 38.

Madsen, A.T., Murray, A.S., 2009. Optically stimulated luminescence dating of young sediments: A review. Geomorphology 109, 3-16.

Madsen, A.T., Murray, A.S., Andersen, T.J., Pejrup, M., Breuning-Madsen, H., 2005. Optically stimulated luminescence dating of young estuarine sediments: a comparison with 210Pb and 137Cs dating. Marine Geology 214, 251-268.

Mejdahl, V., 1979. Thermoluminescence Dating: Beta-Dose Attenuation in Quartz Grains. Archaeometry 21, 61-72.

Murray, A.S., Wintle, A.G., 2003. The single aliquot regenerative dose protocol: potential for improvements in reliability. Radiation Measurements 37, 377-381.

Murray, A.S., Wintle, A.G., 2000. Luminescence dating of quartz using an improved single-aliquot regenerative-dose protocol. Radiation Measurements 32, 57-73.

Prescott, J.R., Hutton, J.T., 1994. Cosmic ray contributions to dose rates for Luminescence & ESR dating: large depth & long-term time variations. Radiation Measurements 23, 497-500.

Reimann, T., Tsukamoto, S., 2012. Dating the recent past (<500 years) by post-IR IRSL feldspar – Examples from the North Sea and Baltic Sea coast. Quaternary Geochronology 10, 180-187.

Reimann, T., Tsukamoto, S., Naumann, M., Frechen, M., 2011. The potential of using K-rich feldspars for optical dating of young coastal sediments – A test case from Darss-Zingst peninsula (southern Baltic Sea coast). Quaternary Geochronology 6, 207-222.

Reimann, T., Tsukamoto, S., Harff, J., Osadczuk, K., Frechen, M., 2011. Reconstruction of Holocene coastal foredune progradation using luminescence dating - An example from the Świna barrier (southern Baltic Sea, NW Poland). Geomorphology 132, 1-16.

Rodnight, H., 2008. How many equivalent dose values are needed to obtain a reproducible distribution? Ancient TL 26, 1-9.

Sun, F., Zhao, C., 2002. Characteristics of temperature variations for recent a hundred years in Liaoning Province. Liaoning meteorological quarterly 3, 14, 22. (in Chinese with English Abstract)

Sun J., 2000. Origin of Eolian Sand Mobilization during the Past 2300 Years in the Mu Us Desert, China. Quaternary Research 53: 78-88.

Tamura, T., Kodama, Y., Bateman, M. D., Saito, Y., Yamaguchi, N., Matsumoto, D. 2016. Late Holocene aeolian sedimentation in the Tottori coastal dune field, Japan Sea, affected by the East Asian winter monsoon. Quaternary International, v. 397, pp. 147-158.

Tamura, T., Bateman, M.D., Kodama, Y., Saitoh, Y., Watanabe, K., Yamaguchi, N., Matsumoto, D., 2011. Building of shore-oblique transverse dune ridges revealed by ground-penetrating radar and optical dating over the last 500 years on Tottori coast, Japan Sea. Geomorphology 132, 153-166.

Thiel, C., Buylaert, J.-P., Murray, A.S., Terhorst, B., Hofer, I., Tsukamoto, S., Frechen, M., 2011. Luminescence dating of the Stratzing loess profile (Austria)–Testing the potential of an elevated temperature post-IR IRSL protocol. Quaternary International 234, 23-31.

Thomsen, K. J., Murray, A. S., Jain, M., Bøtter-Jensen, L., 2008. Laboratory fading rates of various luminescence signals from feldspar-rich sediment extracts. Radiation Measurements 43, 1474-1486.

Wang, H., Fan, C., 2005. The 14C database (II) on the circum-Bohai sea-coast. Quaternary Sciences 25, 141-156. (in Chinese with English Abstract)

Wang, H., Li, F., Fan, C., Frechen, M., M., v.S., Fei, D., Wang, Y., 2004. The 14C database (I) on the circum-Bohai sea-coast. Quaternary Sciences 24, 601-613. (in Chinese with English Abstract)

Wang, S., Wang, R., 1990. Variations of seasonal and annual temperatures during 1470 - 1979 AD in eastern China. Acta Meteorologica Sinica 48, 26-35. (in Chinese with English Abstract)

Wang, S., Ye, J., Gong, D., Zhu, J., Yao, T., 1998. Construction of mean annual temperature series for the last one hundred years in China. Quarterly journal of applied meteorology 9, 392-401. (in Chinese with English Abstract)

Wintle, A.G., Murray, A.S., 2006. A review of quartz optically stimulated luminescence characteristics and their relevance in single-aliquot regeneration dating protocols. Radiation Measurements 41, 369-391.

Xiao, Z., 2010. Change of geographical range of Liao Ze in history. China's boarder land history and geography studies 20, 106-114. (in Chinese with English Abstract)

Xu, J., 1994. Changes of sea level and chenier along Huanghua beach of the Bohai bay. Acta Oceanologica Sinica, 68-77. (in Chinese with English Abstract)

Xue, C., 2009. Historical Changes of Coastlines on West and South Coasts of Bohai Sea since 7 000 a B. P. Scientia Geographica Sinica 29, 217-222. (in Chinese with English Abstract)

Xue, C., Ding, D., 2008. Weihe River-Mihe River delta in South Coast of Bohai Sea, China: Sedimentary Sequence and Architecture. Scientia geographica sinica 28, 672-676. (in Chinese with English Abstract)

Yang, L., Long, H., Yi, L., Li, P., Wang, Y., Gao, L., Shen, J., 2015. Luminescence dating of marine sediments from the Sea of Japan using quartz OSL and polymineral pIRIR signals of fine grains. Quaternary Geochronology 30, 257-263.

Yang, L., Wang, T., Zhou, J., Lai, Z., Long, H., 2012. OSL chronology and possible forcing mechanisms of dune evolution in the Horqin dunefield in northern China since the Last Glacial Maximum. Quaternary Research 78, 185-196.

Yao, Z., Guo, Z., Chen, Y., Xiao, G., Shao, Y.X., Wang, X.L., Hao, Q., Lu, Y.C., 2006. Magnetostratigraphy of marine-terrigenous facies deposits in Bohai Bay. Marine Geology and Quaternary Geology 26, 9-15. (in Chinese with English Abstract)

Yi, L., Deng, C., Xu, X., Yu, H., Qiang, X., Jiang, X., Chen, Y., Su, Q., Chen, G., Li, P., Ge, J., Li, Y., 2015. Paleo-megalake termination in the Quaternary: Paleomagnetic and water-level evidence from south Bohai Sea, China. Sedimentary Geology 319, 1-12.

Yi, L., Yu, H., Ortiz, J. D., Xu, X., Chen, S., Ge, J., Hao, Q., Yao, J., Shi, X., Peng, S., 2012. Late Quaternary linkage of sedimentary records to three astronomical rhythms and the Asian monsoon, inferred from a coastal borehole in the south Bohai Sea, China. Palaeogeography, Palaeoclimatology, Palaeoecology 329–330, 101-117.

Zhang, J., Tsukamoto, S., Grube, A., Frechen, M., 2014. OSL and 14C chronologies of a Holocene sedimentary record (Garding-2 core) from the German North Sea coast. Boreas 43, 856-868.

Zhao, S., Yang, G., Cang, S., Zhang, H., Huang, Q., Xia, D., Wang, Y., Liu, F., Liu, C., 1978. On the marine stratigraphy and coastlines of the western coast of the gulf of Bohai. Oceanologia and Liminologia Sinica 9. (in Chinese with English Abstract)

Zhao, X., Geng, X., Zhang, J., 1979. Sea level changes of the eastern China during the past 2000 years. Acta Oceanologia Sinica, 269-281. (in Chinese with English Abstract)

Zhao, Y., 2004. The quantitative analysis population in the northeast China of Qing Dynasty. Population journal 146, 49-53. (in Chinese with English Abstract)

Zhu, K., 1973. A primary study on climatic change in past 5000 years in China. Science in China, Ser. A, 2, 168-189. (in Chinese with English Abstract)

Chapter 4 Quartz and K-feldspar luminescence dating of sedimentation in the North Bohai coastal area (NE China) since the late Pleistocene

Yan Li [1,2], Zhiwen Shang [3], Sumiko Tsukamoto [1], Toru Tamura [4], Liang Yi [5], Hong Wang [3], Manfred Frechen [1,2], Jianfen Li [3], Xingyu Jiang [3]

[1]Leibniz Institute for Applied Geophysics (LIAG), Hanover, 30655, Germany

[2]Free University of Berlin, Berlin, 12249, Germany

[3]Tianjin Centre of Geological Survey, China Geological Survey, Tianjin, 300170, China

[4]Geological Survey of Japan, AIST, Central 7, 1-1-1 Higashi, Tsukuba City 305-8567, Japan

[5]State Key Laboratory of Marine Geology, Tongji University, Shanghai, 200092, China

Published in ***Journal of Asian Earth Sciences***

Volume 152 (February 2018), pages 103-115

https://doi.org/10.1016/j.jseaes.2017.10.036

Chapter 5 Timing of the three transgressions in the Bohai Coast since the Middle Pleistocene by luminescence dating

Yan Li[1,2,*], Sumiko Tsukamoto[1], Zhiwen Shang[3], Hong Wang[3], Manfred Frechen[1,2]

[1]Leibniz Institute for Applied Geophysics (LIAG), 30655 Hannover, Germany

[2]Free University of Berlin, 12249 Berlin, Germany

[3]Tianjin Centre of Geological Survey, China Geological Survey, 300170 Tianjin, China

Abstract

Three major Quaternary transgressions documented in the sediment record of the modern Bohai Coast have been widely recognised. However, there is no consensus of the timing of these transgressions. Optically Stimulated Luminescence (OSL) dating using multiple luminescence signals was carried out on a sediment core to figure out the chronological framework of the three major transgressions in the Bohai Coast. Reliabilities of the luminescence ages were firstly investigated in terms of 1) signal bleaching and 2) anomalous fading for the feldspar infrared stimulated luminescence signals. Our results show that the quartz OSL and K-feldspar $pIRIR_{225}$ signals were generally well bleached. The laboratory determined fading rates of ca. 1-1.5 %/decade for the K-feldspar $pIRIR_{290}$ signal reflect an actual fading process instead of the previous statement of laboratory artefact. The quartz OSL dating is applicable within ca. 50 ka, and dating upper limits for the K-feldspar $pIRIR_{225}$ and $pIRIR_{290}$ could reach to ca. 300 ka. The fine-grained polymineral pIRIR dating yields lower upper dating limit than that for the coarse-grained K-feldspar. The reliable quartz OSL and K-feldspar $pIRIR_{225}$ ages were used to reconstruct the accumulation history in the Bohai Coast. The earliest transgression correlates to the Marine Isotope Stage (MIS) 7, and the second transgression probably started from MIS 5. The latest transgression was triggered by the Holocene sea-level rise. According to the Bacon age-depth model, a sedimentation rate (SR) of ca. 0.2-0.3 m/ka is estimated for the duration between 250 and 30 ka. The sedimentation rate increased dramatically during the last deglaciation.

Keywords: transgression, luminescence dating, K-feldspar post-IR IRSL, anomalous fading, Bohai Coast

5.1 Introduction

The semi-enclosed Bohai Sea, located in northeastern China and at the west margin of the Pacific Ocean, is sensitive to the marine-terrestrial interaction due to the shallow water depth of ca. 20 m (Fig. 5.1). The thick sediments deposited in the Bohai sediment basin have been widely studied in respect of Quaternary sedimentary processes and climate changes (e.g. IOCAS, 1985, Liu et al., 2009, 2016; Shi et al., 2016; Yao et al., 2014; Yi et al., 2012, 2015). Three major transgressive layers were identified in a wealth of onshore cores using micro- or macro-fossils (IOCAS, 1985; Yi et al., 2012). The cyclical transgression-regression sequences were triggered by the glacio-eustatic sea-level fluctuations over the last 1 Ma (Shi et al., 2016) postdating the subsidence of the Miaodao Archipelago (Yi et al., 2015, 2016). The maximum range for each transgression has been determined by stratigraphic correlation of buried transgressive strata (Fig. 5.1. IOCAS, 1985; Liaoning Geology Bureau, 1983; Wang et al., 1986; Zhao et al., 1986).

It is crucial to determine the timing of each transgression for further climatological and geological interpretations. Several dating approaches have been exploited to date the transgression-regression

cycles in the Bohai Coast. The palaeomagnetic dating results show that the three transgressions postdated the Brunches-Matuyama reversal (Yi et al., 2015; Liu et al., 2016). Radiocarbon chronology restricted the three transgressions to Marine Isotope Stages 5, 3 and 1, respectively. However, radiocarbon dates for the earlier two transgressions are doubtful, as they are in general at the dating limit (~40 cal ka BP. Long et al., 2015; Pigati et al., 2007; Yi et al., 2013). Optically Stimulated Luminescence (OSL) was applied to determine the timing of transgressions largely in the South and West Bohai Coast using quartz and K-feldspar. The quartz OSL ages are consistent with radiocarbon dates for the latest transgression (T-1), and timing of the second transgression (T-2) was modified to MIS 5-3 by quartz OSL dating (Chen et al., 2008; Yi et al., 2013. Fig. 5.2). Nevertheless, the quartz OSL ages for the earliest transgression (T-3) are underestimated (Chen et al., 2008; Liu et al., 2016; Yan et al., 2006), as indicated by the dating upper limit at a maximum of ca. 50-100 ka for quartz, yielded using the saturation dose of ca. 200 Gy with typical dose rate of ca. 2-4 Gy/ka in Bohai (Chen et al., 2008; Liu et al., 2016; Timor-Gabor et al., 2010; Yi et al., 2013). Alternatively, the K-feldspar infrared stimulated luminescence (IRSL) signal could extend dating range. However, the published K-feldspar luminescence ages for a coastal core in Chen et al., (2012) are regarded unreliable owing to the problems of partial bleaching and anomalous fading. Therefore, the onset timing of the transgressions since middle Pleistocene has not been well constrained by numerical dating.

Although K-feldspar IRSL signal is a promising method to extend dating range, it is hampered by anomalous fading which results in age underestimation. To overcome anomalous fading for K-feldspar IRSL, the novel two-step and multi-elevated temperature (MET) post-IR IRSL (pIRIR) signals are regarded more athermally stable and have less fading with the increase of stimulation temperature (Buylaert et al., 2009; Li and Li, 2011; Thomsen et al., 2008; Zhang et al., 2015). The two-step pIRIR signals stimulated at 290 °C ($pIRIR_{290}$) and MET-pIRIR signal stimulated at 250 °C ($MET\text{-}pIRIR_{250}$) show negligible fading (Thiel et al., 2011; Li and Li, 2011). However, the pIRIR signal appears to be more difficult to bleach with the increase of the stimulation temperature (e.g. Colarossi et al., 2015; Kars et al., 2014), which could result in age overestimation. In addition, to the contrary of the former observation (Thiel et al., 2011), significant fading for the $pIRIR_{290}$ signal was measured in the laboratory (e.g. Li et al., 2014 and reference therein; Li et al., in press). It thus requires further investigations to understand fading for the pIRIR signal at very high stimulation temperature. An alternative way is to date the sediments using the lower-temperature stimulated pIRIR signals with proper fading correction models (Huntley and Lamothe, 2001; Lamothe et al., 2003; Kars et al., 2008). It seems to be more reasonable, especially for sediments with potential bleaching problem (e.g. water-lain sediments). The fading correction method following Huntley and Lamothe (2001) is theoretically applicable for ages not older than 20-50 ka. The recent Kars et al. (2008) model, on the basis of quantum-mechanical

tunnelling model (Huntley, 2006), is applicable to correct ages close to field saturation (Kars et al., 2009; Li et al., in press; Li et al., in prep.).

In this study, we exploit luminescence dating on a 100-m core (LZK06) to determine the timing of the three transgressions in the Bohai Coast after validations of the K-feldspar pIRIR dating for the Bohai sediments using materials from the upper 20 m of core LZK06 in Li et al. (in press). Samples collected from the interval of 20-100 m in core LZK06 are carefully dated in this study. The degree of signal bleaching for the three young 'T-2' samples is assessed by comparison of the quartz OSL, K-feldspar $pIRIR_{150}$ and $pIRIR_{225}$ ages. K-feldspar samples below the second transgression layer were measured using the $pIRIR_{225}$ and $pIRIR_{290}$ protocols. The degree of bleaching and fading for the pIRIR signals are fully investigated. The luminescence age-based age-depth model is subsequently built to determine the timing of the transgressions and to reconstruct the accumulation history in the Bohai Coast.

5.2 Study area and materials

5.2.1 Geological settings

The Bohai Sea consists of the Central basin, Bohai strait and three bays: the Liaodong Bay (north), Bohai Bay (west) and Laizhou Bay (south). The entire Bohai sediment basin, comprising the Bohai Sea and the adjacent coastal plains, is surrounded by the Yanshan Orogen, Jiao-Liao Uplift and Luzhong Mountain (Fig. 5.1). Large amount of sediments were transported by the local streams and deposited in the Bohai sediment basin as a consequence of subsidence since the late Cenozoic (Allen et al., 1997). The North Bohai Coast is part of the Lower Liaohe Plain, receiving sediments from the local streams, such as the Liaohe, Dalinghe, Daliaohe and Xiaolinghe Rivers. The upper succession with a thickness of 300-400 m comprises a wealth of information to understand the Quaternary climate change and environmental evolution (IOCAS, 1985).

5.2.2 Core LZK06 and sampling strategy

The borehole LZK06 is located in the west Lower Liao Plain. It is situated on the east bank of the modern channel of the Dalinghe River, 10 km north to the estuary. The core was drilled in June 2015. The length of the core is 100 m and the recovery rate is approximately 92%. The upper 60 m of core LZK06 is studied in this thesis and described below.

0-0.7 m, artificially filled layer.

0.7-3.8 m, yellowish silt with high moisture, including vegetation fragments at 1.6 m.

3.8-4.7 m, horizontally bedded grey clayey silt with a thin organic-rich layer, containing vegetation and mollusc fragments in millimetre scale throughout the layer.

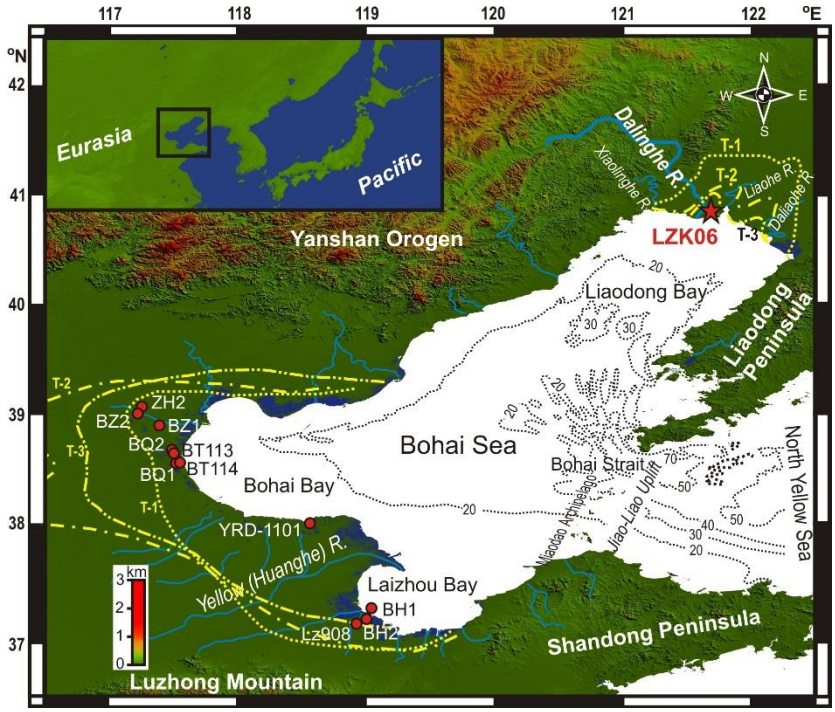

Fig. 5.1 The Bohai Sea and location of borehole. The three transgression ranges (T-1, T-2 and T-3) in the Bohai Coast are modified from Wang et al. (1986) and Zhao et al. (1986). The main local streams and OSL dated cores are shown. The studied core LZK06 is located in the North Bohai Coast, fed mainly by the Dalinghe River. The inset shows the location of Bohai Sea, as the transition area between the Eurasia and Pacific.). The OSL dated coastal cores are from Chen et al. (2008) (BZ1 and BZ2), Chen et al. (2012) (BT113 and BT114), Liu et al. (2016) (YRD-1101), Yan et al. (2006) (BQ1 and BQ2), Yi et al. (2013) (Lz908, BH1 and BH2), Zhao et al. (2002) (ZH2).

4.7-8.4 m, grey silty fine sand to fine sand (coarsening-upwards) with high moisture. It contains Umbonium thomasi, Potamocorbula laevis shells and mollusc fragments in millimetre scale.

8.4-9.7 m, grey lenticular bedded clay and silt with several high-moist sand intercalations, containing mollusc fragments.

9.7-10.7 m, high-moist grey fine sand with vegetation fragments at the bottom. It contains Mactra veneriformis and Umbonium thomasi shells and numerous mollusc fragments in millimetre scale.

10.7-12.2 m, this layer contains high-moist sand layer with mollusc fragments (12.1-12.2 m), fining-upwards silt-clay with thin sand intercalations and one Potamocorbula laevis shell (11.5-12.1 m), clayey silt-sand interlayers with ripples (11.2-11.5 m), parallel clay-silt layer with lenticulars sands (10.9-11.2 m), and silty clay with rich organic matters (11.7-11.9 m).

12.1-13.6 m, grey silty sand with high moisture and rich in mollusc fragments, including lens-like intercalations of silt from 12.4 to 13.0 m.

13.6-15.5 m, grey clayey silt and silt. The uppermost 20 cm is blackish grey organic-rich silty clay layer.

15.5-20.0 m, light grey silt to fine sand (fining-upwards) with high moisture, containing organic rich matters at the bottom.

20.0-20.8 m, core absence.

20.8-21.1 m, grey silt with clay aggregates and mollusc shells.

21.1-23.5 m, high-moist fine sand without bedding, containing shell fragments.

23.5-24.3 m, silty clay with silt pellets and shell fragments.

24.3-27.0 m, high-moist fine sand with Genus Potamocorbula shell and shell fragments. No bedding.

27.0-27.7 m, core absence.

27.7-28.7 m, blackish-grey clayey silt layer (fining-upwards). It is rich in mollusc shells and the basal well-rounded carbonate concretions (diameter of ca. 4 cm). It overlies the lower sand layer with an erosional surface.

28.7-29.0 m, light grey sand layer. No bedding.

29.0-30.1 m, core absence.

30.1-34.5 m, massive fine sand with high-moisture.

34.5-35.0 m, medium-fine sand (fining-upwards) with carbonate concretions.

35.0-39.0 m, medium-find sand with high moisture. A well-rounded carbonate concretion (2 cm) is found at depth of 35.8 m.

39.0-40.0 m, dark-grey clay with small carbonate concretions, fining-upwards.

40.0-42.1 m, brownish-grey silt-clay with silt pellets and interlayers.

42.1-43.2 m, grey clay with carbonate concretions.

43.2-47.0 m, fining upwards medium-fine sand with small carbonate concretions in the upper 40 cm.

47.0-48.6 m, massive fine-medium sand.

48.6-49.0 m, core absence.

49.0-49.6 m, blackish-grey coarse sand layer with mollusc shells and gravels, highly moist.

49.6-50.4 m, medium sand with gravel and shell fragments in millimetre size.

50.4-56.0 m, grey medium sand, including a dark-grey clay interlayer occurring at 51.6-51.8 m. No bedding.

56.6-59.6 m, grey fine-medium sand from 56.6 to 59.2 m, overlying a coarse sand bedded layer with gravels. This layer is unconformably contacted with the underlying layer.

59.6-60.0 m, light grey clay layer. No bedding.

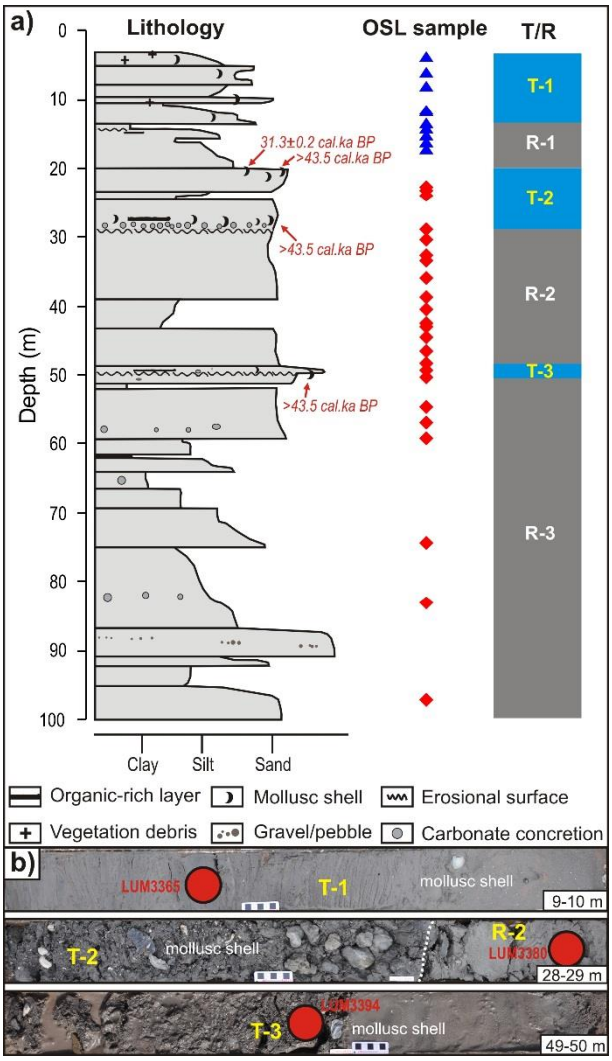

Fig. 5.2 Lithology of core LZK06. a) shows the lithological variations, OSL sample positions and definition of transgression or regression layers. Radiocarbon dates for the lower two transgression layers are shown (Shang et al., in prep.). b) shows pictures of the representative transgressive deposits. The position of OSL samples, mollusc shells and boundary between R-2 and T-2 are sketched.

All the OSL samples were collected using stainless steel cylinders. The cylinders fully filled with sediments were covered and sealed with black plastic sheets and tapes to prevent light exposure. 24 OSL samples were collected between 20 and 100 m of core LZK06 (Fig. 5.2). It is not possible to collect OSL samples from the losse lower T-2, and only three samples were taken from the upper T-2. 18 OSL samples were collected with high resolution from 28.9 to 60.0 m, including R-2 (28.9-49.0 m), T-3 (49.0-50.1 m) and the upper R-3 (50.1-60.0 m). The three lowermost samples, LUM3417, LUM3425 and LUM3435, were taken at depths of 74.73 m, 83.52 m and 97.64 m, respectively, to investigate the upper limits of luminescence dating.

5.3 Methods

5.3.1 Sample preparation

The OSL samples were prepared in the subdued red light-equipped luminescence laboratory at the Leibniz Institute for Applied Geophysics (Hannover, Germany). The quartz and K-feldspar fractions with grain size intervals of 100-150, 100-200, 150-200 or 150-250 μm were separated from the coarse-grained samples. The inner non-light exposed material in the cylinder was collected for luminescence dating (Table 5.1). The fine silt fraction (4-11 μm) in the FG samples was separated by Stokes' settling. Detailed preparation procedures can be found in Li et al. (in press). We exploited large aliquots with diameters of 6 and 2.5 mm for CG quartz and K-feldspar measurement, respectively, by mounting the grains on stainless steel discs using silicone oil as adhesive. FG quartz and polymineral fractions were settled from distilled water onto aluminium discs for measurement.

Table 5.1 Dose rate determination.

Sample	Depth (m)	Grain size (μm)	U (ppm)	Th (ppm)	K (%)	Water content (%)	Dose rate (Gy/ka)	
							K-feldspar	quartz
LUM3377	22.93	150-200	1.28±0.09	5.25±0.31	2.93±0.17	30±10	3.39±0.18	2.63±0.22
LUM3378	23.50	4-11	2.47±0.16	10.16±0.58	2.41±0.14	20±5	3.80±0.19	3.45±0.19
LUM3379	24.06	4-11	2.54±0.16	10.33±0.60	2.32±0.14	20±5	3.76±0.19	3.40±0.19
LUM3380	28.95	150-200	1.79±0.12	3.71±0.25	2.62±0.15	20±10	3.40±0.20	
LUM3381	30.59	150-200	1.94±0.12	3.05±0.20	2.55±0.15	20±10	3.50±0.20	
LUM3382	32.90	100-200	1.84±0.12	4.48±0.29	2.80±0.16	20±10	3.92±0.21	
LUM3383	33.68	150-200	2.05±0.13	6.09±0.37	2.06±0.12	20±10	3.14±0.19	
LUM3384	36.14	150-200	1.02±0.07	4.02±0.24	2.92±0.16	20±10	3.50±0.20	
LUM3385	38.84	150-200	1.75±0.12	4.63±0.29	3.22±0.18	20±10	4.18±0.22	
LUM3386	39.32	4-11	2.74±0.16	10.90±0.62	2.32±0.14	15±5	4.07±0.21	
LUM3388	41.80	4-11	1.85±0.12	9.39±0.54	2.30±0.14	15±5	3.61±0.19	
LUM3390	43.22	4-11	1.93±0.13	8.63±0.51	2.39±0.14	15±5	3.64±0.19	
LUM3391	44.82	150-200	0.86±0.07	3.09±0.21	2.64±0.15	20±10	3.19±0.20	
LUM3392	46.90	150-200	1.28±0.10	3.91±0.26	2.79±0.17	20±10	3.44±0.20	
LUM3393	48.52	150-200	1.03±0.07	3.30±0.23	2.76±0.16	20±10	3.33±0.20	
LUM3394	49.64	100-200	1.67±0.11	8.23±0.49	2.44±0.14	30±10	3.81±0.22	
LUM3395	50.72	150-250	1.18±0.08	5.03±0.32	2.44±0.14	20±10	3.18±0.22	
LUM3398	54.90	150-200	0.78±0.06	3.44±0.23	3.08±0.17	20±10	3.55±0.20	
LUM3399	57.32	150-200	1.05±0.07	4.41±0.27	3.00±0.17	20±10	3.59±0.20	
LUM3400	59.50	100-200	1.00±0.07	4.75±0.30	2.60±0.15	20±10	3.31±0.20	
LUM3401	59.90	4-11	1.49±0.11	7.30±0.46	2.00±0.13	15±5	3.01±0.17	
LUM3417	74.75	150-200	1.27±0.10	5.23±0.33	2.73±0.16	20±10	3.46±0.19	
LUM3425	83.54	150-200	0.82±0.07	3.54±0.24	2.58±0.15	20±10	3.16±0.20	
LUM3435	97.66	150-200	1.21±0.08	5.87±0.34	3.03±0.17	20±10	3.73±0.20	

5.3.2 Equipment and protocols

The measurements were carried out on an automated Risø TL/OSL system (DA-15) equipped with a $^{90}Y/^{90}Sr$ beta source with a dose rate of ca. 0.1 Gy/s. The quartz grains were stimulated using blue light-emitting diodes (LEDs, 470±30 nm), and the OSL signal was detected through a 7.5 mm Hoya U-340

filter. The emitted signals of CG K-feldspar and FG polymineral grains were detected through a combined blue filter pack (Schott BG-39 and Corning 7-59) after stimulation using infrared (870±40 nm) LEDs.

The single-aliquot regenerative dose (SAR) protocol was applied for quartz OSL dating (Table 5.2; Murray and Wintle, 2000, 2003). The quartz equivalent dose (D_e) was calculated by subtracting the initial OSL signal integrated over 0.80 s (first 5 channels) by the 'early background' (6-20 channels, 0.8-3.2 s) (Cunningham and Wallinga, 2010). We exploited the pIRIR measurements with three different preheat and pIRIR stimulation temperature combinations on the CG feldspar and FG polymineral samples. The feldspar aliquots were firstly preheated for 60 s, followed by the pIRIR stimulation for 200 s after the IR stimulation at 50 °C for 100 s (Table 5.2). The preheat and pIRIR stimulation temperatures were set to 180 and 150 °C in the $pIRIR_{150}$ protocol, 250 and 225 °C in the $pIRIR_{225}$ protocol, and 320 and 290 °C in the $pIRIR_{290}$ protocol, respectively. The initial 5 s of both the IR and pIRIR signals were subtracted by the last 15 s of respective signals for D_e calculation.

Table 5.2 SAR protocols [a] for D_e measurements of quartz and K-feldspar.

Quartz blue OSL			K-feldspar post-IR IRSL[c]		
Step	Treatment	Observed	Step	Treatment	Observed
1	N, beta dose		1	N, beta dose	
2	Preheat at 180 °C for 10s		2	Preheat for 60 s at 180/250/320 °C	
3	IR stimulation for 40 °C [b]		3	IR stimulation for 110 s at 50 °C	
4	Blue stimulation for 40 s at 125 °C	L_n, L_i	4	IR stimulation for 210 s at 150/225/290 °C	L_n, L_i
5	Beta dose (Test dose)		5	Beta dose (Test dose)	
6	Cutheat at 160 °C		6	Preheat for 60 s at 180/250/320 °C	
7	Blue stimulation for 40 s at 125 °C	T_n, T_i	7	IR stimulation for 110 s at 50 °C	
8	Return to 1		8	IR stimulation for 210 s at 150/225/290 °C	T_n, T_i
			9	Return to 1	

[a]:Repeated dose was given at last in each protocol to monitor sensitivity change.

[b]:IR stimulation is conducted before blue stimulation in the last recycling step at room temperature.

[c]:Three post-IR IRSL protocols are applied in this study. Preheat temperatures and the corresponding stimulation temperatures are shown.

The three T-2 samples (LUM3377-3379) were measured using the quartz OSL, K-feldspar $pIRIR_{150}$ and $pIRIR_{225}$ protocols. The degree of signal bleaching was evaluated by comparisons of the multiple luminescence ages. For the samples under T-2, we first exploited the quartz OSL measurement on three samples (LUM3380, LUM3382 and LUM3384) to assess signal saturation. CG K-feldspar or FG polymineral samples were measured using the $pIRIR_{225}$ and $pIRIR_{290}$ protocols, and the dose response curves were fully constructed with regenerative dose up to ca. 3300 Gy.

5.3.3 Fading correction for the IRSL signals

To evaluate the extent of signal loss, the fading experiment was conducted following Auclair et al. (2003). Three to six aliquots were used for each pIRIR protocol. The IRSL intensities were measured

repeatedly after different delay times from tens of minutes to several tens of hours. The fading rate (referred to as g_{2days} [%/decade]) and the recombination-centre-density (referred to as ρ') were determined by fitting IRSL intensities against the arbitrary delay time with logarithmic function (Eq. 4-Huntley and Lamothe, 2001) and power-law function (Huntley, 2006), respectively. The Huntley and Lamothe (2001) model was theoretically applicable for the linear growth part of dose response and thus utilised only for the three samples from upper T-2 using g_{2days} values. The Kars et al. (2008) model has an extended correction range up to field saturation and used for the samples collected below T-2 employing ρ'. The g_{2days} values were calculated for all the samples for further discussion.

5.3.4 Dosimetry

The radioactivity of the surrounding sediments for each sample was measured using additional 50 g of dried material. Prior to gamma measurement, these materials were filled in plastic containers and stored at least four weeks to secure equilibrium between radon and its daughters. The concentrations of uranium (U), thorium (Th) and potassium (K) of the surrounding sediments were subsequently calculated from the activity of these nuclides measured by high-resolution gamma spectrometry. The parameters used for determination of environmental dose rate for the Bohai samples can be found in Li et al. (in press). Specifically, according to the alternation of water content in the sequence, the observed water contents were used for dose rate determination with uncertainties of 10 and 5% for CG and FG samples, respectively, representing the variation of water content in antiquity. The results of dose rate are shown in Table 5.1.

5.4 Luminescence characteristics and ages for the T-2 samples

5.4.1 Quartz OSL characteristics and ages

A preheat temperature at 180 °C was employed for the quartz OSL measurement (Li et al., in press). Its reliability was examined by the dose recovery test (Fig. 5.3). 43 of 72 measured aliquots, assessed by criteria of the recycling and depletion ratios with the acceptable ranges of 0.9-1.1, were used to determine D_e for CG sample LUM3377. Six aliquots were measured for FG quartz samples LUM3378 and LUM3379. All the dose response curves (DRC) were fitted with a single saturating exponential function. D_e distributions, decay and growth curves are shown in Fig. 5.4. The quartz OSL mean D_es are between 113±6 and 136±1 Gy, and the quartz ages vary from 39.1±2.2 to 43.0±4.2 ka by dividing the

mean D_e value by the environmental dose rate.

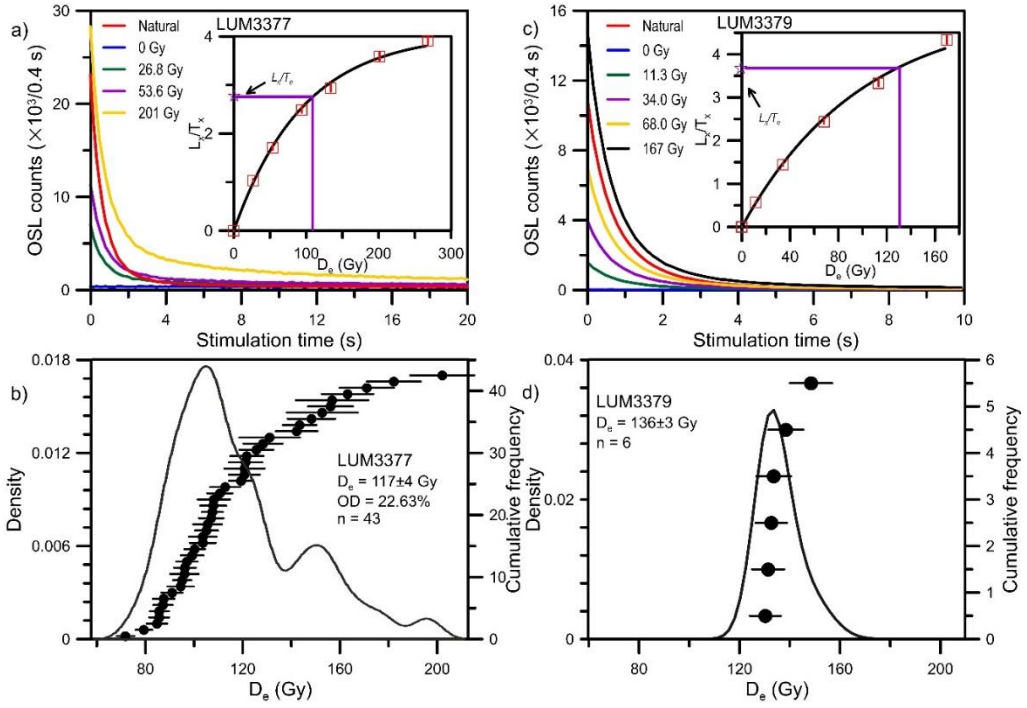

Fig. 5.4 a) and b) show the decay and dose response curves for two young 'T-2' samples LUM3377 and LUM3379. C) and d) show the De distributions for CG sample LUM3377 and FG sample LUM3379.

5.4.2 K-feldspar luminescence characteristics and ages

12 aliquots were measured using each pIRIR protocol for CG feldspar sample LUM3377, while 4 aliquots were used for two FG polymineral samples. The DRCs were fitted with a single saturating exponential function. The apparent ages were determined by dividing the mean D_e value by the feldspar dose rate (Table 5.3). The apparent $pIRIR_{150}$ ages are between 26.4±1.4 and 37.2±3.6 ka, while the corresponding IR_{50} ages are between 20.2±1.0 and 22.1±1.5 ka. The apparent $pIRIR_{225}$ ages are between 30.9±1.8 and 44.9±3.6 ka, and the corresponding IR_{50} ages range from 25.1±1.4 to 27.1±1.7 ka. Dose recovery and residual tests were carried out to assess the reliability of two pIRIR protocols. Three aliquots were used for each test after four-hour bleaching in the Hönle SOL 2 solar simulator. In the dose recovery test, the bleached aliquots were given a known dose close to the measured D_e prior to the measurement. The obtained recovered D_e was first residual dose subtracted and then divided by the given dose to calculate the dose recovery ratio. The dose recovery ratios of both the $pIRIR_{150}$ and $pIRIR_{225}$ signals are within the acceptable range (0.9-1.1) (Fig. 5.3), showing that both the pIRIR protocols are applicable for the T-2 samples.

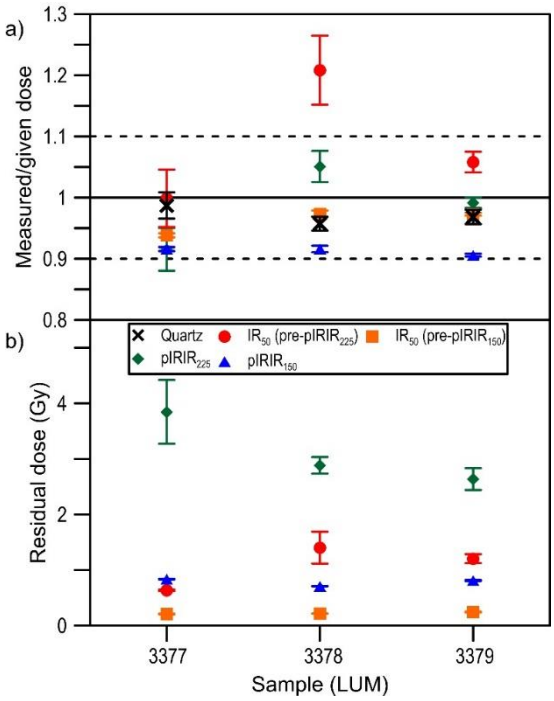

Fig. 5.3 a) Dose recovery ratios for quartz OSL, feldspar $pIRIR_{150}$, $pIRIR_{225}$ and the associated IR_{50} signals. b) Residual doses after 4h SOL2 bleaching for feldspar $pIRIR_{150}$, $pIRIR_{225}$ and the associated IR_{50} signals.

Fading correction was subsequently performed according to Huntley and Lamothe (2001). The pIRIR fading rates are generally between 1-2%, while the IR_{50} fading rates are larger than the associated pIRIR signals (Table 5.3). The fading corrected $pIRIR_{150}$ ages are between 29.3±1.7 and 43.7±4.3 ka, while the fading corrected $pIRIR_{225}$ ages vary from 33.8±2.0 to 52.4±4.5 ka.

5.4.3 Degree of signal bleaching

Dissimilar bleaching rates of different luminescence signals have been observed in previous studies (e.g. Colarossi et al., 2015; Godfrey-smith et al., 1988). Based on this recognition, ages derived from different luminescence signals were compared to evaluate the degree of bleaching of the OSL samples (Murray et al., 2012; Reimann et al., 2015; Yang et al., 2015; Li et al., in press). Bleaching rates for the signals used in this study are quartz OSL > IR_{50} > $pIRIR_{150}$ > $pIRIR_{225}$. We thus compared the quartz OSL, fading corrected feldspar IR_{50}, $pIRIR_{150}$ and $pIRIR_{225}$ ages using the feldspar/quartz (F/Q) age ratio to assess the bleaching characteristics for these signals and to figure out the most reliable luminescence ages. The F/Q age ratios for sample LUM3377 are in general close to 1, while the $pIRIR_{225}$ and the associated IR_{50} ages slightly overestimate the quartz age. The overestimation for $pIRIR_{225}$ is probably due to slightly insufficient bleaching, while the associated IR_{50} age is likely fading over-corrected. In general, the F/Q age ratios for the two FG samples are slightly underestimated as derived from fading under-correction, while the $pIRIR_{225}$ ages are broadly consistent with the quartz OSL ages. The results of F/Q ratios indicate that the quartz OSL signal was likely well bleached.

5.5 Luminescence characteristics and ages for samples below T-2

5.5.1 Quartz OSL measurement

Sample LUM3382 was measured using the SAR protocol to examine applicability of the quartz OSL signal. The preheat plateau test was conducted with seven preheat temperatures (180-300 °C with an interval of 20 °C for 10 s) followed by the tracked cutheat temperatures 20 °C lower (Roberts, 2006). Three aliquots were measured for each temperature. The dose response curve for each preheat temperature was fitted using a single saturating exponential function (Fig. 5.5). It shows that the quartz OSL signals after preheating at 180-300 °C are generally in or very close to saturation. The dose recovery ratios for all the temperatures are rejected as they are out of the acceptable range (0.9-1.1) (Fig. 5.6). The unsatisfactory dose recovery results and the limited dating range indicates that the quartz OSL signal is not applicable for the older samples. The $2D_0$ values are generally ca. 200-250 Gy, which is in agreement with the former observation from FG quartz (Timar-Gabor et al., 2010). The K-feldspar $pIRIR_{225}$ and $pIRIR_{290}$ protocols were thus used to date the R-2, T-3 and R-3 samples.

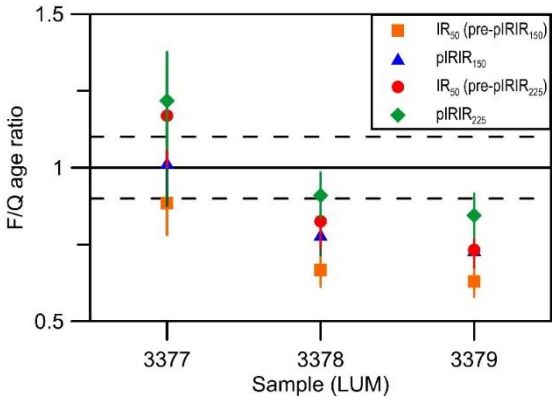

Fig. 5.5 K-feldspar/quartz age ratios for the $pIRIR_{150}$, $pIRIR_{225}$ and the associated IR_{50} signals for the three young 'T-2' samples.

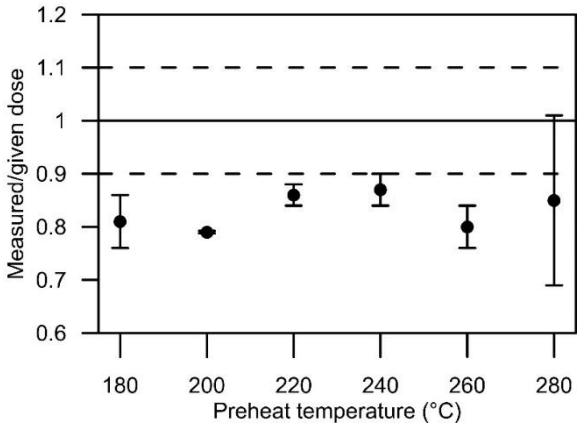

Fig. 5.6 Dose recovery ratio for quartz sample LUM3382.

Table 5.3 Results of quartz OSL and K-feldspar/polymineral pIRIR dating for the upper T-2.

a) Result of quartz D_e and age.

Sample	Depth (m)	Equivalent dose (Gy)	Age (ka)
LUM3377	22.93	113±6	**43.0±4.2**
LUM3378	23.50	135±1	**39.1±2.2**
LUM3379	24.06	136±3	**40.0±2.4**

b) D_es and fading uncorrected ages for the K-feldspar IR_{50}, $pIRIR_{150}$ and $pIRIR_{225}$ signals.

Sample	Depth (m)	Equivalent dose (Gy)				Fading uncorrected age (ka)			
		IR_{50} (pre-$pIRIR_{150}$)	$pIRIR_{150}$	IR_{50} (pre-$pIRIR_{225}$)	$pIRIR_{225}$	IR_{50} (pre-$pIRIR_{150}$)	$pIRIR_{150}$	IR_{50} (pre-$pIRIR_{225}$)	$pIRIR_{225}$
LUM3377	22.93	74.7±3.1	126±10	87.7±4.1	152±9	22.1±1.5	37.2±3.6	25.9±1.8	44.9±3.6
LUM3378	23.50	76.9±0.4	103±3	103±4	122±2	20.3±1.0	27.1±1.6	27.1±1.7	32.1±1.7
LUM3379	24.06	75.9±0.5	99.1±1.8	94.3±1.6	116±3	20.2±1.0	26.4±1.4	25.1±1.4	30.9±1.8

c) Results of g_{2days} value and fading corrected age for the K-feldspar IR_{50}, $pIRIR_{150}$ and $pIRIR_{225}$ signals.

Sample	Depth (m)	g_{2days} (%/decade)				Fading corrected age (ka)			
		IR_{50} (pre-$pIRIR_{150}$)	$pIRIR_{150}$	IR_{50} (pre-$pIRIR_{225}$)	$pIRIR_{225}$	IR_{50} (pre-$pIRIR_{150}$)	$pIRIR_{150}$	IR_{50} (pre-$pIRIR_{225}$)	$pIRIR_{225}$
LUM3377	22.93	5.39±0.01	1.76±0.07	6.24±0.39	1.66±0.26	**38.1±2.6**	**43.7±4.3**	**50.3±5.3**	**52.4±4.5**
LUM3378	23.50	2.74±0.26	1.36±0.27	1.92±0.58	1.16±0.28	**26.1±1.6**	**30.6±2.0**	**32.3±2.9**	**35.6±2.1**
LUM3379	24.06	2.47±0.04	1.17±0.13	2.30±0.30	1.01±0.13	**25.2±1.3**	**29.3±1.7**	**29.3±1.5**	**33.8±2.0**

5.5.2 K-feldspar luminescence characteristics and ages

5.5.2.1 Apparent age

Six aliquots were measured for each pIRIR protocol. The recycling ratio for each measured DRC is close to 1, and all the recuperation is below 5%. The standardised dose response curve (sDRC) of the pIRIR and the associated IR_{50} signals was fitted with a single saturating exponential function using the L_x/T_x values from all measured aliquots for each sample. After projecting the natural luminescence intensities onto the sDRC, the measured D_e was determined for each signal (D_e1 in Fig. 5.7). The apparent age was calculated by dividing the measured D_e by the environmental dose rate. The $pIRIR_{225}$ ages vary from 90±7 to 229±18 ka (Table 5.4), and the associated IR_{50} ages are between 70±7 and 181±15 ka. While the IR_{50} (pre-$pIRIR_{290}$) ages of 71±7 to 242±19 ka are all finite, the finite $pIRIR_{290}$ ages are between 117±10 and 239±20 ka, and two infinite ages of >274±17 and >355±37 ka were calculated for LUM3401 and LUM3425, respectively (Table 5.4), for which the D_es are above the threshold of the associated $2D_0$.

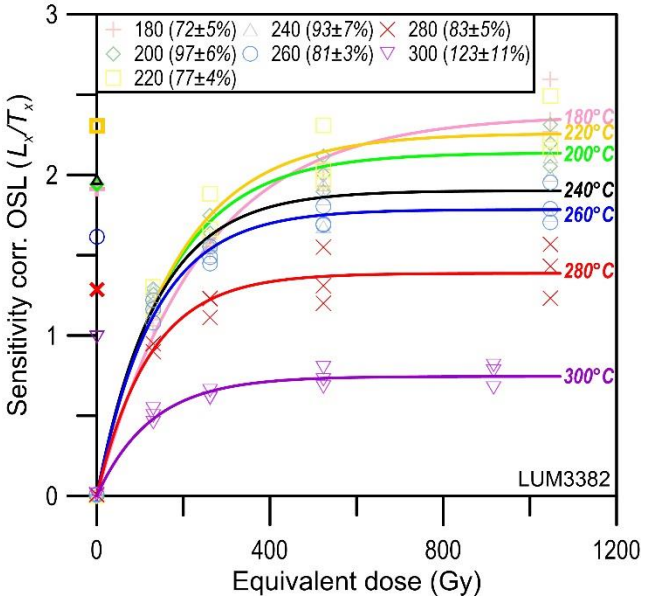

Fig. 5.7 Dose response curves and the associated saturation levels at different preheat temperatures for quartz sample LUM3382.

5.5.2.2 Dose recovery

The 4h-bleached aliquots were used for dose recovery and residual dose measurements. For the samples holding finite equivalent doses, a beta dose close to the equivalent dose was given to three aliquots per sample to measure the recovered doses. In contrast, the given dose of ca. 400 Gy was set for samples holding infinite equivalent dose. The residual dose after four hour SOL2 bleaching was measured using three aliquots. It shows that the residual doses for $pIRIR_{225}$ are between 4.8 and 9.0 Gy, while those for the associated IR_{50} signal are between 1.1 and 3.2 Gy. The residual doses for the $pIRIR_{290}$ and the corresponding IR_{50} signals are 14.1-31.9 and 2.3-10.9 Gy, respectively. The dose recovery ratio per signal was calculated after the residual dose subtraction. It shows that the dose recovery ratios for the $pIRIR_{225}$ signal are broadly around 0.9-1.0, and the corresponding IR_{50} signal mostly yielded acceptable dose recovery ratios (0.9-1.1) (Fig. 5.8). While the dose recovery ratios for the $pIRIR_{290}$ signal are within the acceptable range, the associated IR_{50} signal are generally underestimated due to the trapping sensitivity change after relatively high-temperature preheat (Kars et al., 2014).

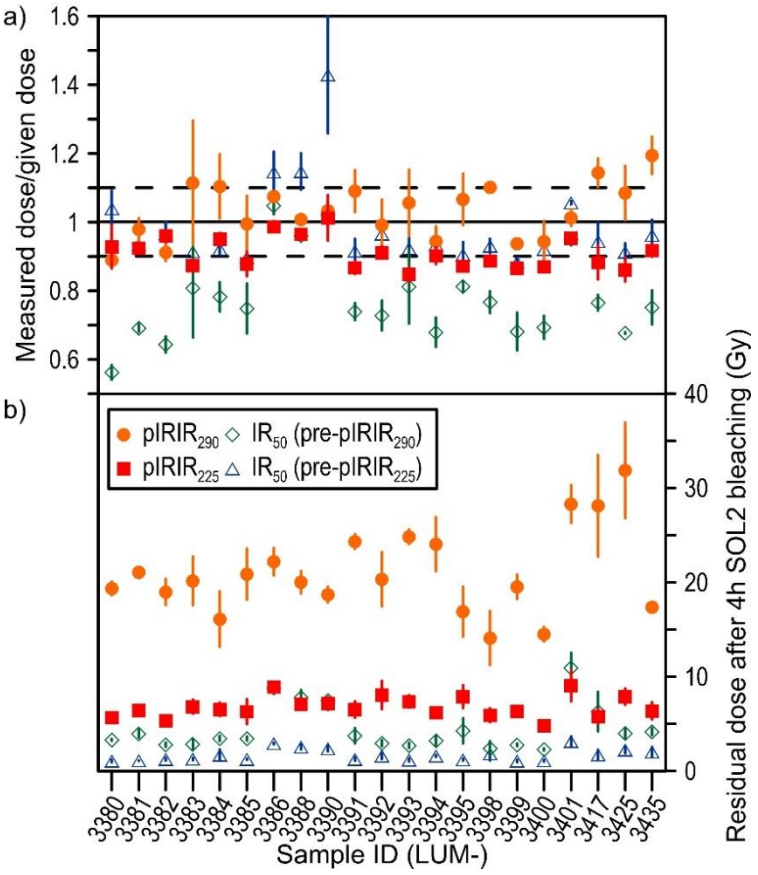

Fig. 5.8 a) dose recovery ratios and b) residual doses after 4h SOL2 bleaching for the IR_{50} and pIRIR signals for samples lower than T-2.

5.5.2.3 Fading correction

The $pIRIR_{225}$ ρ' are between $9.40\pm2.20\times10^{-7}$ and $2.10\pm0.28\times10^{-6}$, whilst the $pIRIR_{290}$ signal yielded generally smaller ρ' values between $3.90\pm4.40\times10^{-7}$ and $1.64\pm0.27\times10^{-6}$. The $pIRIR_{225}$ g_{2days} values range from 1.35±0.32 to 3.15±0.25%/decade, while those for $pIRIR_{290}$ range from 0.60±0.55 to 2.41±0.41%/decade (Table 5.4). The unfaded DRC was subsequently constructed to eliminate fading during D_e measurement (Fig. 5.9). D_0 and saturation value (I_s) of the unfaded DRC, the environmental dose rate, probability distribution of traps and ρ', are the input parameters utilized for construction of the simulated natural DRC (see details in Kars et al., 2008). The natural intensity was plotted onto the simulated natural DRC to determine the fading corrected D_e (D_e2 in Fig. 5.9) according to the simulated I_s and D_0. It is noticed that several fading corrected D_e values are above the threshold for field saturation, thus, minimum ages were presented using $2D_0$ of the simulated natural DRC ($(D_0)_{ss}$ in Table 5.4). The $pIRIR_{225}$ fading corrected ages for the upper 17 samples are finite, ranging from 130±13 to 241±25 ka, while the minimum ages were calculated for the lowermost four samples. Six of twenty-one $pIRIR_{290}$ ages after fading correction are infinite (Table 5.4). The finite $pIRIR_{290}$ ages are between 175±47 and 278±38 ka. The simulated I_s/unfaded I_s ratio, referred to as $(n/N)_{ss}$, is used to predict the

field saturation level. The field saturation levels between 0.70±0.07 and 0.91±0.09 for $pIRIR_{290}$ are generally higher than those of 0.57±0.10 to 0.78±0.06 for $pIRIR_{225}$.

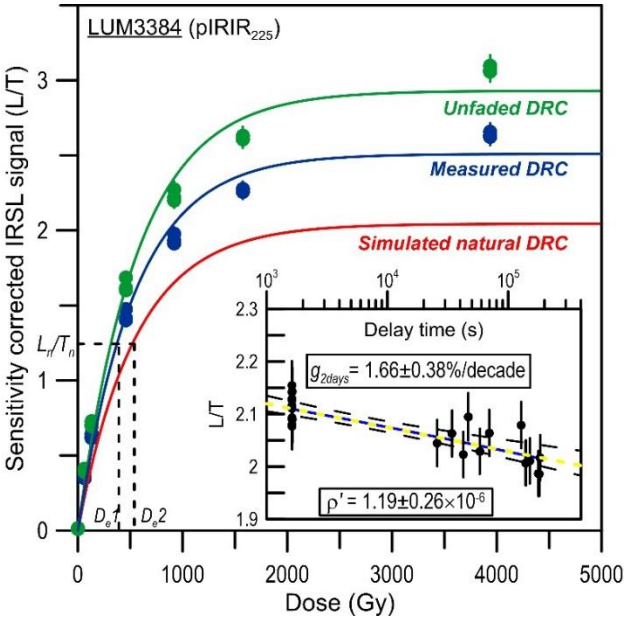

Fig. 5.9 Fading correction results for $pIRIR_{225}$ for sample LUM3384. Three dose response curves (measured, unfaded and simulate natural) following Kars et al. (2008) and the fading uncorrected and corrected D_es are shown. The inset shows the results of fading experiment, including g_{2days} value following Huntley and Lamothe (2001), and ρ' value following Huntley (2006).

5.5.3 Comparison of the $pIRIR_{225}$ and $pIRIR_{290}$ ages

The satisfactory dose recovery ratios indicate that both the $pIRIR_{225}$ and $pIRIR_{290}$ protocols are applicable for the Bohai samples. The fading corrected and uncorrected $pIRIR_{290}$ ages are compared with the associated fading corrected $pIRIR_{225}$ ages to evaluate the degree of bleaching for the two pIRIR signals and to understand the laboratory determined fading for the high-temperature stimulated pIRIR signal. The lowermost four samples are excluded for age comparison as all the $pIRIR_{225}$ and $pIRIR_{290}$ ages are saturated. A tendency of slight age underestimation is demonstrated for the fading uncorrected $pIRIR_{290}$ ages, while the fading corrected $pIRIR_{290}$ ages are generally consistent with the corresponding $pIRIR_{225}$ ages (Fig. 5.10). It is noticed that six fading uncorrected $pIRIR_{290}$ ages are consistent with the fading corrected $pIRIR_{225}$ ages for samples, whilst the corresponding $pIRIR_{290}$ ages after fading correction, including two infinite ages, are overestimated. The dissimilarity appears not to derive from fading over-correction, since both the significant and negligible $pIRIR_{290}$ fading rates are observed for these overestimated ages (Fig. 5.10). On the other hand, age overestimation arises probably due to partial bleaching for the $pIRIR_{290}$ signal (Colarossi et al., 2015), while the $pIRIR_{225}$ signal could be more sufficiently bleached during the same exposure duration. The general consistency between the fading corrected $pIRIR_{225}$ and $pIRIR_{290}$ ages indicates that the $pIRIR_{225}$ signal was well

bleached, which is in agreement with the conclusion in Li et al. (in press), revealing that the $pIRIR_{225}$ dating is applicable in terms of signal bleaching for the pre-Holocene deposits.

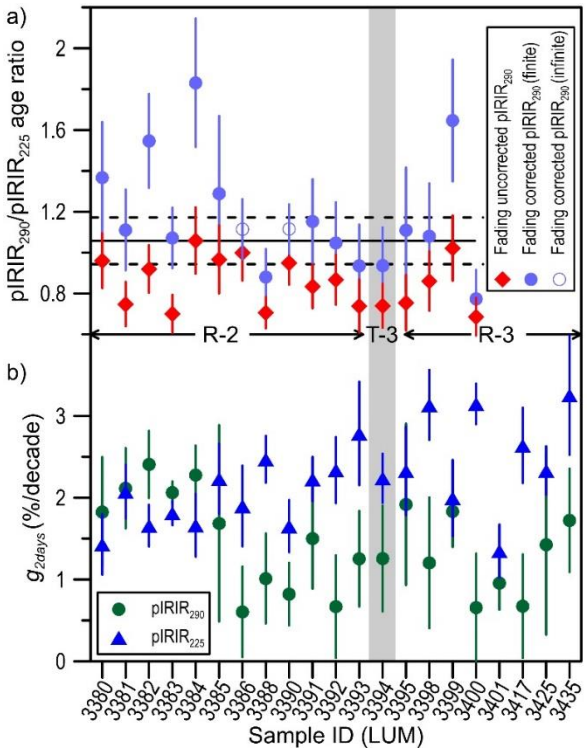

Fig. 5.10 Age comparison between the $pIRIR_{225}$ and $pIRIR_{290}$ signals. a) shows the pIRIR290/pIRIR225 age ratios. The $pIRIR_{290}$ ages are fading uncorrected and corrected. The $pIRIR_{225}$ ages are fading corrected. b) shows the laboratory determined fading rates for the $pIRIR_{225}$ and $pIRIR_{290}$ signals.

For the samples under study, fading rates for the $pIRIR_{290}$ signal is commonly smaller than those for the associated $pIRIR_{225}$ signal. While the lower samples generally yield the $pIRIR_{290}$ fading rate of ca. 1%/decade, significant fading is determined in laboratory for the sand samples in the upper R-2 (Fig. 5.10). Similarly significant fading rates for $pIRIR_{290}$ have been presented (e.g. Li et al., 2014 and the references therein; Li et al., in press), indicating that the $pIRIR_{290}$ signal could also fade. Negligible fading for the $pIRIR_{290}$ signal with g_{2days} values of smaller than 1-1.5%/decade was regarded as an artefact of the measurement procedure (Buylaert et al., 2012), and the apparent $pIRIR_{290}$ ages were thus not corrected for fading. It was suggested that insignificant fading could induce very limited age underestimation, the statement of artefact for the laboratory determined $pIRIR_{290}$ fading rate, however, is still controversial, as the relations between anomalous fading, laboratory and field saturation levels, are not clear. Here, the $(n/N)_{ss}$ after Kars et al. (2008) were plotted against the corresponding g_{2days} values for all the signals. It shows that the field saturation level is higher when less fading occurs. After fitting the plots using a single decaying exponential function with the confidence level of 95% (Fig. 5.11), we notice that the $(n/N)_{ss}$ is close to the threshold of 86% for field saturation, when the associated fading rate is around 1%/decade. It indicates that the approaching or reaching to the laboratory saturation for the $pIRIR_{290}$ signal could derive from indistinguishable field and laboratory saturation levels. Thus, the fading rate of ca. 1%/decade represents a real fading process for the

$pIRIR_{290}$ signal rather than a laboratory artefact, although the fading process results in insignificant signal loss.

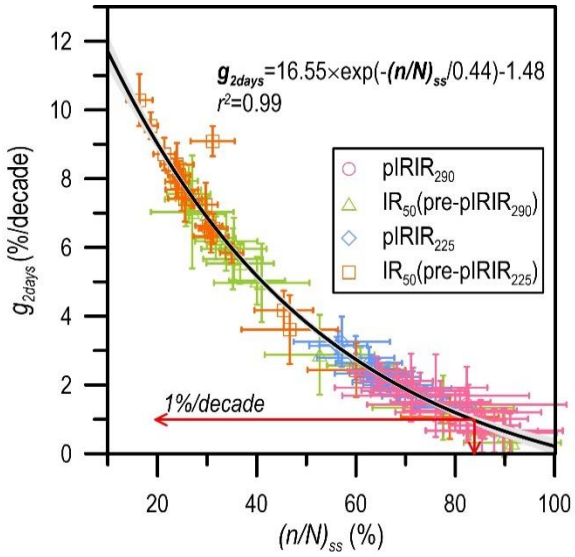

Fig. 5.11 The relation between fading rate g_{2days} and field saturation level $(n/N)_{ss}$. The black solid line reveals the exponential decay fitting with the shaded area of 95% confidence. The 1%.decade fading correlates to ~86% field saturation.

5.6 Dating capabilities for the K-feldspar pIRIR protocols

Twice the characteristic dose (D_0) value for the single saturating exponential fitted DRC, representing 86% of the laboratory saturation value, is used to quantify the dating limit of the luminescence signals (Wintle and Murray, 2006). D_0 values for the measured (M), unfaded (UF) and simulated natural (SN) DRCs in Kars et al. (2008) are first compared to investigate whether the upper dating limit changes before and after fading correction. It shows that the UF D_0 is in general larger than the associated SN D_0. Both the UF and Sn D_0s slightly overestimate the corresponding measured D_0. It is also noticed that this overestimation differs between the IR_{50} and pIRIR signals, which is commonly more significant for the IR_{50} signals than those for the corresponding pIRIR signals, reflected by the slopes of linear fitting (Fig. 5.12 a-d). To investigate the derivation of this discrepancy, the UF/M and SN/M D_0 ratios were calculated and plotted against the recombination-centre-density (ρ'). In Fig. 5.12f, it shows a clear tendency that the increment for UF D_0 is accompanied by the increased fading. The tendency for SN D_0 is relatively negligible, suggesting that D_0 is consistent before and after fading correction. Therefore, we conclude that fading correction is unessential to evaluate minimum ages for the field saturated samples using $2D_0$ value of the simulated natural DRC, which could be substituted by that of the measured DRC.

Table 5.4 Results of $pIRIR_{225}$ and $pIRIR_{290}$ dating for the samples below the second transgressive layer (T-2). [1] Measured (fading uncorrected) D_e. [2] Characteristic dose for the simulated natural DRC.

Sample ID	Depth (m)	Dose rate (Gy/ka)	Signal	g_{2days} (%/decade)	ρ' ($\times10^{-6}$)	I_n/I_{field}	$(n/N)_{ss}$	D_e [1] (Gy)	$(D_0)_{ss}$ [2] (Gy)	Fading corrected D_e (Gy)	Apparent age (ka)	Fading corrected age (ka)
LUM3380	28.95	3.40±0.20	$pIRIR_{225}$	1.43±0.37	0.96±0.25	0.56±0.05	0.77±0.07	369±22	576±25	472±48	108±9	139±16
			$pIRIR_{290}$	1.83±0.67	1.27±0.46	0.67±0.10	0.71±0.10	454±22	579±20	646±96	133±10	190±30
LUM3381	30.59	3.50±0.20	$pIRIR_{225}$	2.07±0.33	1.47±0.22	0.64±0.06	0.65±0.06	374±25	582±33	592±61	107±9	169±20
			$pIRIR_{290}$	2.12±0.49	1.41±0.33	0.65±0.07	0.68±0.07	443±27	621±23	658±79	126±11	188±25
LUM3382	32.90	3.92±0.21	$pIRIR_{225}$	1.66±0.26	1.15±0.18	0.59±0.04	0.73±0.05	372±22	571±29	512±44	95±8	130±13
			$pIRIR_{290}$	2.41±0.41	1.64±0.27	0.76±0.07	0.64±0.06	470±25	561±14	791±75	120±9	202±22
LUM3383	33.68	3.14±0.19	$pIRIR_{225}$	1.81±0.15	1.26±0.11	0.60±0.04	0.71±0.04	371±25	581±30	525±42	118±11	167±17
			$pIRIR_{290}$	2.06±0.14	1.40±0.10	0.70±0.04	0.68±0.03	368±22	470±20	563±41	117±10	179±17
LUM3384	36.14	3.50±0.20	$pIRIR_{225}$	1.66±0.38	1.19±0.26	0.61±0.06	0.72±0.07	372±25	554±25	520±58	106±9	149±19
			$pIRIR_{290}$	2.28±0.36	1.57±0.24	0.80±0.08	0.65±0.05	514±34	559±19	888±90	147±13	273±31
LUM3385	38.84	4.18±0.22	$pIRIR_{225}$	2.23±0.43	1.52±0.29	0.64±0.07	0.67±0.06	377±23	556±13	566±64	90±7	136±17
			$pIRIR_{290}$	1.69±1.20	1.11±0.81	0.68±0.17	0.76±0.19	547±59	634±48	730±192	131±16	175±47
LUM3386	39.32	4.07±0.21	$pIRIR_{225}$	1.90±0.49	1.27±0.33	0.83±0.09	0.71±0.08	465±21	418±14	746±86	114±8	183±22
			$pIRIR_{290}$	0.60±0.55	0.34±0.39	0.89±0.09	0.91±0.09	746±29	416±8	>830±18	183±12	>204±11
LUM3388	41.80	3.61±0.19	$pIRIR_{225}$	2.47±0.29	1.67±0.20	0.83±0.06	0.64±0.04	427±16	441±15	786±60	118±8	218±20
			$pIRIR_{290}$	1.01±0.55	0.62±0.38	0.81±0.09	0.85±0.10	557±15	414±8	695±79	154±9	192±24
LUM3390	43.22	3.64±0.19	$pIRIR_{225}$	1.65±0.32	1.13±0.21	0.81±0.06	0.74±0.05	482±18	438±14	726±55	132±8	199±18
			$pIRIR_{290}$	0.82±0.38	0.57±0.26	0.89±0.08	0.86±0.07	690±32	404±10	>808±20	189±13	>222±13
LUM3391	44.82	3.19±0.20	$pIRIR_{225}$	2.23±0.27	1.53±0.18	0.69±0.05	0.66±0.05	403±16	549±16	639±49	126±9	200±20
			$pIRIR_{290}$	1.50±0.61	0.98±0.42	0.75±0.10	0.77±0.10	534±29	529±21	737±101	167±14	231±35
LUM3392	46.90	3.44±0.20	$pIRIR_{225}$	2.34±0.40	1.61±0.27	0.70±0.06	0.64±0.06	406±18	544±15	655±62	118±9	190±21
			$pIRIR_{290}$	0.67±0.63	0.60±0.42	0.71±0.09	0.85±0.11	568±34	554±24	686±96	165±14	199±30
LUM3393	48.52	3.33±0.20	$pIRIR_{225}$	2.79±0.63	1.90±0.41	0.72±0.09	0.60±0.08	393±16	534±13	689±92	118±8	207±30
			$pIRIR_{290}$	1.25±0.59	0.84±0.39	0.66±0.09	0.80±0.10	509±40	604±34	645±94	153±15	194±30
LUM3394	49.64	3.81±0.22	$pIRIR_{225}$	2.24±0.30	1.52±0.20	0.73±0.05	0.66±0.05	455±19	560±15	725±57	119±9	190±19
			$pIRIR_{290}$	1.26±0.65	0.81±0.45	0.68±0.11	0.81±0.11	536±48	588±30	679±111	140±15	178±31
LUM3395	50.72	3.18±0.22	$pIRIR_{225}$	2.33±0.54	1.69±0.35	0.72±0.09	0.63±0.07	436±29	566±20	725±95	137±12	228±33
			$pIRIR_{290}$	1.92±0.99	1.31±0.69	0.73±0.16	0.71±0.15	547±47	620±39	805±182	172±18	253±59
LUM3398	54.90	3.55±0.20	$pIRIR_{225}$	3.14±0.43	2.10±0.28	0.70±0.08	0.56±0.06	420±26	634±26	766±88	118±10	216±28
			$pIRIR_{290}$	1.20±0.80	0.75±0.55	0.74±0.13	0.83±0.15	659±61	611±42	827±160	186±20	233±47
LUM3399	57.32	3.59±0.20	$pIRIR_{225}$	2.00±0.47	1.39±0.31	0.64±0.06	0.68±0.07	413±16	595±15	607±63	115±8	169±20
			$pIRIR_{290}$	1.83±0.44	1.32±0.29	0.81±0.09	0.70±0.07	620±52	609±26	999±124	173±18	278±38
LUM3400	59.50	3.31±0.20	$pIRIR_{225}$	3.15±0.25	2.10±0.16	0.74±0.05	0.56±0.03	419±21	586±27	797±66	127±10	241±25
			$pIRIR_{290}$	0.66±0.66	0.40±0.40	0.67±0.09	0.90±0.12	547±33	554±15	617±85	165±14	186±28
LUM3401	59.90	3.01±0.17	$pIRIR_{225}$	1.35±0.25	0.94±0.22	0.95±0.07	0.78±0.06	722±24	437±12	1323±106	240±16	>290±18
			$pIRIR_{290}$	0.96±0.33	0.64±0.22	1.07±0.08	0.84±0.06	>826±22	415±10	>830±20	>274±17	>276±17
LUM3417	74.75	3.46±0.19	$pIRIR_{225}$	2.64±0.46	1.73±0.30	0.92±0.10	0.63±0.07	639±44	557±23	1409±171	185±16	>322±22
			$pIRIR_{290}$	0.67±0.63	0.38±0.45	0.86±0.14	0.88±0.14	828±54	540±25	1058±175	239±20	>312±22
LUM3425	83.54	3.16±0.20	$pIRIR_{225}$	2.33±0.30	1.56±0.19	0.94±0.07	0.65±0.04	722±35	587±24	1639±132	229±18	>372±28
			$pIRIR_{290}$	1.43±1.10	0.81±0.78	0.94±0.23	0.82±0.20	>1122±47	566±40	1590±409	>355±37	>358±34
LUM3435	97.66	3.73±0.20	$pIRIR_{225}$	3.26±0.73	2.08±0.48	0.85±0.14	0.57±0.10	552±43	617±38	1169±209	148±14	>331±27
			$pIRIR_{290}$	1.72±0.63	1.19±0.43	0.84±0.12	0.73±0.10	719±47	612±22	1135±167	193±16	>328±22

The D_0 values differ about which grain size fraction is used for dating. It is shown in Fig. 5.12a-d that the FG samples yield much smaller D_0s of ca. 400-500 Gy for all the signals than the CG samples. $2D_0$ values for the pIRIR signals are less than ca. 900 Gy, which is equivalent to a maximum dating limit less than ca. 200 ka when the assumed K-feldspar dose rate is ca. 4 Gy/ka. In contrast, $2D_0$ values for the $pIRIR_{225}$ and $pIRIR_{290}$ signals for CG samples are generally between ca. 1100 and 1200 Gy, suggesting that the upper dating limit could reach to ca. 300 ka. This discrepancy of dating capability requires further investigation, as it could be induced by different luminescence properties for feldspar in different grain size intervals. It could also be explained by variations of the source, since the fine grains can move distally, while the coarse grains are generally indicative of proximal transportation.

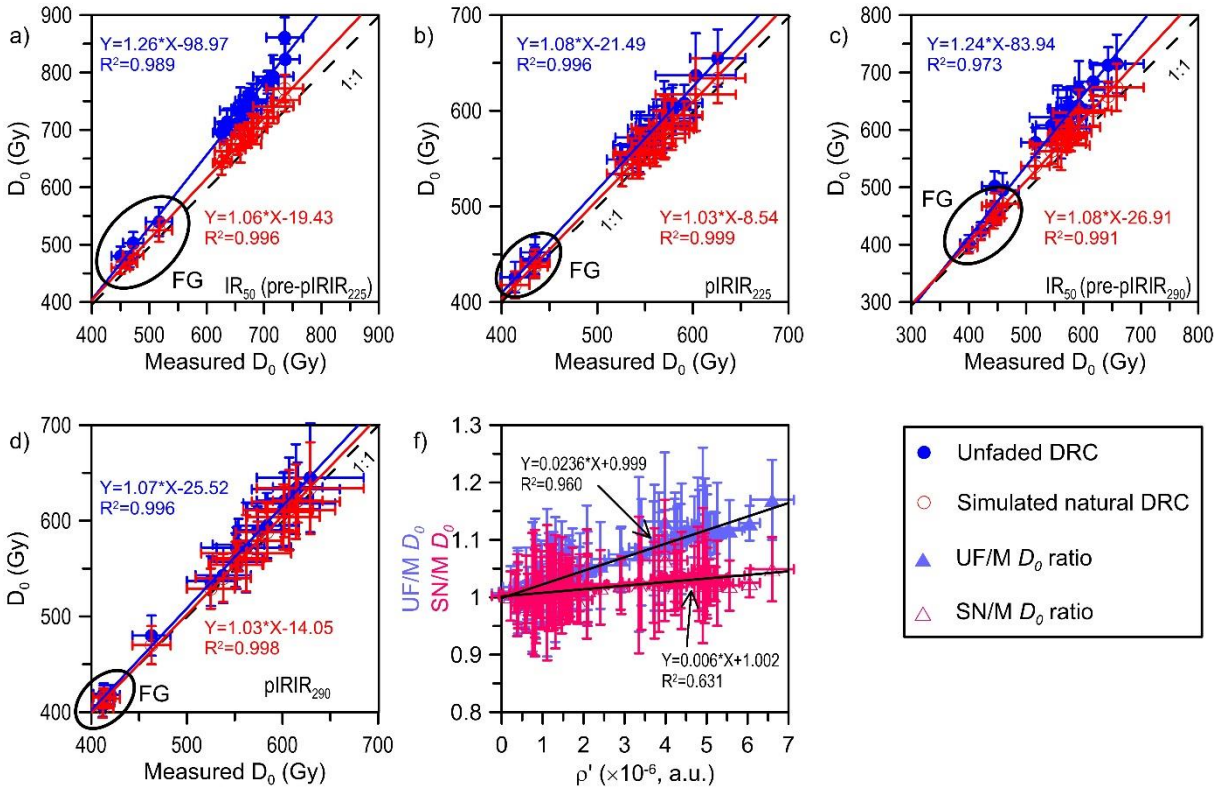

Fig. 5.12 D_0 comparison of measured, unfaded and simulated natural DRCs. a) – d) show the D_0 relations for the $pIRIR_{225}$, $pIRIR_{290}$ and the associated IR_{50} signals. f) shows D_0 variations for the three DRCs with the increase of fading.

5.7 Timing of the Middle Pleistocene transgressions in the Bohai Coast and sedimentation rate variations

After the investigation of signal bleaching and anomalous fading, the luminescence ages in this study and in Li et al. (in press) for core LZK06 are used to establish the chronology. It shows that the quartz OSL signal for the upper 26 m of core LZK06 was well bleached to yield reliable ages (T-1, R-1 and the upper T-2). For the rest core, the quartz OSL signal is in saturation. The $pIRIR_{225}$ signal was generally well bleached after the comparison between the $pIRIR_{225}$ and $pIRIR_{290}$ ages (R-2, T-2 and T-3). The Bacon age-depth model was subsequently used to construct the accumulation history for the last 250

using the most reliable luminescence ages, and to minimise the sample dependent age uncertainties (Blaauw and Christen, 2011). Hiatus occurring at 28.7 m, between T-2 and R-2, was set in the age-depth model with an estimated time gap of 10 ka in the model.

Our new results in this study show that T-3 transgression occurred at ca. 200 ka. In sea-level aspect, the global mean sea-level (GMSL) was between ca. -40 and 10 m a.s.l during this period (Spratt and Lisiecki, 2016), while the thin T-3 transgressive layer was buried at ca. -45 m a.s.l. Therefore, the T-3 layer likely correlate to the period of MIS 7 sea-level highstand. Our results largely extend the timing of T-3 transgression in the literature, which were determined using the saturated quartz ages (Chen et al., 2008; Liu et al., 2016). The timing of T-2 is not very well confirmed by the limited OSL samples. The luminescence age below T-2 shows that this transgression occurred after ca. 130 ka, and the radiocarbon age for the shell-rich bottom layer is saturated (>43.5 cal ka BP. Shang et al., in revision.), whereas no OSL age is available to restrict the period of the observed hiatus between T-2 and R-2. The age-depth model shows that the onset timing of the T-2 transgression is ca. 120 ka, which is reasonable compared with the GMSL in MIS 5. The three OSL ages are available to restrict the timing of the upper T-2. While the quartz OSL ages are related to early-middle MIS 3 (ca. 40 ka), the radiocarbon ages in the uppermost T-2 are generally saturated, and one radiocarbon age is ~30 cal ka BP (Fig. 5.2. Shang et al., in prep.). The upper T-2 is buried at ca. -18 m a.s.l., whilst the GMSL in the early-middle MIS 3 range from ca. -80 to ca. -60 m a.s.l. (Spratt and Lisiecki, 2016), showing a much lower sea-level which is impossible for transgressive deposition in the Bohai Coast. Although the peak sea-level of ca. -38±7 m during 50-37 ka in the Bohai and South Yellow Seas, estimated by Pico et al. (2016), is higher than the GMSL, it is apparently lower than the upper T-2. The discrepancies for the radiocarbon dates, and between OSL and radiocarbon ages, show that most of shell fragments in the upper T-2 appear to be reworked and problematic of old carbon contamination. These shell fragments could be eroded from the old transgressive strata in upstream of Dalinghe River and redeposited on the site of core LZK06. The shell fragments in the upper T-2 do not represent *in situ* deposition and thus not indicative of marine environment. The former chronology showing transgression in MIS 4 and 3 is likely misunderstood by the reworked shells. Termination timing and sedimentary processes for T-2 requires further investigation on the basis of high-resolution chronological constraints. The T-1 transgression occurred in Holocene, which has been indicated by the quartz OSL and radiocarbon ages (Li et al., in press). It agrees with the former radiocarbon chronology in the Bohai coastal area (e.g. IOCAS, 1985; Wang et al., 2004; Wang and Fan, 2005).

The variations of sedimentation rate (SR) is calculated according to the modelled age-depth relation (Fig. 5.13c). In total of 60 bins divide the deposits in ca. 250 ka with bin size of 1 m. It shows that the sedimentation rates of 0.2-0.3 m/ka are roughly constant throughout 250-30 ka, while a rapid

accumulation occurred in the last deglaciation accompanied with a high rate of sea-level rise. The high rate of sedimentation is observed in the last millennia, related to winter monsoon enhancement and human activity (Li et al., in press). Similar variation of sedimentation rate in the South Bohai Coast was revealed by Yi et al. (2015). Our result for the constant sedimentation rate during 250-30 ka is slightly higher than that in the South Bohai Coast. It could be induced by different discharges of the local streams. The discrepancy of the sedimentation rates also likely derives from the dominant grain sizes of the sediments in different locations. The catchment in the North Bohai Coast comprises mainly sand fractions, while the south and west coast holds finer materials. The silt or clay deposits in the south and west coast have higher porosity (Guillocheau et al., 2012), resulting in higher compaction than the common sand deposits in north.

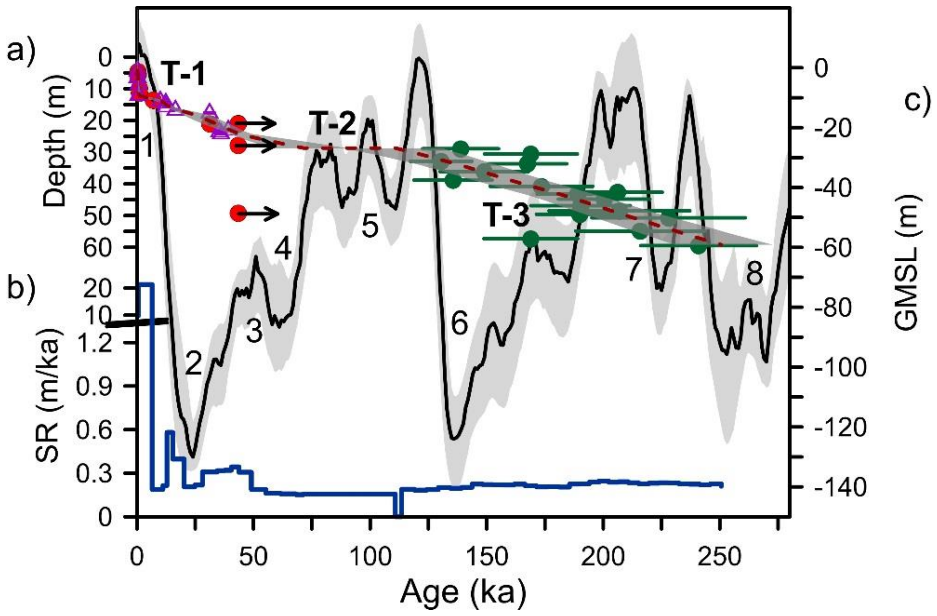

Fig. 5.13 a) Age-depth model for core LZK06. The purple triangles represent quartz ages, and the green filled circles show the fading corrected K-feldspar pIRIR225 ages. The radiocarbon dates for T-2 and T-3 transgressions are referred here using red filled circle. The red circles with arrow represent infinite radiocarbon ages. The red dot line with the shaded area (95% confidence) reveals the results after Bacon age-depth modelling. b) Variations of sedimentation rate in the last 250 ka. c) The global mean sea-level changes following Spratt and Lisiecki (2006). The depth in a) is elevation corrected and comparable with the elevation in c).

5.8 Conclusions

We exploited luminescence dating on a sediment core from the Bohai Coast to explore the timing of the three-major transgression for the Middle and Upper Pleistocene. Multiple luminescence signals were first used to investigate the luminescence characteristics and their reliabilities. The most reliable luminescence ages in this study and in Li et al. (in press) were used to restrict the timing of each transgression. The Bacon age-depth model was employed to reconstruct the accumulation history. We draw our conclusions as follows:

- The quartz OSL signal was well bleached for the sediments since ca. 50 ka. Quartz OSL dating is not applicable for the samples beyond ca. 130 ka, due to an early saturation with equivalent dose of 200-250 Gy.
- Both the K-feldspar $pIRIR_{225}$ and $pIRIR_{290}$ signals were applicable in term of dose recovery. The laboratory determined fading rates of ca. 1-1.5%/decade for the $pIRIR_{290}$ signal reflect actual fading process rather than laboratory artefact. The $pIRIR_{225}$ signal was well bleached after comparison between the $pIRIR_{225}$ and $pIRIR_{290}$ ages.
- Upper dating limits for the two pIRIR signals could reach ca. 300 ka when the dose rate is ca. 4 Gy/ka. In general, the upper dating limit would not change after fading correction. The dating ranges for the IR_{50} and pIRIR signals from FG polymineral are much lower than those for CG K-feldspar.
- The timing of the earliest transgression is constrained to MIS 7 using the fading corrected $pIRIR_{225}$ ages. The onset timing of the second transgression is probably triggered by the MIS 5 sea-level highstand. Termination of the second transgression requires further investigations. The latest transgression is related to the Holocene sea-level rise.
- Sedimentation rate between ca. 250 and 30 ka was 0.2-0.3 m/ka according to the modelled age-depth relation. It is slightly higher than that in the South Bohai Coast (Yi et al., 2015) due to differences of the local discharges and sediment compaction. Sedimentation rate increased dramatically since the last deglaciation, and rapid accumulation in the last millennia is observed.

Acknowledgements

The authors are grateful to the assistance from technicians in LIAG-S3. Yan Li is supported by China Scholarship Council (201406400050). This work is funded by China Geological Survey (CGS) Programme (12120113005800).

References

Allen, M.B., Macdonald, D.I.M., Zhao, X., Vincent, S.J., Brouet-Menzies, C., 1997. Early Cenozoic two-phase extension and late Cenozoic thermal subsidence and inversion of the Bohai Basin, northern China. Marine and Petroleum Geology 14, 951-972.

Auclair, M., Lamothe, M., Huot, S., 2003. Measurement of anomalous fading for feldspar IRSL using SAR. Radiation Measurements 37, 487-492.

Blaauw, M., Christen, J.A., 2011. Flexible paleoclimate age-depth models using an autoregressive gamma process. Bayesian Analysis 6, 457-474.

Bureau, L.G., 1983. Quaternary in Liaoning. Geology Press, Beijing.

Buylaert, J.P., Jain, M., Murray, A.S., Thomsen, K.J., Thiel, C., Sohbati, R., 2012. A robust feldspar luminescence dating method for Middle and Late Pleistocene sediments. Boreas 41, 435-451.

Buylaert, J.P., Murray, A.S., Gebhardt, A.C., Sohbati, R., Ohlendorf, C., Thiel, C., Wastegård, S., Zolitschka, B., 2013. Luminescence dating of the PASADO core 5022-1D from Laguna Potrok Aike (Argentina) using IRSL signals from feldspar. Quaternary Science Reviews 71, 70-80.

Buylaert, J.P., Murray, A.S., Thomsen, K.J., Jain, M., 2009. Testing the potential of an elevated temperature IRSL signal from K-feldspar. Radiation Measurements 44, 560-565.

Chen, Y., Li, Z., Shao, Y., Wang, Z., Gao, W., Yang, X., 2008. Study on the Quaternary chronostratigraphic section in Tianjin Area. Seismology and geology 30, 483-493. (in Chinese with English Abstract)

Chen, Y., Wang, H., Pei, Y., Tian, L., Li, J., Shang, Z., 2012. Division and its geological significance of the late Quaternary marine sedimentary beds in the west coast of Bohai Bay, China. Journal of Jilin University (Earth Science Edition) 42, 747-759. (in Chinese with English Abstract)

Colarossi, D., Duller, G.A.T., Roberts, H.M., Tooth, S., Lyons, R., 2015. Comparison of paired quartz OSL and feldspar post-IR IRSL dose distributions in poorly bleached fluvial sediments from South Africa. Quaternary Geochronology 30, 233-238.

Cunningham, A.C., Wallinga, J., 2010. Selection of integration time intervals for quartz OSL decay curves. Quaternary Geochronology 5, 657-666.

Godfrey-Smith, D.I., Huntley, D.J., Chen, W.H., 1988. Optical dating studies of quartz and feldspar sediment extracts. Quaternary Science Reviews 7, 373-380.

Guillocheau, F., Rouby, D., Robin, C., Helm, C., Rolland, N., Le Carlier de Veslud, C., Braun, J., 2012. Quantification and causes of the terrigenous sediment budget at the scale of a continental margin: a new method to the Namibia-South Africa margin. Basin Research 24, 3-30.

Huntley, D.J., 2006. An explanation of the power-law decay of luminescence. Journal of Physics: Condensed Matter 18, 1359-1365.

Huntley, D.J., Lamothe, M., 2001. Ubiquity of anomalous fading in K-feldspars and the measurement and correction for it in optical dating. Canadian Journal of Earth Sciences 38, 1093-1106.

IOCAS, 1985. Geology of the Bohai Bea. Science Press, Beijing. (in Chinese with English Abstract)

Kars, R.H., Reimann, T., Ankjaergaard, C., Wallinga, J., 2014. Bleaching of the post-IR IRSL signal: new insights for feldspar luminescence dating. Boreas 43, 780-791.

Kars, R.H., Wallinga, J., 2009. IRSL dating of K-feldspars: Modelling natural dose response curves to deal with anomalous fading and trap competition. Radiation Measurements 44, 594-599.

Kars, R.H., Wallinga, J., Cohen, K.M., 2008. A new approach towards anomalous fading correction for feldspar IRSL dating — tests on samples in field saturation. Radiation Measurements 43, 786-790.

Lamothe, M., 2016. Luminescence dating of interglacial coastal depositional systems: Recent developments and future avenues of research. Quaternary Science Reviews 146, 1-27.

Lamothe, M., Auclair, M., Hamzaoui, C., Huot, S., 2003. Towards a prediction of long-term anomalous fading of feldspar IRSL. Radiation Measurements 37, 493-498.

Li, B., Jacobs, Z., Roberts, R., Li, S.-H., 2014. Review and assessment of the potential of post-IR IRSL dating methods to circumvent the problem of anomalous fading in feldspar luminescence. Geochronometria 41.

Li, B., Li, S.-H., 2011. Luminescence dating of K-feldspar from sediments: A protocol without anomalous fading correction. Quaternary Geochronology 6, 468-479.

Li, Y., Shang, Z., Tsukamoto, S., Tamura, T., Yi, L., Rolf, C., Wang, H., Frechen, M., Li, J., Jiang, X., in press. Sediments of rapid delta progradation during the last millennia in the North Bohai Coast, China: their OSL properties and refined chronology. Journal of African Earth Sciences.

Li, Y., Tsukamoto, S., Gabriel, G., Frechen, M., in press. Timing of fluvial sedimentation in the Upper Rhine Graben since the Middle Pleistocene: constraints from quartz and feldspar luminescence dating. Boreas.

Liu, J., Saito, Y., Wang, H., Zhou, L., Yang, Z., 2009. Stratigraphic development during the Late Pleistocene and Holocene offshore of the Yellow River delta, Bohai Sea. Journal of Asian Earth Sciences 36, 318-331.

Liu, J., Wang, H., Wang, F., Qiu, J., Saito, Y., Lu, J., Zhou, L., Xu, G., Du, X., Chen, Q., 2016. Sedimentary evolution during the last ~1.9Ma near the western margin of the modern Bohai Sea. Palaeogeography, Palaeoclimatology, Palaeoecology 451, 84-96.

Long, H., Shen, J., Wang, Y., Gao, L., Frechen, M., 2015. High-resolution OSL dating of a late Quaternary sequence from Xingkai Lake (NE Asia): Chronological challenge of the 'MIS 3a Mega-paleolake' hypothesis in China. Earth and Planetary Science Letters 428, 281-292.

Murray, A.S., Thomsen, K.J., Masuda, N., Buylaert, J.P., Jain, M., 2012. Identifying well-bleached quartz using the different bleaching rates of quartz and feldspar luminescence signals. Radiation Measurements 47, 688-695.

Murray, A.S., Wintle, A.G., 2000. Luminescence dating of quartz using an improved single-aliquot regenerative-dose protocol. Radiation Measurements 32, 57-73.

Murray, A.S., Wintle, A.G., 2003. The single aliquot regenerative dose protocol: potential for improvements in reliability. Radiation Measurements 37, 377-381.

Pico, T., Mitrovica, J.X., Ferrier, K.L., Braun, J., 2016. Global ice volume during MIS 3 inferred from a sea-level analysis of sedimentary core records in the Yellow River Delta. Quaternary Science Reviews 152, 72-79.

Pigati, J.S., Quade, J., Wilson, J., Jull, A.J.T., Lifton, N.A., 2007. Development of low-background vacuum extraction and graphitization systems for 14C dating of old (40-60 ka) samples. Quaternary International 166, 4-14.

Reimann, T., Notenboom, P.D., De Schipper, M.A., Wallinga, J., 2015. Testing for sufficient signal resetting during sediment transport using a polymineral multiple-signal luminescence approach. Quaternary Geochronology 25, 26-36.

Roberts, H.M., 2006. Optical dating of coarse-silt sized quartz from loess: Evaluation of equivalent dose determinations and SAR procedural checks. Radiation Measurements 41, 923-929.

Shi, X., Yao, Z., Liu, Q., Larrasoaña, J.C., Bai, Y., Liu, Y., Liu, J., Cao, P., Li, X., Qiao, S., Wang, K., Fang, X., Xu, T., 2016. Sedimentary architecture of the Bohai Sea China over the last 1 Ma and implications for sea-level changes. Earth and Planetary Science Letters 451, 10-21.

Spratt, R.M., Lisiecki, L.E., 2016. A late Pleistocene sea level stack. Climate of the past 12, 1079-1092.

Thiel, C., Buylaert, J.-P., Murray, A., Terhorst, B., Hofer, I., Tsukamoto, S., Frechen, M., 2011. Luminescence dating of the Stratzing loess profile (Austria) – Testing the potential of an elevated temperature post-IR IRSL protocol. Quaternary International 234, 23-31.

Thomsen, K.J., Murray, A.S., Jain, M., Bøtter-Jensen, L., 2008. Laboratory fading rates of various luminescence signals from feldspar-rich sediment extracts. Radiation Measurements 43, 1474-1486.

Timar-Gabor, A., Vandenberghe, D., Panaiotu, E.C., Panaiotu, C.G., Necula, C., Cosma, C., van den haute, P., 2010. Optical dating of Romanian loess using fine-grained quartz. Quaternary Geochronology 5, 143-148.

Wang, Q., Li, F., Li, Y., 1986. Shoreline changes in west-southern coastal plain of the Bohai Sea since 150 ka in: Qin, Y., Zhao, S. (Eds.), Late Quaternary sea-level changes. China Ocean Press, Beijing, pp. 62-71.

Wintle, A.G., Murray, A.S., 2006. A review of quartz optically stimulated luminescence characteristics and their relevance in single-aliquot regeneration dating protocols. Radiation Measurements 41, 369-391.

Yan, Y., Wang, H., Li, F., Tian, L., 2006. Different depositional processes of boreholes BQ1 and BQ2 in the late Pleistocene on the west coast of Bohai Bay. Quaternary Science 26, 321-326. (in Chinese with English Abstract)

Yang, L., Long, H., Yi, L., Li, P., Wang, Y., Gao, L., Shen, J., 2015. Luminescence dating of marine sediments from the Sea of Japan using quartz OSL and polymineral pIRIR signals of fine grains. Quaternary Geochronology 30, 257-263.

Yao, Z., Shi, X., Liu, Q., Liu, Y., Larrasoaña, J.C., Liu, J., Ge, S., Wang, K., Qiao, S., Li, X., Shi, F., Fang, X., Yu, Y., Yang, G., Duan, Z., 2014. Paleomagnetic and astronomical dating of sediment core BH08 from the Bohai Sea, China: Implications for glacial-interglacial sedimentation. Palaeogeography, Palaeoclimatology, Palaeoecology 393, 90-101.

Yi, L., Deng, C., Tian, L., Xu, X., Jiang, X., Qiang, X., Qin, H., Ge, J., Chen, G., Su, Q., Chen, Y., Shi, X., Xie, Q., Yu, H., Zhu, R., 2016. Plio-Pleistocene evolution of Bohai Basin (East Asia): demise of Bohai Paleolake and transition to marine environment. Scientific Reports 6, 29403.

Yi, L., Deng, C., Xu, X., Yu, H., Qiang, X., Jiang, X., Chen, Y., Su, Q., Chen, G., Li, P., Ge, J., Li, Y., 2015. Paleo-megalake termination in the Quaternary: Paleomagnetic and water-level evidence from south Bohai Sea, China. Sedimentary Geology 319, 1-12.

Yi, L., Lai, Z., Yu, H., Xu, X., Su, Q., Yao, J., Wang, X., Shi, X., 2013. Chronologies of sedimentary changes in the south Bohai Sea, China: constraints from luminescence and radiocarbon dating. Boreas 42, 267-284.

Yi, L., Yu, H.-J., Ortiz, J.D., Xu, X.-Y., Chen, S.-L., Ge, J.-Y., Hao, Q.-Z., Yao, J., Shi, X.-F., Peng, S.-Z., 2012. Late Quaternary linkage of sedimentary records to three astronomical rhythms and the Asian monsoon,

inferred from a coastal borehole in the south Bohai Sea, China. Palaeogeography, Palaeoclimatology, Palaeoecology 329-330, 101-117.

Zhang, J., Tsukamoto, S., Nottebaum, V., Lehmkuhl, F., Frechen, M., 2015. De plateau and its implications for post-IR IRSL dating of polymineral fine grains. Quaternary Geochronology 30, 147-153.

Zhao, S., 1986. Transgression and coastal changes in Bohai Sea and its vicinities since the Late Pleistocene, in: Qin, Y., Zhao, S. (Eds.), Late Quaternary sea-level changes. China Ocean Press, Beijing, pp. 53-61.

Chapter 6 Conclusions and outlook

6.1 Conclusions

Applicability of optically stimulated luminescence (OSL) techniques to establish a robust chronology for coastal sediments sequences in the North Bohai Bay, China, has been investigated. In order to overcome age underestimations due to anomalous fading affecting feldspar luminescence signals, different fading correction models for natural signal lying beyond the linear part of the dose response curve were evaluated using fluvial sediments from the Heidelberg Basin, Germany, and aeolian (loess-palaeosol) deposits from the Chinese Loess Plateau. The Bohai coastal sediments were then dated based on the findings and improvements to tackle fading issues from the "test site" studies. In addition, the degree of pre-depositional bleaching for various luminescence signals at different depositional periods was examined by comparing the luminescence ages.

The luminescence chronology established in this thesis allowed to define a robust chronological framework for the large scale transgression-regression cycles recorded in the Bohai coastal area since the Middle Pleistocene. In addition, late Holocene sedimentary processes reflecting the interplay between climate variation, sea level fluctuation and human activity could be investigated in details.

The conclusions of this thesis can be divided into five parts.

6.1.1 Reliability of fading correction methods for feldspar ages beyond the linear part of the dose response curve

Fluvial samples collected from core Heidelberg UniNord1 and for which it exists a reference chronology from palynological and palaeomagnetic analysis were first measured using $pIRIR_{225}$ and $pIRIR_{290}$

protocols (Chapter 2.1). The fading corrected $pIRIR_{225}$ ages following Kars et al. (2008) are in agreement with the results of palynological interpretation. The fading corrected ages following Lamothe et al. (2003) are underestimated when compared with the biostratigraphy for the Early and Middle Pleistocene. The $pIRIR_{290}$ signal yielded overestimated ages due to poor bleaching. In addition, this study reveals that fading rates of 1-1.5%/decade for $pIRIR_{290}$ relate to a natural fading process rather than a laboratory artefact (Chapter 2.1 and 6). The feldspar $pIRIR_{225}$ chronology also suggests that the previous and younger infrared radiofluorescence ages by Lauer et al. (2011) are most likely affected by anomalous fading.

Analyse carried out on the loess-palaeosol samples from the Chinese Loess Plateau (Chapter 2.2) show that the simulated dose response curves after fading correction following Kars et al. (2008) and Lamothe et al. (2003) are both comparable with the reconstructed natural dose response curves. The fading corrected ages are also broadly consistent with the reference ages derived from high resolution grain size analysis tuned with orbital cycles. Both the simulated and natural dose response curves yield an upper dating limit of ca. 200, 250 and 130 ka for $pIRIR_{225}$, IR_{50} (pre-$pIRIR_{225}$) and pulsed IR_{50}, respectively. Fading corrected age after Lamothe et al. (2003) broadly agrees with that after Kars et al. (2008) correction when fading rate is smaller than 4-5%/decade. Overall, the fading corrected method following Kars et al. (2008) has been validated using both fluvial and aeolian deposits from Heidelberg Basin and Chinese Loess Plateau, respectively, in aspects of comparisons of age and dose response curve.

6.1.2 Applicability of quartz OSL dating for the Bohai sediments

Compared with the quartz OSL signal, the dating range is largely extended by the feldspar luminescence signals (i.e. IR_{50} and the pIRIR signals stimulated at different temperatures). For young deposits covering the last millennia, the $pIRIR_{150}$ and $pIRIR_{225}$ ages are significantly overestimated, if compared with the associated quartz OSL ages. The apparent IR_{50} ages are broadly consistent with the quartz OSL ages, whilst the fading corrected ages are systematically overestimated (Chapter 2 and 3). The age overestimation for the young samples derives from the dominant residual signal for the pIRIR signals, and from possible fading over-correction (with fading rates of >5%/decade) for the IR_{50} signal. The residual component for pIRIR becomes negligible with the increase of accumulated signal. Feldspar ages for the marsh deposits (IR_{50} and $pIRIR_{150}$) underlying the sand dune and for the pre-Holocene sediments in core LZK06 (IR_{50}, $pIRIR_{150}$ and $pIRIR_{225}$) ranging from *ca.* 5-1 ka are generally consistent with the quartz OSL ages, indicating that the feldspar pIRIR signals stimulated at relatively low temperatures were well bleached and thus are applicable for dating of the older samples above the limit of quartz OSL dating.

The quartz OSL dating method was applied to date the young sand dune in the Lower Liao Plain and the core samples from the North Bohai Coast, which are presented in Chapter 3, 4 and 5. The relatively high dose rate of ca. 3 Gy/ka for all the samples enabled the dating of relatively young sand dune, which rapidly accumulated between 1890 and 1940 AD. The reliable quartz OSL ages for the core samples range from ca. 0.2 to 40 ka. The quartz OSL signal was well bleached at deposition, as the quartz OSL ages are consistent with the feldspar luminescence ages for the pre-Holocene sediments and with the radiocarbon dates for the Holocene samples. In addition, the quartz ages measured using different aliquot size were in agreement, further supporting that the quartz grains were bleached homogenously before burial.

6.1.3 Validation of feldspar luminescence dating for the Bohai sediments

Compared with the quartz OSL signal, the feldspar luminescence signal (i.e. IR_{50} and the pIRIR signals stimulated at different temperatures) allows to largely extend the dating range of sediments when using luminescence techniques. However, for young deposits covering the last millennia, the $pIRIR_{150}$ and $pIRIR_{225}$ ages significantly overestimate the associated quartz OSL ages. The apparent IR_{50} ages are broadly consistent with the quartz OSL ages, whilst the fading corrected ages are systematically overestimated (Chapter 3 and 4). The age overestimation for the young samples was derived from the dominant residual signal for the pIRIR signals, and from possible fading over-correction (with fading rates of >5%/decade) for the IR_{50} signal. The residual component for pIRIR becomes negligible with the increase of accumulated signal. Feldspar ages from the marsh deposits (IR_{50} and $pIRIR_{150}$) underlying the sand dunes) ranging from *ca.* 5-1 ka and from the pre-Holocene sediments in core LZK06 (IR_{50}, $pIRIR_{150}$ and $pIRIR_{225}$ are generally consistent with the quartz OSL ages. This indicates that the applied feldspar pIRIR signals were well bleached for the deposits older than 1 ka and thus are applicable for dating of the older samples above the limit of quartz OSL dating.

6.1.4 Timing of the three transgressions since the Middle Pleistocene in the Bohai Coast

Timing of the three transgressions in the Bohai Coast was controversial, as the chronologies published in the literature were proven to be unreliable. In this study, the degree of bleaching for all the luminescence signals and anomalous fading for feldspar luminescence signals were thoroughly investigated. Quartz OSL and feldspar pIRIR dating were applied to determine the timing of the three periods of transgression since the Middle Pleistocene in the Bohai Coast. The luminescence based chronology was further complemented with the application of the Bacon age-depth model was applied to reconstruct the accumulation history of the past ca. 250 ka. For the earliest transgression, the feldspar $pIRIR_{225}$ signal was well bleached, as indicated by the agreement between most of the fading corrected $pIRIR_{225}$ and $pIRIR_{290}$ ages. The feldspar $pIRIR_{225}$ ages show that the earliest transgression

occurred at ca. 200 ka, correlating with the sea-level highstand during Marine Isotope Stage (MIS) 7 (Spratt and Lisiecki, 2016). Based on the age-depth relation, the second transgression very likely occurred during MIS 5. Both the radiocarbon dates and the quartz OSL ages show that there was no regional sea-level highstand during MIS 3. The last transgression correlates with the Holocene sea-level rise. The chronology established using the quartz OSL and radiocarbon dates, in conjunction with historical records of shoreline migration, reveals that the sea-level stayed at highstand between 6 and 1 ka, and then retreated rapidly with the delta progradation.

6.1.5 Holocene accumulation history in the Bohai Coast

According to the high-resolution quartz OSL chronology, the Holocene sedimentation in the Northern Bohai Coast was an episodic instead of a gradual process. The sea-level rose rapidly during the early and middle Holocene and reached to the sea-level highstand at 6 ka, resulting in thin transgressive deposits in the Northern Bohai Coast due to the flat relief and the limited sediment supply from the local streams, i.e. the Dalinghe River. In the sea-level highstand system, the quartz OSL and radiocarbon ages, as well as historical records of shoreline migration show that a rapid progradation occurred during the last millennia. The annual sediment increment between 6 and 1 ka was 2.7×10^{4} $m^{3}\cdot a^{-1}$, while it dramatic increased to 9.1×10^{6} $m^{3}\cdot a^{-1}$ during the last millennia. Furthermore, the quartz OSL chronology shows a peak in the sediment input at ca. 700 a, filling the accommodation space with 4 m thick deposits. The sediment structures indicate that this episodic deposition was very likely triggered by frequent flooding events, which were also documented in the historical records. The rapid progradation was related to the enhancement of winter monsoon and human activity, resulting to less vegetation cover and soil erosion. Quartz OSL ages range from ca. 5 to 1 ka for the marsh deposits underlying the sand dune in the forest park and support a comparable tendency of shoreline migration in the Liaohe fluvial system. The sand dune accumulated from 1890 to 1940 AD and was out of the influence from sea-level fluctuation, as the shoreline retreated close to the modern Liaohe estuary. The sand accumulation was very likely related to the human activity, i.e. the ''Immigrant and Reclamation Policy'' at the end of Qing Dynasty, and not related to climate change.

6.2 Outlook for further study

In this thesis, the chronology of the three main transgressions in the Bohai Coast since the Middle Pleistocene was investigated in detail using the improved luminescence dating methods developed after testing the reliability of the dating approaches, in term of dating ranges and luminescence properties. Reliability of the fading correction methods for feldspar luminescence signals was assessed more specifically. Three main questions, however, require further investigations, which are listed below.

6.2.1 Sedimentary processes for the second transgression

Although the chronological framework for the three main transgressions in the Bohai Coast has been established, there were not enough luminescence samples to interpret in detail the sedimentary processes associated with the second transgression for core LZK06. For a better understanding on the sedimentary processes of T-2, a core with high recovery rate, especially for layer T-2, is needed. Further research should focus on two aspects. First, the age comparison between quartz OSL and feldspar luminescence signals should be carefully conducted, to evaluate the reliability of both dating approaches in terms of dating range and signal bleaching. Second, the sedimentary processes should be well constrained by high-resolution luminescence chronology.

6.2.2 Rapid progradation along the Bohai Coast in the last Holocene

The late Holocene rapid progradation has been widely reported in different coastal areas (e.g. Gao et al., 2017; Hori et al., 2001; Tamura et al., 2009; Wang et al., 2015; Zhang et al., 2014). Although similar event was revealed by the luminescence chronology in the North Bohai Coast, the sedimentary process in association with this rapid progradation should be carefully re-interpreted after establishment of an integrated chronology for other areas in the Bohai Coast. An integrated study should be conducted in terms of coastal relief, sediment supply of local streams and sea-level fluctuation in the entire Bohai Sea.

Appendix 1: Curriculum vitae

For reasons of data protection, the Curriculum vitae is not published in the online version.

Appendix 2: Publications

First-authored publications

1. **Yan Li**, Sumiko Tsukamoto, Ke Hu, Manfred Frechen, 2017. Quartz OSL and K-feldspar post-IR IRSL dating of sand accumulation in the Lower Liao Plain (Liaoning, NE China). Geochronometria 44, 1-15.
2. **Yan Li**, Sumiko Tsukamoto, Manfred Frechen, Gerald Gabriel. Timing of fluvial sedimentation in the Upper Rhine Graben since the Middle Pleistocene: constraint from quartz and feldspar luminescence dating. Boreas, in press. doi: 10.1111/bor.12266.
3. **Yan Li**, Zhiwen Shang, Sumiko Tsukamoto, Toru Tamura, Liang Yi, Christian Rolf, Hong Wang, Manfred Frechen, Jianfen Li, Xingyu Jiang. Sediments of rapid delta progradation during the last millennia in the Bohai Coast, Northern China: their OSL properties and refined chronology. Journal of Asian Earth Sciences, in press. doi: 10.1016/j.jseaes.2017.10.036.

Co-authored publications

1. Michael Kenzler, Henrik Rother, Heiko Hüneke, Peter Frenzel, Jaqueline Strahl, Sumiko Tsukamoto, **Yan Li**, Stefan Meng, Julia Gallas, Manfred Frechen. A multi-proxy palaeoenvironmental and geochronological reconstruction of the Saalian-Eemian-Weichselian succession at Klein Klütz Höved (SW Baltic Sea, NE-Germany). Boreas, in press. doi: 10.1111/bor.12255.
2. Liang Yi, Chenglong Deng, Xingyong Xu, Hongjun Yu, Xiaoke Qiang, Xingyu Jiang, Yanping Chen, Qiao Su, Guangquan Chen, Ping Li, Junyi Ge, **Yan Li**, 2015. Paleo-megalake termination in the Quaternary: Paleomagnetic and water-level evidence from south Bohai Sea, China. Sedimentary geology 319, 1-12.
3. Liang Yi, Xingyong Ye, Junbing Chen, **Yan Li**, Hao Long, Xulong Wang, Jinhua Du, Songling Zhao, Chenglong Deng, 2014. Magnetostratigraphy and luminescence dating on a sedimentary sequence from northern East China Sea: Constraints on evolutionary history of eastern marginal seas of China since the Early Pleistocene. Quaternary International 384, 316-326.

Appendix 3: Conference contributions

1. International Luminescence and Electron Spin Resonance Dating conference. 11-15 Sep, Cape Town, South Africa. **Oral** presentation.
2. German Luminescence and Electron Spin Resonance Dating conference. 4-6 November, 2016, Freiburg. **Poster** presentation.
3. Asia Oceania Geosciences Society 13th Annual Meeting. 31 Jul-5 Aug, 2016, Beijing, China. **Oral** presentation.
4. Workshop: Ice Age Earth. 21-25 June, 2016, Budapest, Hungary. **Oral** presentation.
5. German Luminescence and Electron Spin Resonance Dating conference. 4-6 November, 2016, Freiburg. **Poster** presentation.
6. German Luminescence and Electron Spin Resonance Dating conference. 4-6 November, 2016, Berlin. **Poster** presentation.
7. Workshop: Interdisciplinary Quaternary Investigations. 15 October, 2015, Zagreb, Croatia. **Oral** presentation.

Appendix 4: Eidesstattliche Erklärung

Hiermit erkläre ich, dass ich die vorgelegte Arbeit selbständig und ohne fremde Hilfe verfasst habe. Die Beiträge der Co-Autoren der wissenschaftlichen Veröffentlichungen sind im Rahmen der Danksagung (Acknowledgements) dargelegt. Ich erkläre, dass die Arbeit erstmalig am Fachbereich Geowissenschaften der Freien Universität Berlin eingereicht wurde und somit noch keiner anderen Fakultät oder Universität zur Prüfung vorgelegt wurde. Der Inhalt der dem Verfahren zugrunde liegenden Promotionsordnung ist mir bekannt.

Yan Li

Hannover, 16. Nov. 2017